EFFECT OF NUTRIENT MOMENTUM AND MASS TRANSPORT ON MEMBRANE GRADOSTAT REACTOR EFFICIENCY

by

BUNTU GODONGWANA

Thesis submitted in fulfilment of the requirements for the degree

DOCTOR TECHNOLOGIAE (ENGINEERING: CHEMICAL)

in the

FACULTY OF ENGINEERING

at the

CAPE PENINSULA UNIVERSITY OF TECHNOLOGY

SUPERVISOR: **Prof MARSHALL S. SHELDON**
CO-SUPERVISOR: **Dr DEON M. SOLOMONS**

CAPE TOWN
March 2016

DECLARATION

I, **Buntu Godongwana**, declare that the contents of this thesis represent my own unaided work, except where specifically acknowledged in the text, and that the thesis has not previously been submitted for academic examination towards any qualification. Furthermore, it represents my own opinions and not necessarily those of the Cape Peninsula University of Technology, Montana State University, the Fulbright Program (USA), the Deutscher Akademischer Dienst (Germany) nor the National Research Foundation.

B. Godongwana

March 2016

ABSTRACT

Since the first uses of hollow-fiber membrane bioreactors (MBR's) to immobilize whole cells were reported in the early 1970's, this technology has been used in as wide ranging applications as enzyme production to bone tissue engineering. The potential of these devices in industrial applications is often diminished by the large diffusional resistances of the membranes. Currently, there are no analytical studies on the performance of the MBR which account for both convective and diffusive transport. The purpose of this study was to quantify the efficiency of a biocatalytic membrane reactor used for the production of enzymes. This was done by developing exact solutions of the concentration and velocity profiles in the different regions of the membrane bioreactor (MBR). The emphasis of this study was on the influence of radial convective flows, which have generally been neglected in previous analytical studies. The efficiency of the MBR was measured by means of the effectiveness factor.

An analytical model for substrate concentration profiles in the lumen of the MBR was developed. The model was based on the solution of the Navier-Stokes equations and Darcy's law for velocity profiles, and the convective-diffusion equation for the solute concentration profiles. The model allowed for the evaluation of the influence of both hydrodynamic and mass transfer operating parameters on the performance of the MBR. These parameters include the fraction retentate, the transmembrane pressure, the membrane hydraulic permeability, the Reynolds number, the axial and radial Peclet numbers, and the dimensions of the MBR. The significant findings on the hydrodynamic studies were on the influence of the fraction retentate. In the dead-end mode it was found that there was increased radial convective flow, and hence more solute contact with the enzymes/biofilm immobilised on the surface of the membrane. The improved solute-biofilm contact however was only limited to the entrance half of the MBR. In the closed shell mode there was uniform distribution of solute, however, radial convective flows were significantly reduced. The developed model therefore allowed for the evaluation of an optimum fraction retentate value, where both the distribution of solutes and radial convective flows could be maximised.

Recent designs of MBRs seek to overcome diffusional limitations inherent in these devices by exploiting radial convective flows. The developed model from the current study allowed for the evaluation of the influence of axial diffusion, membrane resistance and radial convective flows on the solute concentration profiles in the MBR.

A numerical scheme was developed for the second-order elliptic differential balance equation, with non-linear kinetics, for concentration profiles in the MBR. The numerical scheme was executed using the Newton-Raphson algorithm, and was shown to be unconditionally stable for different step sizes. The significant findings from the FDM scheme was that the uniform solute distribution, in the open-shell mode, was more favourable for microbial growth than the dead-end mode. This result was consistent with the findings from the analytical solution.

The effectiveness factor for the MBR was calculated as a function of the Thiele modulus (Φ), the Sherwood number, the Peclet number and dimensions of the MBR. Effectiveness factor plots and their asymptotes were developed and compared to experimental data. Three regions of Φ were defined from the plots, corresponding with: kinetic control ($\Phi < 0.01$), internal-diffusion control ($0.01 < \Phi < 0.1$), and external mass transfer limitation ($\Phi > 0.1$). It was shown that operation of the MBR at low Thiele moduli was not optimal since substrate conversion at these values was minimal. Conversely, at high Thiele moduli solute transport was limited by diffusion through the membrane. The developed model provides a basis for parametric optimisation studies.

The theoretical model developed for the effectiveness factor confirmed previous experimental studies and numerical analysis, on the importance of radial convective flows on the performance of the MBR. The more significant finding from the current study was that radial convective flows improve bioreactor performance in a limited range of Thiele moduli, and this range was found to coincide with the region of internal diffusion limitation ($0.01 < \Phi < 0.1$). Outside this range, the effectiveness factor was shown to be improved only by increased Sherwood numbers. The maximum relative increase in the effectiveness factor was observed to be in the transitional region from kinetic to internal-diffusional control ($\Phi \approx 0.01$), and minimal in the boundary region between internal-diffusional control and external mass transfer limitation. The production of lignin peroxidase and manganese peroxidase from the fungus *Phanerochaete chrysosporium*, in a membrane gradostat reactor, was used to validate the developed models

***Keywords**:* Convection-diffusion equation; Effectiveness factor; Mass transfer with reaction; Membrane bioreactor; Monod kinetics; Regular perturbation; Substrate transport; Thiele modulus; Peclet number; Sherwood number.

DEDICATION

To Chulekazi Mokhatla

ACKNOWLEDGEMENTS

I would like to express my sincere appreciation and gratitude to the following persons and institutions for their support:

- To my supervisors: Prof Marshall Sheldon, for putting her faith in me, her guidance and motivation throughout the duration of my undergraduate and postgraduate studies. Dr Deon Solomons, for his continued support and priceless advice on mathematical principles covered in this thesis. Prof Phillip Stewart, for his mentorship during my visit at Montana State University (MSU).
- Prof Jeff Heys (MSU) for his assistance in developing the MATLAB code for the Newton-Raphson algorithm used in Chapter 4.
- The National Research Foundation for financial support towards the completion of this research.
- The Deutsche Akademischer Austausch Dienst (DAAD) for funding part of the study.
- The Fulbright Program for sponsoring a study visit to the United States, and their interest in my personal development.
- The Center for Biofilm Engineering at MSU for their hospitality and academic input during my visit.
- Hannelene Small, Elizma Alberts, and Denise February (of the Fundani centre at CPUT) for assistance with procurement of the project requirements.
- Prof Seteno Karabo Ntwampe, Dr Patrick Ndakidemi, Dr Sheku Kanu, Dr Patricia Mathabe, Dr Debbie de Jager, Innocentia Erdogan, Moses Basitere, Kevin Ncube, and Vincent Ntunja for their encouragement.
- The memory of my uncles Ndzondelelo “Bra Andy” and Sabelo “Big Joe” Godongwana.
- My mother Thofisa Hellen Godongwana, my dearest sister Noluvuyo Godongwana, Eric Godongwana, and all my family and friends.
- Yolanda Zihlangu from whom I continue to draw infinite inspiration.
- Special thanks to Amanda Mokhatla without whom this work would never be complete. Her greatest contribution was the expansion on the principle of mass conservation to include: “Mass is conserved regardless of its deficiencies”.

RESEARCH OUTPUTS

Published articles

[i] Godongwana, B., Solomons, D. & Sheldon, M.S. 2015. A finite difference solution of solute transport through a membrane bioreactor. *Mathematical Problems in Engineering*, 2015: 1-8.

[ii] Godongwana, B., Solomons, D. & Sheldon, M.S. 2010. A solution of the convective-diffusion equation for solute mass transfer inside a capillary membrane bioreactor. *International Journal of Chemical Engineering*, 2010: 1 – 12.

Articles under review

[iii] Godongwana, B. 2015. Effectiveness factors and conversion in a biocatalytic membrane reactor. *PLoSONE,* **minor revisions required**.

Conference presentations

[iv] Godongwana, B., Solomons, D.M. & Sheldon, M.S. A theoretical analysis of solute transport through a membrane bioreactor. *Proceedings of the 2nd International Conference on Fluid Flow, Heat and Mass Transfer.* Ottawa, Ontario, Canada, May 2015. Paper No. 147.

[v] Godongwana, B., Sheldon, M.S. & Solomons, D. A finite difference solution of solute transport through a membrane bioreactor. *CPUT Annual Postgraduate Conference,* Cape Town, November 2014.

PREFACE

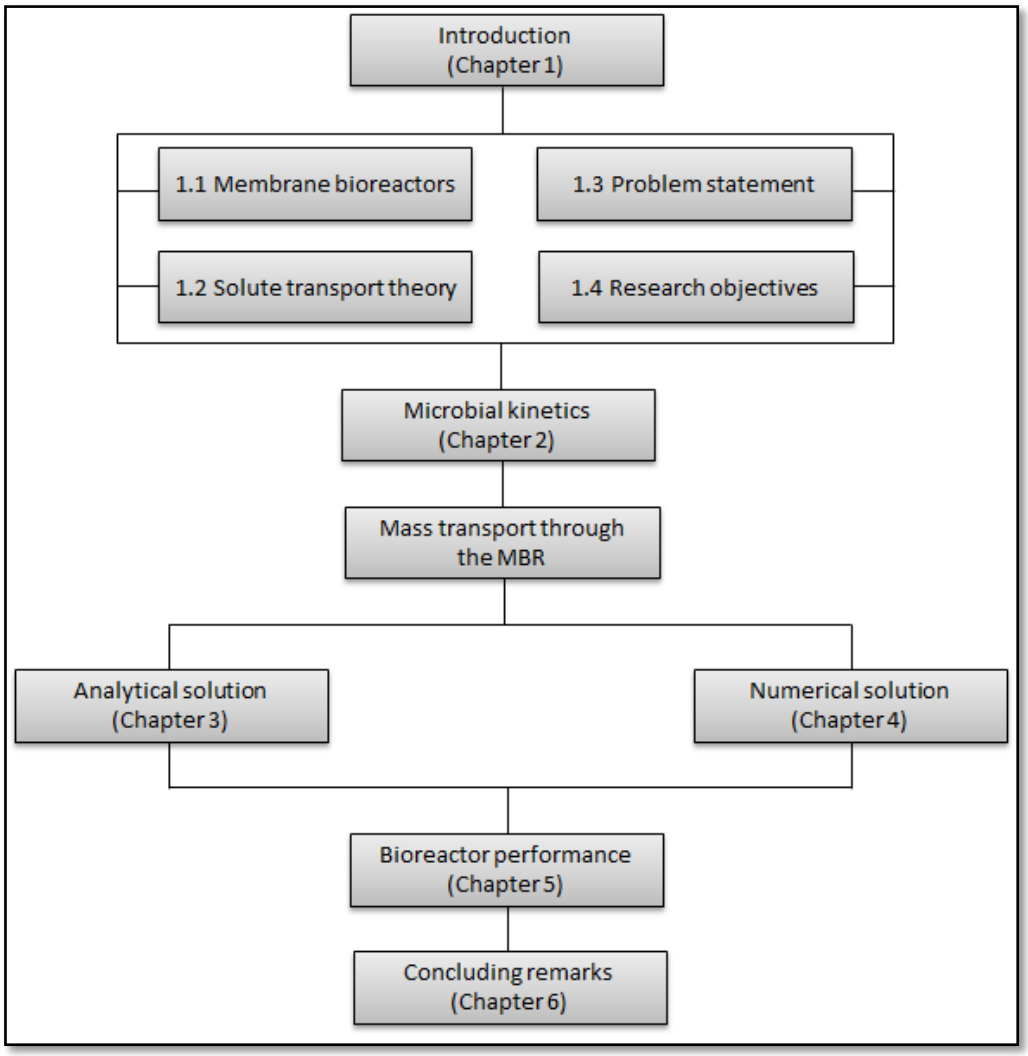

Figure 0: Road map of the thesis.

The potential of membrane bioreactors (MBRs) as an alternative to traditional reaction (and separation) technology, in enzyme production, is often diminished by the large diffusional resistances of the membranes. The concept of overcoming these diffusional limitations by introducing convective flows has been experimentally validated by a number of researchers. However, a precise mathematical analysis of this phenomenon is not available in literature. The current thesis presents analytical solutions of the convection-diffusion equation with reaction, with the intention of developing a functional relation between the convective flows and bioreactor performance. The bioreactor performance is measured by means of the effectiveness factor.

The emphasis of this thesis is on the mathematical solutions and the historical development of MBRs is kept to a minimum. The thesis is written in article format, consisting of 6 chapters. Chapters 1, 2, and 6 are written according to the CPUT thesis guidelines, and Chapters 3, 4, and 5 following the writing and reference style of the specific journals in which they were published. The appendices have been removed from the respective chapters and included as separate auxiliary chapters at the end of the thesis. Chapters not published in research journals follow the Harvard method of referencing.

A road map of the thesis is given in Figure 0. Chapter 1 provides an introduction to the thesis where the research problem and the research objectives are outlined. The relevant theory of simultaneous convection, diffusion and reaction in an MBR is provided. Chapter 2 provides a literature review of microbial kinetics, beginning with the elementary unstructured and distributed models and a brief overview of the more complex structured and segregated models. The theory from this chapter was utilized in Chapters 3 and 4 where simultaneous diffusion, convection and reaction differential balance equations were solved for the transport of the rate limiting solute inside the lumen of the MBR. Chapter 3 presents an analytical approach for solving the mass balance equation with and without reaction. The resulting non-linear elliptic equation is only amenable to an analytical solution when assuming zero-order or first-order kinetics. This restriction limits the range of applicability of the model. Hence in Chapter 4 a finite difference scheme was presented for the lumen concentration profile when the reaction kinetics were non-linear. This chapter also serves to validate the perturbation technique employed in Chapter 3. Chapter 5 extends the analysis to include the membrane matrix, where the actual conversion of solutes takes place. This chapter also includes a theoretical analysis of the effectiveness factor of the bioreactor. The influence of operating parameters, particularly radial convective flow, on the performance of the MBR was examined. Chapter 6 presents a summary of the findings and prospects from the current study.

The mathematical architecture and solution techniques employed in solving the governing differential equations in the lumen and matrix regions of the MBR are presented in Appendix A and B, respectively. Appendix C provides a description of the materials and methods that were used to validate the theoretical models developed. The numerical code used in MATLAB in Chapter 4 has not been included, and will be made available on request.

TABLE OF CONTENTS

LIST OF FIGURES

LIST OF TABLES

CHAPTER 1: INTRODUCTION

1. INTRODUCTION

1.1 Membrane bioreactors

A membrane bioreactor (MBR) is broadly defined as a flow reactor within which membranes are used to separate cells or enzymes from the feed or product streams of a process (Salmon & Robertson, 1994). The membranes can either be tubular (e.g. hollow fibers) or in the form of flat-sheets, the former being the most common geometry (Nagy, 2012). A common characteristic of most MBR's is that feed streams are delivered continuously. Products may also be removed continuously or harvested intermittently, or at the end of the run. Hollow-fiber MBR's are characterized by high packing cell densities of the fibers. A conventional hollow-fiber MBR is considered in this study, and is shown in Figure 1.1. The application of MBR's as an emerging technology is globally gaining popularity in a wide range of industries including industrial and municipal wastewater treatment (Cicek, 2003; Sartor *et al.*, 2008; De Jager, 2013); artificial organ devices (Moussy, 2003; Ye *et al.*, 2006; De Napoli *et al.*, 2014); the production of enzymes (Ntwampe & Sheldon, 2006; Sheldon, 2008; Godongwana *et al.*, 2009) and biotherapeutics (Taylor *et al.*, 1994; van Reis & Zydney, 2007).

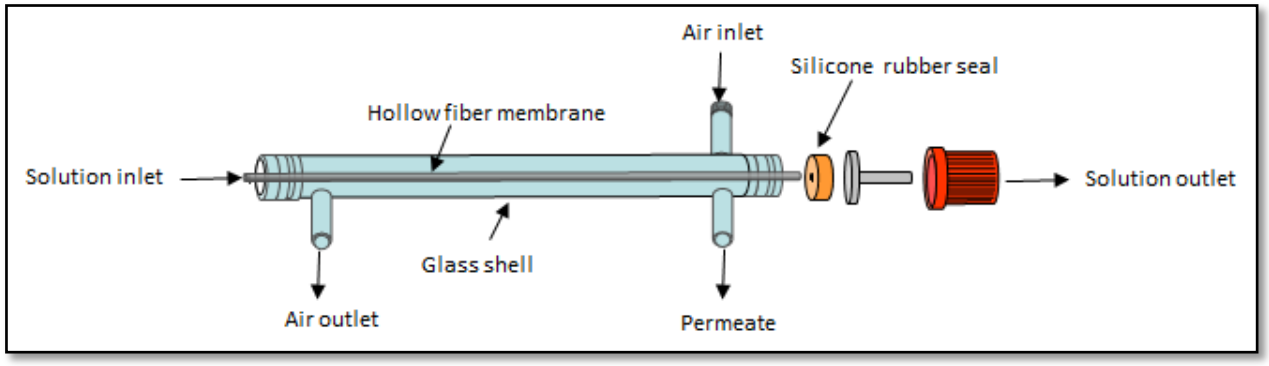

Figure 1.1: A schematic of a membrane bioreactor (MBR).

This technology emerged in the 1970's as an integration of the two disciplines of membrane technology and biotechnology. The first successful uses of MBR's to immobilize enzymes and whole cells were reported by Rony (1971) and Knazek and co-workers (1972). Since then a number of studies have been conducted which have indicated the effectiveness of these devices relative to traditional unit operations (e.g. chemostat reactors). Some of the advantages are: increased surface areas per unit reactor volume; protection of cells (or biofilm) from shear stresses; higher volumetric productivities; higher cell densities; and the possibility of

simultaneous reaction and separation (Montgomery, 2004; Curcio *et al.*, 2006; Nagy *et al.*, 2012). MBR's are favoured by recent trends towards environmentally-friendly technologies, particularly because MBR's do not require additives, function at moderate operating conditions, and reduce by-product formation (Giorno & Drioli, 2000).

The performance of an MBR is determined in large by the transport rate of the key nutrients, through the membranes, to the immobilised biomass (Curcio *et al.*, 2006; Godongwana *et al.*, 2007; Nagy, 2012). The carbon, nitrogen, and oxygen sources are of particular importance because of their high demand by the cells (Salmon & Robertson, 1994; Doran, 2013). The diffusional resistance offered by the membrane can adversely affect the transport of these nutrients in an MBR, and remain a major challenge in the use of these devices. A number of experimental and theoretical investigations have been dedicated to the problem of diffusional limitations in hollow-fiber MBR's (Catapano *et al.*, 1990; Kelsey *et al.*, 1990; Brotherton & Chau, 1995; Labecki *et al.*, 2001; Moussy, 2003; Curcio *et al.*, 2006; Godongwana *et al.*, 2007; Abdullah *et al.*, 2009; Nagy, 2009; Nagy *et al.*, 2012; De Napoli *et al.*, 2014; Nagy *et al.*, 2015). The majority of these studies have demonstrated the substantive role of convective transport in overcoming diffusive mass transfer limitations of nutrients. Consequently hollow fiber MBR's have been designed to exploit radial convective flows (Leukes, 1999; Sheldon, 2008; De Napoli *et al.*, 2014).

1.2 Solute transport theory

The performance of an MBR is analyzed by first developing concentration profiles in the different regions of the MBR. This entails performing a differential material balance of the form (Godongwana *et al.*, 2010):

$$\frac{\partial c}{\partial \tau} = \nabla^2 c - Pe(\boldsymbol{v} \cdot \nabla c) - \phi^2 f(c) \tag{1.1}$$

where c is a dimensionless solute concentration, τ is a dimensionless time, $\mathbf{v}$ is the velocity vector, Pe is the Peclet number, ϕ is the Thiele modulus, and $f(c)$ is the dimensionless rate of solute consumption. The functional forms of $f(c)$ are explicated in Chapter 2 of this thesis, with the majority of experimental data for single substrate limited kinetics fitting the empirical relation (Truskey *et al.*, 2009):

$$f(c) = \frac{c}{K_M + c} \tag{1.2}$$

where K_M is the dimensionless Michaelis (or Monod constant). The Thiele modulus ϕ in Eq. (1.1) represents the relative rates of reaction and diffusion, and is defined as:

$$\phi = \sqrt{\frac{V_M R^2}{c_0 D_{AB}}} \tag{1.3}$$

where V_M is the maximum rate of reaction, D_{AB} is the effective diffusivity, and R is a characteristic length (generally taken as the radius of the membrane). When ϕ >> 1, the transport is diffusion-limited since the rate of reaction is much faster than the rate of diffusion. Ideally, an MBR should operate in a reaction-limited regime rather than a diffusion-limited regime (Giorno & Drioli, 2000). The Peclet number represents the relative rates of convection and diffusion, and for radial convective flows is defined as:

$$Pe = \frac{v_0 R}{D_{AB}} \tag{1.4}$$

where ν_0 is the permeation velocity through the membrane of the MBR governed by Darcy's law (Nagy, 2012):

$$v_0 = -\frac{k}{\mu}\frac{\Delta p}{l} \tag{1.5}$$

where k is the membrane hydraulic permeability, μ is the dynamic viscosity of the fluid, and $\Delta p/l$ is the pressure gradient across the membrane of thickness l. Membranes used in MBRs are usually made of polymers (Chang & Furusaki, 1991) but other materials, particularly ceramics, have also been used (Sheldon & Small, 2005). The hydraulic permeability k of both polymeric and ceramic membranes is much smaller than unity, generally of the order of magnitude 10^{-17} m^2 (Koska *et al.*, 1997; Godongwana *et al*., 2009; Nagy & Kulcsar, 2009).The magnitude of k is an important consideration in the solution of Eq. (1.1), especially when perturbation methods are employed, as will be done in the current study. When k is sufficiently small, the solution of Eq. (1.1) can be represented by asymptotic expansions in terms of k.

The velocity vector $\boldsymbol{\nu}$ in Eq. (1.1) is evaluated from the dimensionless Navier-Stokes equation (Bird *et al.*, 2002; Godongwana *et al.*, 2010):

$$\frac{\partial \boldsymbol{v}}{\partial \tau} + Re(\boldsymbol{v} \cdot \nabla \boldsymbol{v}) = \nabla^2 \boldsymbol{v} - \nabla p + \frac{Re}{Fr} \tag{1.6}$$

Table 1.1: Limiting forms of the convective-diffusion equation, Eq. (1.1).

	Assumptions	Simplification	Comments	References
1.	Steady-state	$\frac{\partial c}{\partial \tau} = 0$	This assumption is generally valid, except during start-up.	Calabro *et al*. (2002); Ye *et al*. (2006); Nagy *et a*l. (2015).
2.	Constant velocities	$u = u_0; \quad v = v_0$	This assumption is not valid when large pressure gradients exist in the MBR.	Heath & Belfort (1987); Nagy (2012).
3.	Radial convection-limited transport	$[\boldsymbol{v} \cdot \nabla c]_r = 0$	At large radial Peclet numbers (*Pe* >> 1) this assumption is not valid.	Willaert *et al* (1999); Li & Tan (2001); Ye *et al*. (2006).
4.	Axial diffusion-limited transport	$[\nabla^2 c]_z = 0$	At low axial Peclet numbers (*Pe* << 1) this assumption is not valid.	Dall-Bauman *et al*. (1990); Cabrera *et al*. (2001); Calabro *et al*. (2002).
5.	Zero-order kinetics	$f(c) = c^0 = 1$	This assumes the rate of reaction is maximal.	Webster *et al*. (1979) Willaert *et al*. (1999); Nagy *et al*. (2012).
6.	First-order kinetics	$f(c) = c^1 = c$	This assumes the rate of reaction is much less than the maximum rate.	Jayaraman (1992) Willaert *et al*. (1999); Nagy *et al*. (2012).

where *Fr* and *Re* are the Froude and Reynolds number, respectively given by:

$$Fr = \frac{v_0^2}{\boldsymbol{g}R}$$
$$Re = \frac{\rho v_0 R}{\mu} \tag{1.7}$$

Equation (1.1) is a second-order (elliptic) nonlinear partial differential equation with variable coefficients, and is the most general form of the differential balance equation for solute transport in a catalytic reactor. This equation is generally solved by numerical techniques, however in a few special cases analytical solutions may be obtained. These solutions are generally based on perturbation theory, and make use of one or more of the assumptions listed in Table 1.1.

The solution of Eq. (1.1) in the membrane region is subject to either the Dirichlet boundary condition (B.C.) or the Robin-type boundary condition. The Dirichlet B.C. assumes negligible

external mass transfer resistance, and is the most often used because of its simplicity. Strictly speaking, however, this B.C. should only be applied at low Thiele moduli (Aris, 1975; Webster *et al.*, 1979). The Robin B.C. accounts for external mass transfer limitations, and is the most general of the two boundary condition types. Once the solute concentration profiles have been established, the effectiveness factor (η) is evaluated from the following equation (Lee & Kim, 2006; Truskey *et al.*, 2009):

$$\eta = \int_0^1 c(r)dr = \frac{1}{\phi^2}\frac{\partial c}{\partial r}\Big|_{r=1} \tag{1.8}$$

The effectiveness factor is defined as the ratio of the observed rate of reaction to the hypothetical rate in the absence of mass transfer limitations, and is generally used to evaluate the performance of a catalytic reactor.

1.3 Problem statement

The assumption of negligible axial diffusion and radial convection, in solving Eqs. (1.1) and (1.8), is common in the majority of analytical models currently in use for the evaluation of MBR performance. Radial convective flows have been shown, both experimentally and by numerical analysis, to significantly improve MBR efficiency as discussed in Section 1.1. In the dead-end ultrafiltration mode, particularly, the assumption of negligible radial convective flow is not justifiable. At axial Peclet numbers (*Pe*) smaller than unity large concentration gradients exist in the membrane lumen and ignoring axial diffusion is also not justified. To the author's knowledge, there are currently no analytical (or closed-form) solutions to Eqs. (1.1) and (1.8) which account for both diffusive and convective mass transfer inside a biocatalytic MBR.

1.3.1 Hypothesis

The rate of nutrient (or solute) transport through the membrane is the primary determinant of biofilm-attached MBR efficiency, and this transport phenomenon is significantly improved by convective flows. The dependence of the performance of an MBR on convective flows can be simulated by defining an effective factor for the MBR.

1.3.2 Research questions

The following questions were addressed in this study:

- Is the growth of biofilm (*P. chrysosporium*) limited by one or more than one substrate?

- Which single or multiple-substrate-limited model is best suitable to quantify the growth kinetics?
- Are the coupled momentum and mass transfer differential balance equations amenable to analytical evaluation in the different regions of the MBR? If not, which numerical scheme would work best to achieve this?
- What is the nature of the dependence of the MBR effectiveness on convective mass and momentum transfer?
- Which parameters are to be used to quantify bioreactor efficiency?

1.4 Research objectives

The aim of this study was to quantify, from basic principles, the efficiency of a biocatalytic membrane reactor used for the production of enzymes. The production of lignin peroxidase and manganese peroxidase from the fungus *Phanerochaete chrysosporium*, in a membrane gradostat reactor, was used to validate the developed models. The specific objectives were to:

- Estimate velocity profiles for the different regions of the MBR from the Navier-Stokes equation, with the hydraulic permeability of the capillary membrane as a process variable.
- Estimate concentration profiles from differential material balances and the appropriate kinetic model of substrate consumption.
- Compare the analytical models developed (with the assumptions of zero-order and first-order kinetics) to a finite-difference solution of the general kinetics problem.
- Generate effectiveness factor versus Thiele modulus plots, and from these identify the optimum operating conditions of the MBR, with specific reference to the effect of radial convective flows.
- Validate the developed model with experimental data.

1.5 Delineation of the study

This study did not investigate oxygen mass transfer characterisation; biofilm morphology; membrane fouling and concentration polarisation; optimisation of enzyme production and purification of enzymes. The theoretical models accounted for the different modes of operation and different orientations of MBR's but the verification of these models was restricted to the dead-end mode of a vertically orientated MGR. Parametric optimisation will not be considered.

Nomenclature

c	dimensionless substrate concentration
c_0	substrate feed concentration (g dm^{-3})
D_{AB}	substrate diffusivity (m^2 s^{-1})
$Fr = u_0^2/gR$	Froude number
$\boldsymbol{g}$	gravitational acceleration (m s^{-2})
k	membrane hydraulic permeability (m^2)
K_M	dimensionless Monod constant
l	membrane thickness (m)
p	fluid pressure (Pa)
$Pe_u = u_0R/D_{AB}$	axial Peclet number
$Pe_v = v_0R/D_{AB}$	radial Peclet number
r	dimensionless radial spatial coordinate
R	membrane lumen radius (m)
$Re = \rho u_0R/\mu$	Reynolds number
u_0	feed axial velocity (m s^{-1})
$\boldsymbol{v}$	dimensionless velocity vector
v_0	permeation velocity (m s^{-1})
V_M	maximum rate of reaction (g dm^{-3} s^{-1})
z	dimensionless axial spatial coordinate

Greek letters

η	effectiveness factor for general kinetics
μ	solution dynamic viscosity (Pa s)
ρ	solution density (kg m^{-3})
ϕ	Thiele modulus
τ	dimensionless time

CHAPTER 2: LITERATURE REVIEW

Microbial Growth and Substrate Uptake Kinetics

2. MICROBIAL GROWTH AND SUBSTRATE UPTAKE KINETICS

2.1 Introduction

The mathematical modelling of microbial processes in biological reactors is broadly divided into two aspects of consideration, i.e., microbial growth kinetics and bioreactor performance, as illustrated in Figure 2.1. Bioreactor performance is governed by the transport of the key substrates through the bioreactor to the microorganisms. Microbial growth kinetics on the other hand is concerned with the mathematical descriptions of the rate of consumption of these substrates by the microorganisms, and the mechanisms of growth. This chapter considers kinetic models currently in use in microbial growth studies from the elementary unstructured and distributed models and a brief overview of the more complex structured and segregated models. Mass and momentum transfer models will be considered in Chapters 3 - 5.

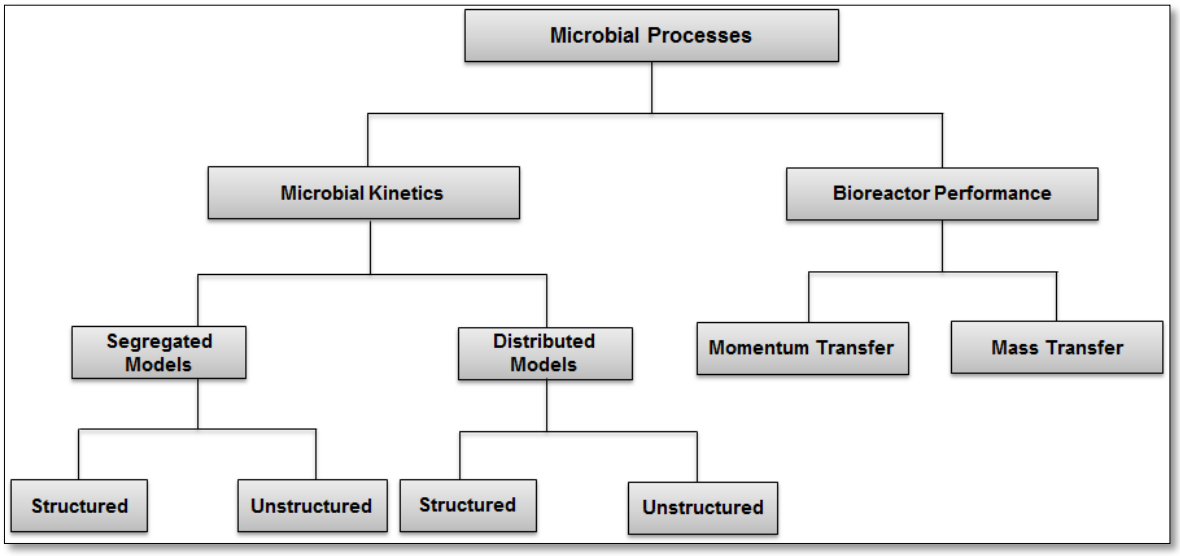

Figure 2.1: Classification of mathematical models of microbial processes (adapted from Ramkrishna, 1979; Nielsen & Villadsen, 1992).

Cell growth processes are characterised by an overwhelming complexity and variety, and mathematical models intended to describe these processes should reflect these characteristics. Over the past 50 years numerous efforts have been made to develop growth kinetic models that are representative of this dynamic and complex nature of microbial processes (Eakman *et al.,* 1966; Ramkrishna, 1979; Liou *et al.*, 1997; Godin *et al.*, 1999; Bizukojc & Ledakowicz, 2003; Sheldon *et al.*, 2008). These models have been developed to account for the intracellular

reactions in the various compartments of the cell (so-called structured models); as well as the variations in metabolic activity from cell to cell within a matrix of cells (referred to as segregated models). Despite these advancements, there still exist difficulties in their application for modelling cell growth. Firstly, this is due to the fact that physiological properties (e.g. growth rate, cell division probability, and partitioning probability), which are input variables, are unknown for most microbial systems (Blanch, 1981; Mantzaris *et al.*, 1999). Secondly, these models are characterised by considerable mathematical complexity. The level of detail required in a model is dictated by what is being described, and the objective is to always choose the simplest model that can describe the system within a tolerable variance.

2.2 Unstructured distributed models

The earliest models of microbial growth kinetics were all unstructured, distributed models. Unstructured means that they assume fixed cell composition, which is similar to assuming all cell components grow at the same rate. This assumption is only valid in single-stage, steady-state, continuous cultures and the exponential phase of batch cultures. It is invalid during any transient condition. In these models the biomass development is a function of one state variable, as opposed to the two or more components in structured models. The unstructured model is based on the following observations concerning microbial growth processes: (1) that the rate of cell mass production is proportional to biomass concentration; (2) that there is a saturation limit for growth rate on each substrate; and (3) that the cells need substrate and may synthesize products even when they do not grow (Nielsen, 2006; Shuler & Kargi, 2014).

Distributed (or non-corpuscular) models are those that assume that there are no variations from cell to cell in a population, and that the cell can be viewed as a lumped biomass. This assumption is satisfactory under many circumstances, exceptions being in their inability to predict a lag phase in batch growth (Tsuchiya *et al.*, 1966) and the growth responses of plasmid-containing cultures (Shuler & Kargi, 2014).

2.2.1 Single-substrate limited growth

The most basic of unstructured microbial growth kinetic models is that of single-substrate limited growth. In this model it is assumed that a single chemical specie, *i*, is growth-rate limiting, and that the kinetics of microbial growth can be expressed in terms of this substrate alone. The specific growth rate, μ, which characterises microbial growth is therefore a function of the concentration of this specie, c_i:

$$\mu = f(c_i) \tag{2.1}$$

The microbial growth rate, d*x*/d*t*, is a linear function of the specific growth rate (Biazar *et al.*, 2003; Doran, 2013):

$$\frac{dx}{dt} = \mu x - Y_{x/c_i} m_x x \tag{2.2}$$

Where *x* is the microbial concentration (or density); *t* is time; Y_{x/c_i} is the maximum yield of cells per unit substrate, *i*, consumed; and m_x is the maintenance coefficient. The maintenance coefficient is defined as the rate of substrate consumption for cellular maintenance (i.e. production of cell mass, oxygen consumption, and product formation). The simplest and most used model for the nature of the dependence of the specific growth rate, μ, on the substrate concentration, c_i, in Equation (2.1) is that proposed by Monod (1949):

$$\mu = \frac{\mu_{max} c_i}{K_s + c_i} \tag{2.3}$$

where μ_{max} is the maximum specific growth rate and K_S is the saturation constant (or half velocity constant), equal to the concentration of the rate-limiting substrate when the specific growth rate is equal to one-half of the maximum. Other models have been proposed for the dependence of Equation (2.1), and can be generally described by a single differential equation (Shuler & Kargi, 2014):

$$\frac{d\upsilon}{dc_i} = K\upsilon^a(1-\upsilon)^b \tag{2.4}$$

where *a*, b, and *K* are constants, and υ is the dimensionless specific growth rate equal to μ/μ_{max}. Equation (2.4) reduces to Tessier's (1942) equation when $a = 0$, $b = 1$, and $K = 1/K_S$:

$$\mu = \mu_{max}\left(1 - e^{-c_i/K_s}\right) \tag{2.5}$$

Moser's (1958) equation when $a = 1 - 1/n$, $b = 1 + 1/n$, and $K = 1/K_s^{1/n}$:

$$\mu = \frac{\mu_{max} {c_i}^n}{K_s + {c_i}^n} \tag{2.6}$$

Contois's (1959) equation when $a = 0$, $b = 2$, $K = 1/K_{sx}$:

$$\mu = \frac{\mu_{max} c_i}{K_{sx} x + c_i} \tag{2.7}$$

Equations (2.3) to (2.7) do not account for the inhibition of microbial growth which occurs at high concentrations of the limiting substrate or a metabolic product formed. This is often accounted for by extending these equations with additional terms. Thus, for inhibition by high concentrations of the limiting substrate, the Monod equation becomes (Truskey *et al.*, 2009; Shuler & Kargi, 2014):

$$\mu = \frac{\mu_{max} c_i}{K_s + c_i + \frac{{c_i}^2}{K_i}} \tag{2.8}$$

and inhibition by a metabolic product is given by (Truskey *et al.*, 2009; Shuler & Kargi, 2014):

$$\mu = \frac{\mu_{max} c_i}{c_i + K_s \left(1 + \frac{p}{K_p}\right)} \tag{2.9}$$

where p is the concentration of the product; K_i and K_p are the substrate and product inhibition coefficients, respectively. The choice of the most suitable equation to use in a given microbial growth process is dependent on the shape of the specific growth rate versus limiting-substrate concentration curve.

2.2.2 Multiple-substrate limited growth

Microorganisms exhibit nutritional preferences. When presented with a mixture of substrates, those that are in the main metabolic pathways are generally consumed first, the rest are consumed later after the common substrates are depleted (Bungay *et al.*, 1998; Sheldon *et al*., 2008). When the substrates concerned are carbon sources, this behaviour is referred to as diauxic growth, and is illustrated in Figure 2.2 by the cell mass growth curve. Diauxic growth curves exhibit an intermediary growth plateau (diauxic lag) between exhaustion of one substrate, exemplified by glucose in Figure 2.2, and commencement of utilization of the next (lactose in Figure 2.2). During this lag period, the enzymes needed for the uncommon substrate are synthesized. These enzymes are not produced during consumption of the first substrate because the enzymes required for the utilisation of the primary substrate show catabolic inhibition for the second substrate (Bungay *et al.*, 1998; Sheldon, 2008; Sheldon *et al*., 2008).

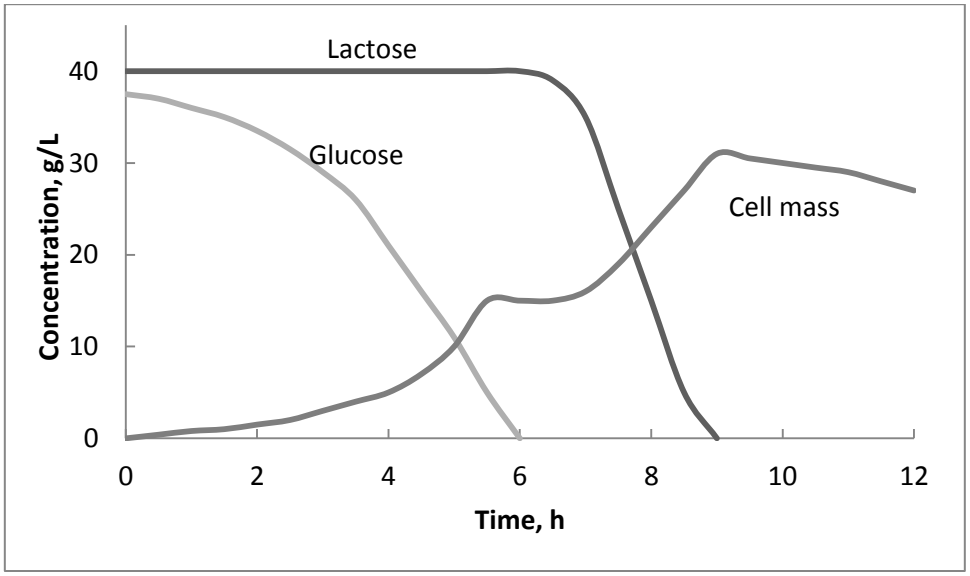

Figure 2.2: A computer simulation of diauxic growth (Bungay *et al*., 1998).

Substrates in a mixture may also be consumed simultaneously (i.e., exhibit non-competitive behaviour) as opposed to the competitive diauxic growth behaviour. In certain instances substrates may even show very weak to no interaction with each other (Narang & Pilyugin, 2007). The modelling of multiple substrate limited growth kinetics is generally based on one of the assumptions: (1) competitive interaction; (2) non-competitive interaction; or (3) non-interaction of substrates.

The specific growth rate for competitive inhibition of the utilization of one substrate by the other (sequential utilization) is given by:

$$\mu = \sum_{i=1}^{N} \omega_i f(c_i) \tag{2.10}$$

Where ω_i is a weighted average of the growth rates under individual nutrient limitations; the function $f(c_i)$ can take the form of any of the equations derived from Equation (2.4). As an illustration, in the case of dual-substrate limitation, assuming Monod kinetics, Equation (2.10) reduces to (Merchuk & Asenjo, 1994; Okpokwasili & Nweke, 2005; Sheldon, 2008):

$$\mu = \mu_{max}\left[\omega_1 \frac{c_1}{K_1 + c_1} + \omega_2 \frac{c_2}{K_2 + c_2}\right] \tag{2.11}$$

Equation (2.10) is often referred to as the additive model for multiple-substrate limited growth. The specific growth rate for non-competitive (simultaneous) utilization of substrates is given by:

$$\mu = \prod_{i=1}^{N} f(c_i) \tag{2.12}$$

Where Π is the product operator. For dual-substrate limitation, assuming Monod kinetics, Equation (2.12) becomes (Merchuk & Asenjo, 1994; Okpokwasili & Nweke, 2005):

$$\mu = \mu_{max}\left[\frac{c_1}{K_1 + c_1} \cdot \frac{c_2}{K_2 + c_2}\right] \tag{2.13}$$

Equation (2.12) is the so-called multiplicative model for multiple-substrate limited growth. In non-interactive models the growth rate of the microorganism is assumed to be equal to the lowest growth rate that would be predictable from the separate single substrate models (Sonmezisik *et al.*, Lewandowski & Beyenal, 2007):

$$\mu = f(c_1) \quad or \quad f(c_2) \quad or \quad f(c_N) \tag{2.14}$$

There is no reason to prefer non-competitive kinetics to competitive, but most experimental data has been fitted to the non-competitive models (Blanch, 1981; Sonmezisik *et al.*, 1998). It is important to note that multiple-substrate limited growth is best described by structured models and, in general, the unstructured (or black box) models of Section 2.2 should be used for single-substrate limited growth only (Nielsen, 2006).

2.3 Structured models

The unstructured models, described previously, constitute the majority of available literature models on fermentation processes. These models are normally restricted to one reactor type and to one mode of operation, and do not apply to transient operations. Structured models are not subject to these restrictions, and may be used in steady-state as well as transient operations. Although the mathematical formalism of structured models is quite complex, this is often outweighed by the amount of detail and degree of realism obtained from these models. There are various interpretations of structured microbial models, Nielsen and Villadsen (1992) have presented a general framework of these models, and a summary thereof is presented in this section.

Generally, there are two types of structured models applicable to microbial growth processes: (1) intracellularly structured models, and (2) morphologically structured models (Bizukojc & Ledakowicz, 2003). In the former models, kinetic expressions for the intracellular reactions of basic metabolic pathways are formulated, whereas in the latter models biomass is divided into subsections or compartments of various function and biochemical properties (Bizukojc & Ledakowicz, 2003). Morphologically structured models are mainly used to describe the growth of filamentous fungi (Nielsen, 1992; Bizukojc & Ledakowicz, 2003).

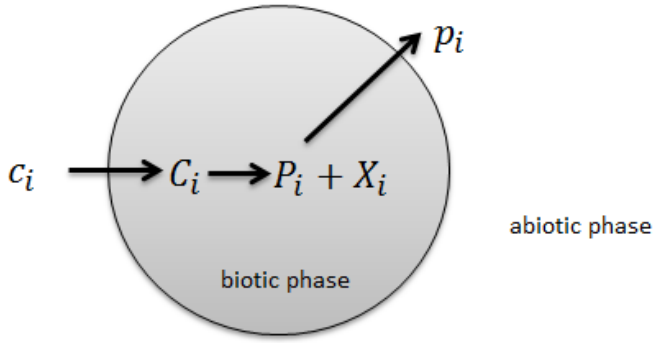

Figure 2.3: Reactions involved in cellular growth.

In developing a structured model the intention is to represent the kinetics in terms of species which are present only inside the cells, i.e., the microbial and reactor kinetics are decoupled. This is done by introducing the intracellular components C_i and P_i which are in pseudo-steady-state equilibrium with the extracellular substrates and products, c_i and p_i, respectively. Considering a system where the microorganism grows on N different substrates and M metabolic products are formed, as shown in Figure 2.3. A stoichiometric equation for each extracellular substrate, c_i, becomes (Nielsen *et al.*, 1991; Nielsen & Villadsen, 1992):

$$\sum_{j=1}^{N} \alpha_{c,ij} C_j + \sum_{j=1}^{L} \gamma_{c,ij} X_j + \sum_{j=1}^{M} \beta_{c,ij} P_j - c_i = 0; \quad i = 1,2,\dots,N \tag{2.15}$$

Where $\alpha_{c,ij}$, $\beta_{c,ij}$, and $\gamma_{c,ij}$ are stoichiometric coefficients which may be positive, zero, or negative (positive if there is a net production of species i in the j^{th} reaction); ***C*** and ***P*** are vectors of the intracellular concentrations of substrates and products; ***X*** is the vector of intracellular concentrations of the L biomass components. In most cases, however, the influence of the M metabolic products on the substrate uptake reactions is negligible (i.e. $\beta_{c,ij} = 0$). The uptake of each of the i^{th} substrate is often independent of the intracellular concentrations of the other substrates, and hence, $\alpha_{c,ij} = 0$ for $i \neq j$. Also, the transport of substrates across the membrane is

normally carried out without loss of mass, i.e. $\alpha_{c,jj}$ = 1. Considering the above conditions, Equation (2.15) reduces to (Nielsen *et al.*, 1991; Nielsen & Villadsen, 1992):

$$C_i + \sum_{j=1}^{L} \gamma_{c,ij} X_j - c_i = 0; \quad i = 1,2,\dots,N \tag{2.16}$$

For most microorganisms very little is known of the mechanisms involved in the substrate uptake, and empirical expressions are used to relate C_i to c_i and other environmental variables (e.g. temperature and pH). After uptake of substrate the formation of biomass and metabolic products is described by *J* reactions (Nielsen *et al.*, 1991; Nielsen & Villadsen, 1992):

$$\sum_{j=1}^{N} \alpha_{ij} C_j + \sum_{j=1}^{M} \beta_{ij} P_j + \sum_{j=1}^{L} \gamma_{ij} X_j = 0; \quad i = 1,2,\dots,J \tag{2.17}$$

For unstructured models $L = 1$ in Equations (2.15) - (2.17), since the biomass is assumed to be made-up of only one component. For structured models $L > 1$, and the chemical composition (X_i) must be known if stoichiometry is to be applied. The *M* metabolic products formed in the intracellular reactions are transported across the cellular membrane according to the stoichiometric equation (Nielsen *et al.*, 1991; Nielsen & Villadsen, 1992):

$$\sum_{j=1}^{N} \alpha_{p,ij} C_j + \sum_{j=1}^{L} \gamma_{p,ij} X_j + \sum_{j=1}^{M} \beta_{p,ij} P_j + p_i = 0; \quad i = 1,2,\dots,M \tag{2.18}$$

Considering the same arguments used in the simplification of Equation (2.15), Equation (2.18) can be reduced to:

$$\sum_{j=1}^{L} \gamma_{p,ij} X_j - P_i + p_i = 0; \quad i = 1,2,\dots,M \tag{2.19}$$

The rate of change of the intracellular substrate concentrations, when considering the aforementioned quasi-steady-state assumption, is given by (Nielsen *et al.*, 1991; Nielsen & Villadsen, 1992):

$$\frac{d\boldsymbol{C}}{dt} = \boldsymbol{A}^T \boldsymbol{r} + \boldsymbol{A}_c^T \boldsymbol{r}_c + \boldsymbol{A}_p^T \boldsymbol{r}_p - \mu \boldsymbol{C} = 0 \tag{2.20}$$

Where $\boldsymbol{r}_c$ is the rate of substrate uptake for the *N* substrates across the cellular membrane, equal to the specific substrate utilization vector for the *N* extracellular substrates; $\boldsymbol{r}_p$ is the specific product excretion vector for the *M* products; $\boldsymbol{r}$ is the rate vector for the *J* intracellular reactions. The first term on the right hand side of Equation (2.20) is the net substrate formation in the *J* intracellular reactions. The second and third terms represent net substrate formation in the substrate uptake and product excretion reactions, respectively; the last term accounts for dilution of $\boldsymbol{C}$ due to growth.

In the reaction scheme described in this section the specific growth rate of the biomass is calculated as a sum of the net specific formation rates for each component in the intracellular reactions:

$$\mu = \sum_{j=1}^{L} \sum_{i=1}^{J} \gamma_{ij} r_i \tag{2.21}$$

Where $\gamma_{ji} r_j$ specifies the net specific formation of the j^{th} component in the i^{th} reaction.

2.4 Segregated models

Segregated models are those that view the population as segregated into individual cells that are different from one another with respect to some distinguishable traits (Ramkrishna, 1979). The selection of the basis for this distinguishing trait is experimentally difficult, due primarily to the small size of bacterial, yeast and most fungal cells. Cell age and cell mass have often been proposed as a means of characterising cells, but without any experimental means of verifying the predictions of these models (Tsuchiya *et al.*, 1966; Blanch, 1981). Advances in flow microfluorimetry coupled with light scattering, cytometry and automatic image analysis now allows monitoring of individual cell content (Liou *et al.*, 1997; Mantzaris *et al.*, 1999).

Segregation is based on the presumption that growth is a manifestation of physiological activity of the cell. The extent of the physiological activity of the cell is a function of the physiological state and the constitution of the cell's environment. The physiological state of the cell can be determined by the quantitative amounts of one or more of the cellular constituents (Ramkrishna, 1979). The most commonly used segregated, structured population balance model is that developed by Eakman *et al.* (1966) for a well-stirred continuous bioreactor, using cell mass as the single index of the physiological state:

$$\frac{\partial W(t,m)}{\partial t} + \frac{\partial [r(m,c_i)W(t,m)]}{\partial m} = 2\int_{m}^{\infty} \Gamma'(m',c_i)W(t,m')p(m,m')dm - \left[\frac{1}{\theta} + \Gamma'(m,c_i) + \Theta(m,c_i)\right]W(t,m) \quad (2.22)$$

Where *W(t,m)* is the cell mass distribution function, representative of a number of cells per volume at time *t* with a mass between *m* and *m* + *dm*; *r(m, c_i)* is the single cell growth rate of a cell of mass *m*, growing in a medium with a limiting substrate concentration c_i; $\Gamma'(m', c_i)$ is the transition probability function; *p(m,m')* is the distribution of mass into daughter cells from mother cell; $\Theta(m,c_i)$ is the specific probability of death; θ is the holding time; c_i is the limiting substrate concentration.

The partial integro-differential Equation (2.22) is extremely difficult to solve analytically, and only amenable to such solutions after restrictive assumptions. A number of numerical solutions have been developed to overcome these restrictions. However, the majority of these models used cell age as the index of physiological state. Cell age implies the time elapsed since the cell has visibly detached from its mother, and has very limited practical value due to difficulties in its measurement (Liou *et al.*, 1997; Mantzaris *et al.*, 1999). Current research is focused on numerical solutions of mass-structured population balances, mass being a general term for any cell property which obeys the conservation law (Mantzaris *et al.*, 1999).

2.5 Empirical models

Transport equations for biological reactor systems give rise to a set of partial differential equations which are quite complex and difficult to solve (Mitchell *et al.*, 2004, Godongwana *et al.*, 2010). Coupling these equations with the structured and segregated kinetic models of Sections 2.3 and 2.4 gives the most general and accurate account of bioreactor performance. The solution of such a model, however, would require a lot of computational power, even for the simplest of microbial systems. This is typically avoided by using empirical kinetic models, instead of the growth kinetic models of Section 2.2 - 2.4 (Mitchell *et al.*, 2004).

Generally, there are four types of empirical correlations for solid-state fermentations, namely: the linear, exponential, logistic, and the two-phase model (Mitchell *et al.*, 2004), and these are presented in Table 2.1 These equations are fitted to experimental growth profiles by non-linear

Table 2.1: Differentiated and integrated forms of the empirical correlations of growth (Mitchell et al., 2004).

	Differentiated form		Integrated form	
Linear	$\frac{dX}{dt} = K$	(2.23)	$X = Kt + X_0$	(2.24)
Exponential	$\frac{dX}{dt} = \mu X$	(2.25)	$X = X_0 e^{\mu t}$	(2.26)
Logistic	$\frac{dX}{dt} = \mu X\left(1 - \frac{X}{X_m}\right)$	(2.27)	$X = \frac{X_m}{1 + \left(\frac{X_m}{X_0} - 1\right)e^{-\mu t}}$	(2.28)
Two phase	$\frac{dX}{dt} = \mu X, \quad t < t_a$ $\frac{dX}{dt} = \left[\mu L e^{-k(t-t_a)}\right]X, \quad t \geq t_a$	(2.29)	$X = X_0 e^{\mu t}, \quad t < t_a$ $X = X_0 exp\left[\frac{\mu L}{k}\left(1 - e^{-k(t-t_a)}\right)\right]X, \quad t \geq t_a$	(2.30)

Where X is microbial biomass, t is time, K is the linear growth rate, μ is the specific growth rate, X_0 is the initial biomass, X_m is the maximum microbial biomass, L is the ratio of the specific growth rate at the start of the deceleration phase to the specific growth rate during the previous exponential phase, k is a first-order rate constant describing the deceleration phase, and t_a is the time at which the switch from exponential to deceleration phase occurs.

regression, and the model that most closely resembles the experimental profiles is chosen as the model for growth. The logistic equation is the most commonly used of the four models, since it simulates the characteristic S-shape curve of population growth dynamics. This model is also favoured over the two-phase model because of its simplicity; the rate constant, *k*, and the specific growth rate ratio, *L*, of the two-phase model are difficult parameters to measure (Mitchell *et al.*, 2004). A disadvantage of these empirical models is that they do not include the effect of environmental conditions (e.g. nutrient concentration) on growth, which can make their usage questionable (Blanch, 1981; Mitchell *et al.*, 2004; Shuler & Kargi, 2014).

2.6 Summary

This section of the thesis presents a literature review of microbial kinetics, beginning with the elementary unstructured and distributed models and a brief overview of the more complex structured and segregated models. The theory from this chapter was utilized in Chapters 3 and 4 where simultaneous diffusion, convection and reaction differential balance equations were solved for the transport of the rate limiting solute inside the lumen of the MBR.

Nomenclature

a	constant in the generalized specific rate equation, Eq. (2.4)
$\boldsymbol{A}$	stoichiometric matrix for the substrates
b	constant in the generalized specific rate equation, Eq. (2.4)
$\boldsymbol{c}$	extracellular substrate concentration vector
$\boldsymbol{C}$	intracellular substrate concentration vector
J	number of intracellular reactions
K	constant in the generalized specific rate equation, Eq. (2.4)
L	number of intracellular components
m	mass of cells
m_x	maintenance coefficient
M	number of metabolic products
N	number of substrates
$\boldsymbol{p}$	extracellular product concentration vector
$\boldsymbol{P}$	intracellular product concentration vector
$\boldsymbol{r}$	rate vector for the intracellular reactions
r_i	rate of the ith reaction
$\boldsymbol{r}_p$	specific product formation rate vector
$\boldsymbol{r}_c$	specific substrate utilization rate vector
t	time
$W(t,m)$	cell mass distribution function
x	biomass concentration
$\boldsymbol{X}$	state vector for the biotic phase
Y_{x/c_i}	maximum yield of cells per unit substrate, i, consumed

Greek symbols

α_{ij}	stoichiometric coefficient for the i^{th} substrate in the j^{th} reaction
β_{ij}	stoichiometric coefficient for the i^{th} metabolic product in the j^{th} reaction
γ_{ij}	stoichiometric coefficient for the i^{th} element in the biotic phase in the j^{th} reaction
μ	specific growth rate for the biomass
υ	dimensionless specific growth rate
ω	weighted average of the growth rate of the biomass
θ	holding time

CHAPTER 3: RESULTS

Solute Transport Through the Lumen of a Membrane Bioreactor

Published as: **Godongwana, B., Solomons, D.M. & Sheldon, M.S.** 2010. A solution of the convective-diffusion equation for solute mass transfer inside a capillary membrane bioreactor. *International Journal of Chemical Engineering,* vol. 2010, 1-12.

3. SOLUTE TRANSPORT THROUGH THE LUMEN OF A MEMBRANE BIOREACTOR

Abstract

This paper presents an analytical model of substrate mass transfer through the lumen of a membrane bioreactor. The model is a solution of the convective-diffusion equation in two dimensions using a regular perturbation technique. The analysis accounts for radial-convective flow as well as axial-diffusion of the substrate specie. The model is applicable to the different modes of operation of membrane bioreactor (MBR) systems (e.g. dead-end, open-shell, or closed-shell mode), as well as the vertical or horizontal orientation. The first-order limit of the Michaelis-Menten equation for substrate consumption was used to test the developed model against available analytical results. The results obtained from the application of this model, along with a biofilm growth kinetic model, will be useful in the derivation of an efficiency expression for enzyme production in an MBR.

***Keywords**:* Convection-diffusion equation; Laplace transform; Mass transfer with reaction; Membrane bioreactor; Regular perturbation; Substrate transport.

3.1 Introduction

Since the first uses of hollow-fiber membrane bioreactors (MBR's) to immobilize whole cells were reported in the early 1970's, this technology has been used in as wide ranging applications as enzyme production to bone tissue engineering. One of the current research areas of interest into biofilm-attached membrane bioreactors (MBR's) is the development of cost effective and environmentally friendly methods of producing various primary and secondary metabolites from bacterial, fungal, and yeast cells. These include: manganese and lignin peroxidase, secreted by the fungus *Phanerochaete chrysosporium* [1,2]; actinorhodin, a non-commercial antibiotic produced by the filamentous bacterium *Streptomyces coelicolor* [3]; glutamic acid, an ingredient in flavour enhancers of meats and vegetables, secreted by the bacterium *Corynebacterium glutamicum* [4]; ethanol, extracted from the yeast *Saccharomyces cerevisiae* [5]; and many others. With the exception of ethanol, these bioproducts are generally classified as products of intermediate value [6]. It has been reported that bioreactor productivity, in the production of these types of products, greatly impacts on the product cost [7].

The productivity of biofilm-attached MBR's is determined in large by the biomass growth, and one of the most important factors that influence biomass growth is the availability and transport of nutrients through the bioreactor [8,9]. The momentum transfer of solutes through MBR's has been thoroughly studied, from a theoretical and experimental perspective, for a number of configurations [10-15]. Similarly, the mass transfer has received considerable attention [8,9,16-22]. With the exception of the models developed by Heath and Belfort [17]; Li and Tan [19]; Willaert et al. [22], the mass transfer models were solved using numerical procedures such as finite difference schemes and control volumes. A difficulty in implementing such schemes is the choice of the appropriate technique for a specific MBR system [21], and these techniques are subject to discretization errors and stringent stability criterion. In the models presented by Heath and Belfort [17]; Willaert et al. [22]; Li and Tan [19], the convective-diffusion equation governing mass transfer was solved analytically. These authors, however, neglected the effects of axial diffusion and radial convective flow in their models. Both these assumptions may not be justified in all cases. A number of theoretical and experimental investigations have demonstrated the significance of radial convective flows in improving MBR efficiencies [9,15,21]. In the dead-end ultrafiltration mode, particularly, the assumption of negligible radial convective flow is not justifiable. At axial Peclet numbers (Pe_u) smaller than unity large concentration gradients exist, and under these circumstances ignoring axial diffusion is also not justified.

The current study presents an analytical solution of the convective-diffusion equation, for solute transport trough a single fiber isotropic capillary membrane, in two dimensions. This study will not include the growth kinetics of the microorganism, as conversion is assumed to take place in the shell-side of the MBR; the current analysis is restricted to the lumen-side. The developed model, however, is easily adjustable to account for solute consumption. For comparison with literature models, the first-order limit of the Michaelis-Menten equation will be superimposed on the developed model in the results section.

3.2 Model development

3.2.1 The membrane gradostat reactor

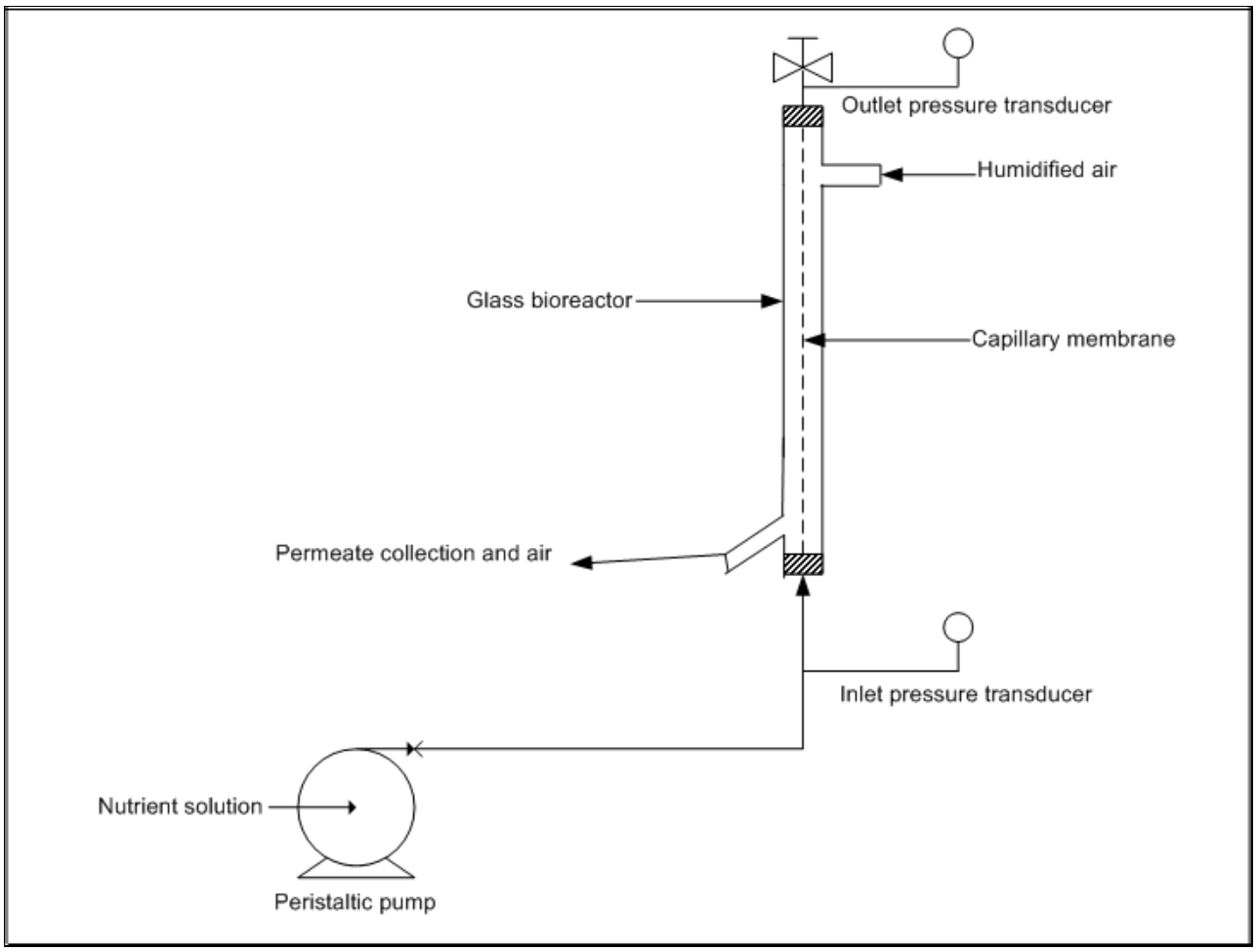

Figure 3.1: A schematic diagram of the single capillary membrane gradostat reactor (MGR).

The models developed in this study are applicable to a hollow-fiber MBR system, consisting of either a single fibre or a bundle of fibres; with nutrient flowing on the lumen-side of the membrane and the micro-organism immobilised either on the lumen-side or on the shell-side.

The notation used, however, is specifically for a single hollow-fiber membrane gradostat reactor (MGR). The construction of the MGR, as patented by Edwards et al. [23], is illustrated schematically in Figure 3.1. It consists of a single hollow-fibre, made of surface modified polysulphone, encased in a glass bioreactor. The membranes are asymmetric and characterized by an internally skinned and externally un-skinned region of microvoids; approximately 0.15mm long and 0.015mm thick. These membranes have inner and outer diameters of approximately 1.395mm and 1.925mm, respectively. The nutrient solution permeates from the lumen-side to the shell-side of the MGR due to the transmembrane pressure gradient. The micro-organism is immobilised on the shell-side of the MGR. Humidified air is supplied on the shell-side, and two pressure transducers are fitted at the inlet and outlet of the MGR as shown in Figure 3.1. A detailed description of the set-up and operation of the MGR is provided in Appendix C.

3.2.2 Model assumptions

The theoretical models to be developed will be based on the following conditions of operation and assumptions: (1) the system is isothermal, meaning the energy equation has been decoupled from the mass and momentum transfer; (2) the flow regime within the membrane lumen is fully developed, laminar, and homogeneous; (3) the physical and transport parameters (e.g. density, viscosity and diffusivity) are constant; (4) in the dense and spongy layers of the membrane matrix the flow is only one dimensional (that is, there are no axial components of the velocity profiles in the membrane matrix); (5) the aspect ratio of the membrane is much smaller than unity. The aspect ratio, φ, is the ratio of the membrane inner radius to the effective membrane length (i.e. R_L/L), and if it is much smaller than unity then normal stress effects are negligible in the momentum transfer analysis.

3.3 Mathematical formulation

The starting point of the analysis is the convective-diffusion equation [24]:

$$\frac{Dc}{Dt} = D_{AB}\nabla^2 c + r_A \tag{3.1}$$

where c is the local substrate concentration; t is time; D_{AB} is the substrate diffusivity, assumed to be constant; and r_A is the rate of substrate production (or consumption), which is a function of the local biofilm density. Eq. (3.1), for steady-state, two-dimensional flow, without reaction, in cylindrical co-ordinates may be written as:

$$u\frac{\partial c}{\partial z} - D_{AB}\frac{\partial^2 c}{\partial z^2} = \frac{D_{AB}}{r}\left(\frac{\partial c}{\partial r} + r\frac{\partial^2 c}{\partial r^2}\right) - v\frac{\partial c}{\partial r} \tag{3.2}$$

It is convenient to express this equation in dimensionless form by introducing the following dimensionless variables:

$$U = \frac{u}{u_0};\quad V = \frac{v}{v_0};\quad C = \frac{c}{c_0};\quad Z = \frac{z}{L};\quad R = \frac{r}{R_1};\quad \varphi = \frac{R_1}{L} \tag{3.3}$$

The expressions of *u* and *v* in Eqn. (3.2) are obtained from the momentum transfer analysis given in Appendix A (Section A.1). Substituting the dimensionless variables in Eq. (3.3) into Eq. (3.2) results in:

$$\varphi Pe_u U\frac{\partial C}{\partial Z} - \varphi^2\frac{\partial^2 C}{\partial Z^2} = \frac{1}{R}\left(\frac{\partial C}{\partial R} + R\frac{\partial^2 C}{\partial R^2}\right) - Pe_v V\frac{\partial C}{\partial R} \tag{3.4}$$

where the axial and radial Peclet numbers ($Pe_{u,v}$) are defined as:

$$Pe_u = \frac{u_0 R_1}{D_{AB}};\quad Pe_v = \frac{v_0 R_1}{D_{AB}} \tag{3.5}$$

The boundary conditions which match the imposed operating conditions of the MBR system are presented in Table 3.1. Boundary condition 1 (B.C.1) corresponds to a uniform inlet substrate concentration; B.C.2 and B.C. 5 corresponds to cylindrical symmetry at the centre of the membrane lumen; B.C.3 corresponds to continuity of the substrate flux at the lumen-matrix interface [17]. The boundary conditions B.C.4-8 are employed in the solution of the velocity profiles given in Appendix A. A cross-section of the MGR illustrating the three regions of the reactor, with the notation used in the model development, is shown in Figure 3.2.

If *U* in Eq. (3.4) is radially-averaged, to become U_{av}, then the L.H.S. of Eq. (3.4) is only a function of *Z* and the R.H.S. only a function of *R*. This can only be true if both the L.H.S and R.H.S. are independent of the variables *R* and *Z*. Eq. (3.4) may therefore be solved by separation of variables to give a solution of the form:

$$C = F(Z)T(R) \tag{3.6}$$

Table 3.1: The boundary conditions of the MBR[1].

B.C.	*R,Z*	*C, U, V, P*	Equation
B.C. 1	$Z=0$	$C=1$	(3.7a)
B.C. 2	$R=0$	$\frac{\partial C}{\partial R}=0 \quad (or\ C=finite)$	(3.7b)
B.C. 3	$R=1$	$\frac{\partial C}{\partial Z}=\frac{2}{\varphi Pe_u}\frac{\partial C}{\partial R}$	(3.7c)
B.C. 4	$R=1$	$U=0$	(3.7d)
B.C. 5	$R=0$	$\frac{\partial U}{\partial R}=0 \quad (or\ U=finite)$	(3.7e)
B.C. 6	$R=0$	$V=0$	(3.7f)
B.C. 7	$R=1$	$V=V_M$	(3.7g)
B.C. 8	$Z=0$	$P=P_0; P'=\varphi a$	(3.7h)

[1]The boundary conditions presented in Godongwana *et al.* (2010) are revised.

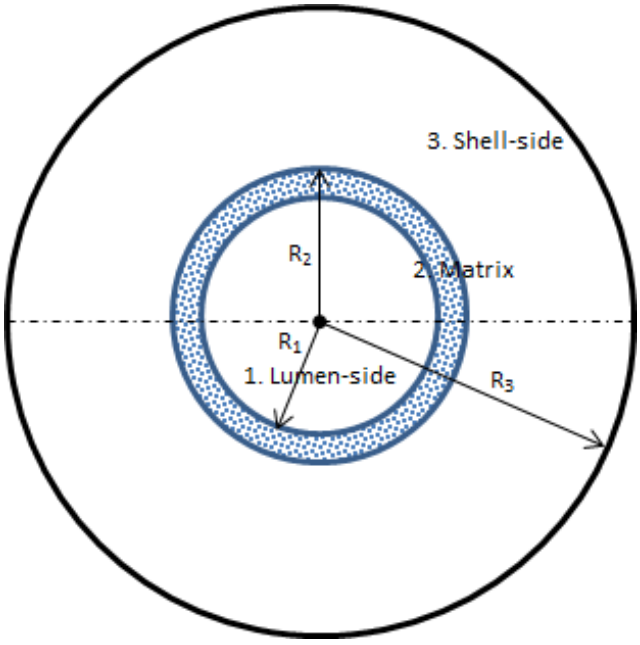

Figure 3.2: A cross-section of the single fibre MGR.

Substituting Eq. (3.6) into (3.4) gives:

$$\frac{\varphi Pe_u U_{av}}{F}\frac{dF}{dZ}-\frac{\varphi^2}{F}\frac{d^2F}{dZ^2}=\frac{1}{RT}\left(\frac{dT}{dR}+R\frac{d^2T}{dR^2}\right)-\frac{Pe_v V}{T}\frac{dT}{dR}=-\lambda^2 \tag{3.8}$$

The equating of the two ordinary differential equations to the arbitrary constant $-\lambda^2$ in Eq. (3.8) is due to the fact that the two ODEs are independent of the variables *R* and *Z*.

3.3.1 Solution of the axial concentration function F(Z)

To solve for the axial function *F*(*Z*) of the substrate concentration profile the ODE on the L.H.S. of Eq. (3.8) is considered:

$$\frac{d^2F}{dZ^2} - \frac{Pe_u U_{av}}{\varphi}\frac{dF}{dZ} - \frac{\lambda^2}{\varphi^2}F = 0 \tag{3.9}$$

The radially-averaged axial velocity U_{av} in Eq. (3.9) is defined as:

$$U_{av} = 2\int_0^1 URdR = -\frac{1}{8}\left(\frac{dP}{dZ} - \frac{Re}{Fr}\right) \tag{3.10}$$

where *Fr* and *Re* are the Froude and Reynolds number, respectively given by:

$$\begin{aligned} Fr &= \frac{u_0^2}{gR_1} \\ Re &= \frac{\rho u_0 R_1}{\mu} \end{aligned} \tag{3.11}$$

where *g* is the gravitational acceleration; ρ is the solution density; and μ the solution dynamic viscosity. The solution of the axial velocity *U* in Eq. (3.10) is given in Appendix A as:

$$U = -\frac{1}{4}(1 - R^2)\left(\frac{dP}{dZ} - \frac{Re}{Fr}\right) \tag{3.12}$$

with the axial pressure gradient given by:

$$\frac{dP}{dZ} = 4\sqrt{\varphi^{-1}\kappa}\beta sinh\left(4\sqrt{\varphi^{-1}\kappa}\right)Z + \varphi a cosh\left(4\sqrt{\varphi^{-1}\kappa}\right)Z \tag{3.13}$$

where *P* is the dimensionless fluid pressure; β is the dimensionless transmembrane pressure; *a* is the dimensionless entrance pressure drop; and κ is the dimensionless membrane hydraulic permeability. The entrance pressure drop *a* in Eq. (3.13) is given by:

$$a = \frac{4\sqrt{\varphi^{-1}\kappa}\beta sinh\left(4\sqrt{\varphi^{-1}\kappa}\right) - ReFr^{-1}(1-f)}{\varphi\left[f - cosh\left(4\sqrt{\varphi^{-1}\kappa}\right)\right]} \tag{3.14}$$

where *f* is the fraction retentate (*f* = 0 for the dead-end mode and *f* = 1 for the closed-shell mode). The membrane hydraulic permeability κ in Eq. (3.13) is much smaller than unity (κ<<1), therefore this equation can be approximated by the following expression:

$$\frac{dP}{dZ} \approx \varphi a + 16\beta\varphi^{-1}\kappa Z \tag{3.15}$$

This approximation makes Eq. (3.9) a confluent hypergeometric type differential equation. This is more evident if the following sequential substitutions are made:

Substitution 1

$$\xi = -\frac{Pe_u}{8\varphi}\left(a\varphi + \frac{16\beta\kappa Z}{\varphi} - \frac{Re}{Fr}\right) \tag{3.16}$$

The substitution in Eq. (3.16) transforms Eq. (3.9) to:

$$\frac{d^2F}{d\xi^2} - A\xi\frac{dF}{d\xi} - \frac{A^2\lambda^2}{\varphi^2}F = 0 \tag{3.17}$$

where

$$A = -\varphi^2(2Pe_u\beta\kappa)^{-1} \tag{3.18}$$

Substitution 2

$$\theta = \frac{1}{2}A\xi^2 \tag{3.19}$$

Transforming Eq. (3.17) to:

$$\theta\frac{d^2F}{d\theta^2} + \left(\frac{1}{2} - \theta\right)\frac{dF}{d\theta} - \frac{A\lambda^2}{2\varphi^2}F = 0 \tag{3.20}$$

Eq. (3.20) is the standard Kummer hypergeometric equation and has two solutions, the Kummer function of the first kind $M(\alpha,\gamma,\theta)$ and the Tricomi function $\Phi(\alpha,\gamma,\theta)$, respectively [25]:

$$M(\alpha,\gamma,\theta) = 1 + \frac{\alpha}{\gamma}\theta + \frac{(\alpha)_2}{(\gamma)_2 2!}\theta^2 + \cdots + \frac{(\alpha)_n}{(\gamma)_n n!}\theta^n \tag{3.21}$$

where

$$(\alpha)_n = \alpha(\alpha+1)(\alpha+2)+\cdots(\alpha+n-1), \quad (\alpha)_0 = 1$$

and

$$\Phi(\alpha,\gamma,\theta) = \frac{\pi}{sin\pi\gamma}\left\{\frac{M(\alpha,\gamma,\theta)}{\Gamma(1+\alpha-\gamma)\Gamma(\gamma)} - \theta^{1-\gamma}\frac{M(1+\alpha-\gamma,2-\gamma,\theta)}{\Gamma(\alpha)\Gamma(2-\gamma)}\right\} \tag{3.22}$$

where $\Gamma(n)$ is the gamma function. Therefore, the solution of Eq. (3.20) becomes:

$$F(\theta) = F_0 M\left(\frac{A\lambda^2}{2\varphi^2},\frac{1}{2},\theta\right) + F_1\Phi\left(\frac{A\lambda^2}{2\varphi^2},\frac{1}{2},\theta\right) \tag{3.23}$$

where F_0 and F_1 are constant coefficients. The Tricomi function approaches infinity as values of θ approach zero [26], therefore, the coefficient F_1 in Eq. (3.23) must be zero for this equation to satisfy Eq. (3.7a). The coefficient F_0 can be arbitrarily put equal to unity without loss of generality. The solution of the axial function of the dimensionless concentration profile, $F(\theta)$, is therefore:

$$F(\theta) = M\left(\frac{A\lambda^2}{2\varphi^2},\frac{1}{2},\theta\right) \tag{3.24}$$

3.3.2 Solution of the radial concentration function T(R)

3.3.2.1 Zero-order approximation

To solve for the radial function $T(R)$ of the substrate concentration profile, the ODE on the R.H.S. of Eq. (3.8) is solved:

$$\frac{d^2T}{dR^2} + \left(\frac{1}{R} - Pe_v V\right)\frac{dT}{dR} + \lambda^2 T = 0 \tag{3.25}$$

The radial velocity V in Eq. (3.25) is given in Appendix A as:

$$V = \varphi\left(\frac{u_0}{v_0}\right)\left[\frac{R}{8}\left(1-\frac{R^2}{2}\right)\right]\frac{d^2P}{dZ^2} \tag{3.26}$$

From the approximation in Eq. (3.15):

$$\frac{d^2P}{dZ^2} \approx 16\beta\varphi^{-1}\kappa, \quad \kappa \ll 1 \tag{3.27}$$

Eq. (3.25) is solved by a regular perturbation technique:

$$T(R) = \sum_{n=0}^{\infty} \kappa^n T_n \tag{3.28}$$

The magnitude of the membrane hydraulic permeability κ is very small; hence validity of the perturbation method is assured. The equations to solve for the zero-order approximation, T_0, of Eq. (3.25) are:

$$\frac{d^2T_0}{dR^2} + \frac{1}{R}\frac{dT_0}{dR} + \lambda^2 T_0 = 0 \tag{3.29}$$

and,

$$T_0(0) - B_1 = 0; \quad \frac{dT_0(0)}{dR} - B_2 = 0 \tag{3.30}$$

Eq. (3.29) is the Bessel equation, and has a standard solution of the form:

$$T_0(R) = B_1 J_0(\lambda R) + B_2 Y_0(\lambda R) \tag{3.31}$$

As R approaches zero in Eq. (3.31), the Webber function Y_0 tends to minus infinity; and therefore, B_2 must be zero for the equation to satisfy B.C.2 at R is equal to zero. Thus,

$$T_0(R) = B_1 J_0(\lambda R) \tag{3.32}$$

There are many positive values of λ that satisfy B.C.3 when the axial function $F(\theta)$ and radial function $T(R)$ are returned for $C(R,Z)$ in Eq. (3.6). This means there are many functions $T_0(R)$ that satisfy Eq. (3.25). The sum of these functions is the most general result:

$$T_0(R) = \sum_{m=1}^{\infty} B_{1m} J_0(\lambda_m R) \tag{3.33}$$

The solution for the coefficient B_{1m} in Eq. (3.33) is given in Appendix A (Section A.2); the eigenvalues λ_m are derived from B.C.3 and are presented in Table 4.1 (Chapter 4) and for brevity will not be repeated here.

3.3.2.2 First-order and second order approximations

The equations to solve for the first-order approximation, T_1, of Eq. (3.25) are:

$$\frac{d^2T_1}{dR^2} + \frac{1}{R}\frac{dT_1}{dR} + \lambda_m^2 T_1 = \delta\left[R\left(1 - \frac{R^2}{2}\right)\right]\frac{dJ_0(\lambda_m R)}{dR} \tag{3.34}$$

and,

$$T_1(0) = 0; \quad \frac{dT_1(0)}{dR} = 0 \tag{3.35}$$

where

$$\delta = 2Pe_u\beta\sum_{m=1}^{\infty} B_{1m} \tag{3.36}$$

Eq. (3.34) is evaluated by making use of the following identity of Bessel functions [25]:

$$\frac{dJ_0(\lambda_m R)}{dR} = -\lambda_m J_1(\lambda_m R) \tag{3.37}$$

Substituting Eq. (3.37) into Eq. (3.34) results in the following inhomogeneous O.D.E:

$$\frac{d^2T_1}{dR^2} + \frac{1}{R}\frac{dT_1}{dR} + \lambda_m^2 T_1 = -\delta\lambda_m\left[R\left(1 - \frac{R^2}{2}\right)\right]J_1(\lambda_m R) \tag{3.38}$$

Eq. (3.38) is further simplified by making use of the following substitution:

$$x = \lambda_m R \tag{3.39}$$

This substitution simplifies Eq. (3.38) to:

$$x\frac{d^2T_1}{dx^2} + \frac{dT_1}{dx} + xT_1 = -\frac{\delta x^2}{\lambda_m^2}\left(1 - \frac{x^2}{2\lambda_m^2}\right)J_1(x) \tag{3.40}$$

Some mathematical architecture is required to solve Eq. (3.40) and this is described in Appendix A (Section A.3). The solution of this equation is given in Section A.4 as:

$$T_1(x) = i_3\left[\frac{x^2 J_2(x)}{3!!} + i_1\frac{x^3 J_3(x)}{5!!} + i_2\frac{x^4 J_4(x)}{7!!}\right] \tag{3.41}$$

where

$$i_1 = -\frac{20}{3\lambda_m^2}, \quad i_2 = \frac{35}{4\lambda_m^2}, \quad i_3 = -\frac{3\delta}{4\lambda_m^2} \tag{3.42}$$

The differential equations to solve for the second-order approximation, T_2, of Eq. (3.25) are:

$$x\frac{d^2T_2}{dx^2} + \frac{dT_2}{dx} + xT_2 = -\frac{\delta x^2}{\lambda_m^2}\left(1 - \frac{x^2}{2\lambda_m^2}\right)T_1'(x) \tag{3.43}$$

and,

$$T_2(0) = 0; \quad \frac{dT_2(0)}{dx} = 0 \tag{3.44}$$

The mathematical architecture required for the solution of these equations is also given in Section A.3, and the solution is given in Section A.5:

$$\begin{aligned} T_2(x) = \frac{3\delta^2}{2\lambda_m^6}\Bigg\{&\frac{20}{3}\lambda_m^2\frac{x^3 J_3(x)}{5!!} - \left[105 - \frac{7}{3}\lambda_m^2(6i_1 - 5)\right]\frac{x^4 J_4(x)}{7!!} \\ &+ \frac{9}{10}[7(60 - 48i_1) + 2\lambda_m^2(8i_2 - 7i_1)]\frac{x^5 J_5(x)}{9!!} \\ &- \frac{9\cdot 11}{12}[(35 - 112i_1 + 80i_2) + 2\lambda_m^2 i_2]\frac{x^6 J_6(x)}{11!!} \\ &- \frac{9\cdot 11\cdot 13}{14}(7i_1 - 20i_2)\frac{x^7 J_7(x)}{13!!} - \frac{9\cdot 11\cdot 13\cdot 15}{16}i_2\frac{x^8 J_8(x)}{15!!}\Bigg\} \end{aligned} \tag{3.45}$$

Substituting Eqs. (3.24) and (3.28) into Eq. (3.6), the solution of the dimensionless luminal concentration profile is therefore:

$$C(\theta, x) = \sum_{m=1}^{\infty}\sum_{n=0}^{N} F_m(\theta)T_n(x)\kappa^n \tag{3.46}$$

The perturbation solution is only extended up to second-order approximation; therefore Eq. (3.46) reduces to:

$$C(\theta, R) = \sum_{m=1}^{\infty} F_m(\theta)[T_0(\lambda_m R)\kappa^0 + T_1(\lambda_m R)\kappa^1 + T_2(\lambda_m R)\kappa^2] \tag{3.47}$$

3.4 Results

The small diameters of the capillary membranes used in the construction of the MBR's render it a very difficult task to validate the accuracy of the developed models experimentally, and thus the predictive power of the models will be compared to currently available results for similar MBR systems; in particular the model developed by Heath and Belfort [17]. The approach used by these authors in solving the convective-diffusion equation was to assume a constant cross sectional concentration profile in the membrane lumen and matrix regions, and negligible membrane resistance to mass transfer. The lumen side axial concentration profile was then correlated to the shell (or annulus) by a mass flux balance. This approach is equivalent to assuming that the substrate consumption takes place in the lumen-side of the MBR; in which case the convective-diffusion equation given in Eq. (3.1) becomes:

$$u\frac{\partial c}{\partial z} - D_{AB}\frac{\partial^2 c}{\partial z^2} = \frac{D_{AB}}{r}\left(\frac{\partial c}{\partial r} + r\frac{\partial^2 c}{\partial r^2}\right) - v\frac{\partial c}{\partial r} - \frac{V_M c}{K_m + c} \tag{3.48}$$

where V_M is the maximum rate of reaction and K_m is the Michaelis constant. This equation is made dimensionless by introducing the variables in Eqs. (3.3) and (3.5), and two additional variables the Thiele modulus ϕ and the dimensionless Michaelis constant K_m^*, respectively:

$$\phi = \sqrt{\frac{V_M R_1^2}{c_0 D_{AB}}}, \quad K_m^* = \frac{K_m}{c_0} \tag{3.49}$$

Eq. (3.48) then becomes:

$$\varphi Pe_u U\frac{\partial C}{\partial Z} - \varphi^2\frac{\partial^2 C}{\partial Z^2} = \frac{1}{R}\left(\frac{\partial C}{\partial R} + R\frac{\partial^2 C}{\partial R^2}\right) - Pe_v V\frac{\partial C}{\partial R} - \frac{\phi^2 C}{K_m^* + C} \tag{3.50}$$

Assuming the first-order limit of the Michaelis-Menten equation (i.e. $K_m^* >> C$) the solution of Eq. (3.50) takes the same general approach as that of Eq. (3.4). The solution of this equation is identical to Eq. (3.47) with an adjustment of the axial function $F_m(\theta)$ and the coefficient of the perturbation solution B_{1m} to account for the reaction rate:

$$C(\theta, R) = \sum_{m=1}^{\infty} \tilde{F}_m(\theta)[T_0(\lambda_m R)\kappa^0 + T_1(\lambda_m R)\kappa^1 + T_2(\lambda_m R)\kappa^2] \tag{3.51}$$

Table 3.2: Parameter values used to determine the concentration profile [17].

Model parameter	Symbol	Unit	Basic measured value
Membrane hydraulic permeability[a]	k_m	m/Pas	3.82×10^{-11}
Fraction retentate[a]	f		0.80
Membrane inner radius	R_L	m	1.30×10^{-4}
Annulus radius	r_3	m	4.08×10^{-4}
Effective membrane length	L	m	5.7×10^{-2}
Lumen-side entrance axial velocity	u_0	m s^{-1}	1.67×10^{-3}
Permeation velocity	v_0	m s^{-1}	3.82×10^{-7}
Lumen-side inlet fluid pressure[a]	p_0	Pa	106 325
Shell-side fluid pressure[a]	p_S	Pa	101 325
Glucose diffusivity	D_{AB}	m^2 s	1.0×10^{-10}
solution density[a]	ρ	kg m^{-3}	998
solution viscosity[a]	μ	Pas	9.7×10^{-4}
Glucose inlet concentration	c_0	g dm^{-3}	2.00
Kinetic constants	V_M/K_m	s^{-1}	1.00

[a] Typical operational values are used

where

$$\tilde{F}_m(\theta) = M\left\{\frac{A(\lambda_m^2 K_m^* + \phi^2)}{2\varphi^2 K_m^*}, \frac{1}{2}, \theta\right\} \tag{3.52}$$

and

$$\tilde{B}_m = \frac{2}{\lambda_m M\left[\frac{A(\lambda_m^2 K_m^* + \phi^2)}{2\varphi^2 K_m^*}, \frac{1}{2}, \theta_0\right]}\left[\frac{J_1(\lambda_m)}{J_0^2(\lambda_m) + J_1^2(\lambda_m)}\right] \tag{3.53}$$

The input variables used in validating Eq. (3.51) are obtained from Heath and Belfort [17] and are given in Table 3.2. The values of the membrane hydraulic permeability (k_m), the fraction retentate (f), the lumen-side inlet fluid pressure (p_0), the shell-side fluid pressure (p_S), the solution density (ρ) and viscosity (μ) are not specified by these authors; therefore, typical operational values of these parameters will be used. A transmembrane (TMP) pressure of 5kPa is assumed across the MBR, and the solution properties are assumed to be those of water at 30°C.

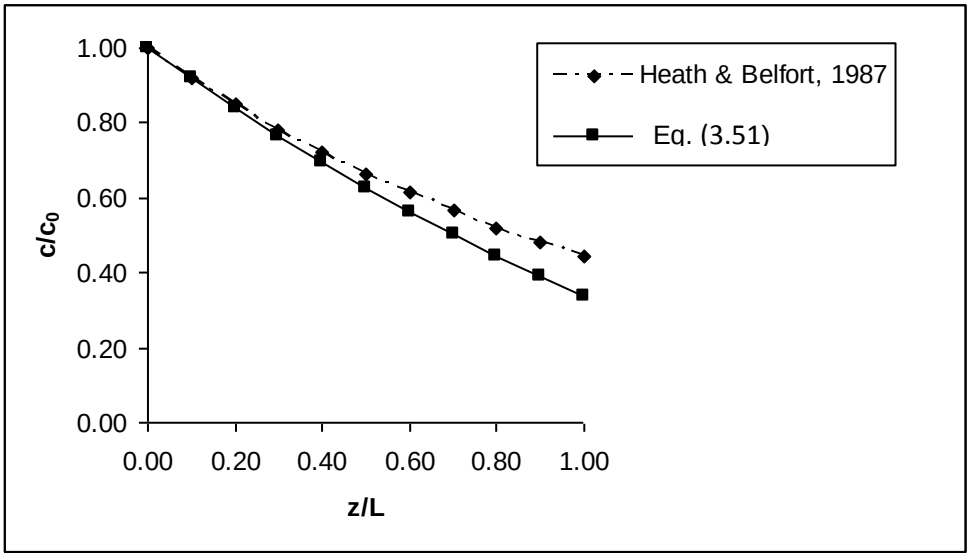

Figure 3.3: A comparison of the concentration profiles resulting from Eq. (3.51) with Heath and Belfort [17] assuming a first-order limit for substrate consumption (at *R* = 0).

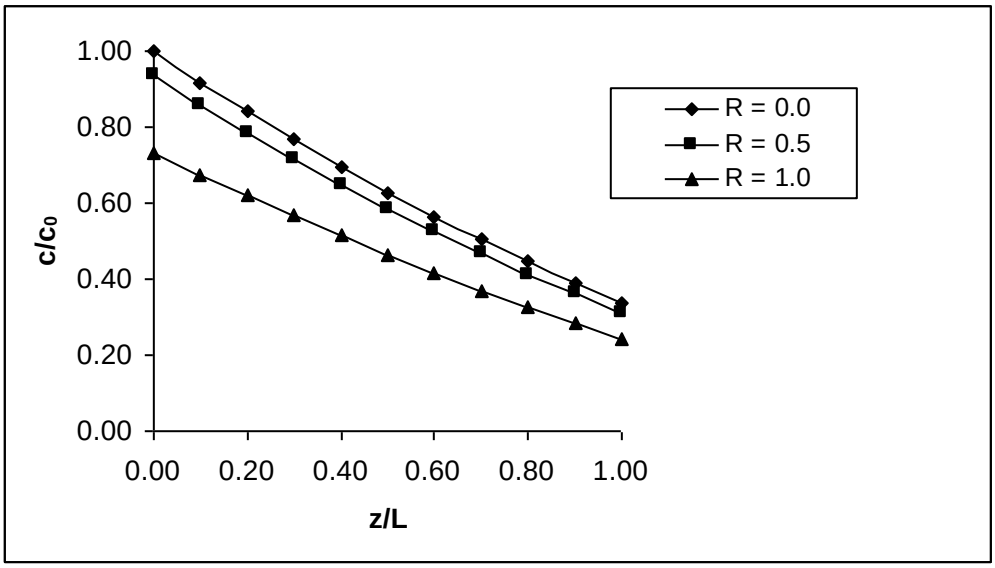

Figure 3.4: Substrate concentration profiles assuming a first-order limit for substrate consumption at different radial positions.

In Figure 3.3 it can be seen that Eq. (3.51) compares satisfactorily with the model of Heath and Belfort [17] for the parameter values listed in Table 3.2, with a standard deviation of 0.048. The significant difference is that the axial concentration gradient is a function of the radial position in Eq. (3.51), while in the model of Heath and Belfort [17] the gradient is not influenced by radial position. At the centre of the MBR (*R* = 0) Eq. (3.51) predicts a 66% decrease in the axial concentration when the applied TMP is 5kPa, and a 76% decrease at the membrane wall (*R* = 1) as shown in Figure 3.4. The model of Heath and Belfort [17] predicts a 56% decrease for all

values of R for the corresponding conditions. It is important to note, however, that only the resulting trends from the two models can be compared, since Eq. (3.51) requires a more detailed description of the MBR system than that required for the model of Heath and Belfort [17].

3.5 Conclusion

A thorough analytical mathematical model for substrate concentration profiles in the lumen of a hollow fiber MBR was developed. The model was based on the solution of the convective-diffusion equation in dimensionless form. The model allows evaluation of the influence of the general operating parameters of a MBR on the concentration profiles. These parameters are the fraction retentate (f); the membrane hydraulic permeability (κ); the axial and radial Peclet numbers ($Pe_{u,v}$); the Thiele modulus (ϕ); the fluid properties; and the dimensions of the MBR. The developed model can be further used to evaluate reactor performance from basic principles, since it allows analytical evaluation of performance parameters (e.g the performance index and the effectiveness factor).

3.6 Summary

In this chapter an analytical approach for solving the mass balance equation with and without reaction was presented. The underlying philosophy was to transform the non-linear partial differential equations into standard forms with known solutions. Applying this principle, the differential mass balance in the lumen was separated into the Bessel equation and the confluent hypergeometric equation (Kummer equation). Both these equations have known solutions. The non-linear elliptic equation was shown to be only amenable to analytical evaluation when assuming zero-order or first-order kinetics. This restriction greatly limited the range of applicability of the model, hence in Chapter 4 a finite difference scheme was presented for the lumen concentration profile when the reaction kinetics were non-linear.

The concentration profiles developed from this chapter were used as a basis for the analysis of bioreactor performance in Chapter 5.

Nomenclature

a	dimensionless entrance pressure drop
B_n	constants of integration of Bessel's equation, n = 1, 2
c	substrate concentration (g dm^{-3})
c_0	substrate feed concentration (g dm^{-3})
$C = c/c_0$	dimensionless substrate concentration
D_{AB}	substrate diffusivity (m^2 s^{-1})
$f = u_1/u_0$	fraction retentate
F_n	coefficients of the solution of Kummer's confluent hypergeometric equation, n = 1, 2
$Fr = u_0^2/(gR_L)$	Froude number
$F(Z)$	dimensionless axial concentration function
g	gravitational acceleration (m s^{-2})
$g(s)$	Laplace transform of the first-order approximation of the function $T(x)$
$h(s)$	Laplace transform of the second-order approximation of the function $T(x)$
i_n	constants in the first and second-order approximations of the function $T(x)$, n = 1, 2, 3
$J_n(\lambda)$	Bessel function of order n of the first kind
k_a	mass transfer coefficient (m s^{-1})
k_m	membrane hydraulic permeability (m Pa^{-1} s^{-1})
K_m	Michaelis constant (g dm^{-3})
$K_m^* = K_m/c_0$	dimensionless Michaelis constant
L	membrane effective length (m)
$M(\alpha,\gamma,\theta)$	Kummer function of the first kind
p	fluid pressure (Pa)
$P = pR_L^2/(\mu u_0 L)$	dimensionless fluid pressure
$Pe_u = u_0 R_L/D_{AB}$	axial Peclet number
$Pe_v = v_0 R_L/D_{AB}$	radial Peclet number
r_A	rate of substrate production/consumption (g dm^{-3} s^{-1})
r	radial spatial coordinate (m)
$R = r/R_L$	dimensionless radial spatial coordinate
R_L	membrane lumen radius (m)
$Re = \rho u_0 R_L/\mu$	Reynolds number
t	time (s)

$T(R)$	dimensionless radial concentration function
u	axial velocity (m s^{-1})
u_0	feed axial velocity (m s^{-1})
$U = u/u_0$	dimensionless axial velocity
v	radial velocity (m s^{-1})
$v_0 = k_m(p_0 - p_S)$	permeation velocity (m s^{-1})
$V = v/v_0$	dimensionless radial velocity
V_M	maximum rate of reaction (g dm^{-3} s^{-1})
$x = \lambda_m R$	substitution variable
$Y_n(\lambda)$	Bessel function of order n of the second kind
z	axial spatial coordinate (m)
$Z = z/L$	dimensionless axial spatial coordinate

Greek letters

α	first parameter in the Kummer functions of the first and second kind
$\beta = P_0 - P_S$	dimensionless transmembrane pressure
δ	lumped parameter in Eq. (41)
ε	membrane porosity
ϕ	Thiele modulus
$\Phi(\alpha,\gamma,\theta)$	Tricomi function/Kummer function of the second kind
γ	second parameter in the Kummer functions of the first and second kind
$\Gamma(n)$	gamma function, n = 1, 2, …
$\varphi = R_L/L$	aspect ratio
$\kappa = \mu k_m L/R_L^2$	dimensionless membrane hydraulic permeability
λ_m	eigen values, m = 1, 2, …
μ	solution dynamic viscosity (Pa s)
θ	substitution variable
ρ	solution density (kg m^{-3})
$\tau = tu_0/R_L$	dimensionless time
ξ	axial gradient/driving force of substrate concentration profile

Subscripts

0	membrane entrance
1	membrane exit
S	shell-side of the MBR

Acknowledgements

The authors would like to thank the Deutscher Akademischer Austausch Dienst (DAAD) for financial support. Dr. Aletta van der Merwe for her contribution in validating some of the mathematical principles.

References

[1] Leukes, W.D., Development and characterisation of a membrane gradostat bioreactor for the bioremediation of aromatic pollutants using white rot fungi, PhD thesis, Rhodes University, Grahamstown (1999).

[2] S.K.O. Ntwampe, M.S. Sheldon, H. Volshenk, The Membrane Gradostat Reactor: Secondary metabolite production, bioremediation and commercial potential. *African Journal of Biotechnology* 6, 1164-1170 (2007).

[3] B. Godongwana, D. De Jager, M. Sheldon, W. Edwards, The effect of *Streptomyces coelicolor* development on the hydrodynamics of a vertically orientated capillary membrane gradostat reactor. *Journal of Membrane Science* 333, 79-87 (2009).

[4] G. Amin, Continuous production of glutamic acid in a vertical rotating immobilized cell reactor of the bacterium *Corynebacterium glutamicum*. *Bioresource Technology* 47, 113-119 (1994).

[5] D.S. Inloes, D.P. Taylor , S.N. Cohen, A.S. Michaels, C.R. Robertson, Ethanol production by *Saccharomyces cerevisiae* immobilized in hollow-fiber membrane bioreactors. *Applied and Environmental Microbiology* 46, 264-278 (1983).

[6] G. Belfort, Membranes and bioreactors: a technical challenge in biotechnology. *Biotechnology and Bioengineering* 33, 1047-1066 (1989).

[7] J.C. Van Suijdam, Trends in bioreactor research, in *Proceedings of the 4th European Congress on Biotechnology,* Vol 3 (O.M. Neijssel, R.R. van der Meer, K.Ch. A.M. Luyben, Eds), Elsevier, Amsterdam (1987).

[8] V. Calabro, S. Curcio, G. Iorio, A theoretical analysis of transport phenomena in a hollow fiber membrane bioreactor with immobilized biocatalyst. *Journal of Membrane Science* 206, 217-241 (2002).

[9] S. Curcio, V. Calabro, G. Iorio, A theoretical and experimental analysis of a membrane bioreactor performance in recycle configuration. *Journal of Membrane Science* 273, 129-142 (2006).

[10] A. Apelblat, A. Katzir-Katchalsky, A. Silberberg, A mathematical analysis of capillary-tissue fluid exchange. *Biorheology* 11, 1-49 (1974).

[11] W.J. Bruining, A general description of flows and pressures in hollow fiber membrane modules. *Chemical Engineering Science* 44, 1441-1447 (1989).

[12] K. Damak, A. Ayadi., B. Zeghmati, P. Schmitz, A new Navier-Stokes and Darcy's law combined model of fluid flow in crossflow filtration tubular membranes. *Desalination* 161, 67-77 (2004).

[13] B. Godongwana, M.S. Sheldon, D.M. Solomons, Momentum transfer inside a vertically orientated capillary membrane bioreactor. *Journal of Membrane Science* 303, 86-99 (2007).

[14] L.J. Kelsey, M.R. Pillarella, A.L. Zydney, Theoretical analysis of convective flow profiles in a hollow fiber membrane bioreactor. *Chemical Engineering Science* 45, 3211–3220 (1990).

[15] J.P. Thakaran, P.C. Chau, Operation and pressure distribution of immobilised cell hollow fiber bioreactors. *Biotechnology and Bioengineering* 28, 1064–1071 (1986.).

[16] N.S. Abdullah, D.R. Jones, D.B. Das, Nutrient transport in bioreactors for bone tissue growth: why do hollow fibre membrane bioreactors work? *Chemical Engineering Science* 64, 109-125 (2009).

[17] C. Heath, G. Belfort, Immobilization of suspended mammalian cells: analysis of hollow fiber and microcapsule bioreactors. *Advances in Biochemical Engineering* 34, 1-31 (1987).

[18] M. Labecki, B.D. Bowen, J.M. Piret, Two-dimensional analysis of protein transport in the extracapillary space of hollow-fibre bioreactors. *Chemical Engineering Science* 51, 4197-4213 (1996).

[19] K. Li, X. Tan, Mass transfer and chemical reaction in hollow-fiber membrane reactors. *American Institute of Chemical Engineers Journal* 47, 427-435 (2001).

[20] A.Y. Patkar, J. Koska, D.G. Taylor, B.D. Bowen, J.M. Piret, Protein transport in ultrafiltration hollow-fiber bioreactors. *American Institute of Chemical Engineers Journal* 41, 415-425 (1995).

[21] P.M. Salmon, S.B. Libicki, C.R. Robertson, A theoretical investigation of convective transport in the hollow-fiber reactor. *Chemical Engineering Communications* 66, 221-248 (1988).

[22] R. Willaert, A. Smets, L. De Vuyst, Mass transfer limitations in diffusion-limited isotropic hollow fiber bioreactors. *Biotechnology Techniques* 13, 317-323 (1999).

[23] W. Edwards, W.D. Leukes, S.J. Fraser, High throughput bioprocess apparatus. SA patent WO 2007/116266 A1 (2007).

[24] R.B. Bird, W.E. Stewart, E.N. Lightfoot, *Transport phenomena*, third ed. John Wiley, New York (2002).

[25] M. Abramowitz, I.A. Stegun, (Eds), *Handbook of mathematical functions*. Dover, New York (1965).

[26] G.N. Georgiev, M.N. Georgieva-Grosse, The Kummer confluent hypergeometric function and some of its applications in the theory of azimuthally magnetized circular ferrite

waveguides. *Journal of Telecommunications and Information Technology,* 3: 112-128 (2005).

CHAPTER 4: RESULTS

Solute Transport Through a Membrane Bioreactor (with Non-Linear Kinetics)

Published as: **Godongwana, B., Solomons, D.M. & Sheldon, M.S.** 2015. A finite difference solution of solute transport through a membrane bioreactor. *Mathematical Problems in Engineering,* vol. 2015, 1-8.

(**Godongwana, B., Solomons, D.M. & Sheldon, M.S.** A theoretical analysis of solute transport through a membrane bioreactor. *Proceedings of the 2nd International Conference on Fluid Flow, Heat and Mass Transfer.* Ottawa, Ontario, Canada, May 2015. Paper No. 147) .

4. SOLUTE TRANSPORT THROUGH A MEMBRANE BIOREACTOR (WITH NON-LINEAR KINETICS)

Abstract

The current paper presents a theoretical analysis of the transport of solutes through a fixed-film membrane bioreactor (MBR), immobilised with an active biocatalyst. The dimensionless convection-diffusion equation with variable coefficients was solved analytically and numerically, for concentration profiles of the solutes through the MBR. The analytical solution makes use of regular perturbation, and accounts for radial-convective flow as well as axial diffusion of the substrate specie. The Michaelis-Menten (or Monod) rate equation was assumed for the sink term, and the perturbation was extended up to second-order. In the analytical solution only the first-order limit of the Michaelis-Menten equation was considered, hence the linearized equation was solved. In the numerical solution, however, this restriction was lifted. The solution of the non-linear, elliptic, partial differential equation was based on an implicit finite-difference method (FDM). An upwind scheme was employed for numerical stability. The resulting algebraic equations were solved simultaneously using the multi-variate Newton-Raphson iteration method. The solution allows for the evaluation of the effect on the concentration profiles of (i) the radial and axial convective velocity, (ii) the convective mass transfer rates, (iii) the reaction rates, (iv) the fraction retentate, and (v) the aspect ratio.

Keywords: Membrane bioreactor; Convection-diffusion equation; Implicit finite-difference; Upwind scheme; Multivariate Newton-Raphson; Regular perturbation.

4.1 Introduction

Membrane bioreactors (MBRs) are finding increasing use in the production of primary and secondary metabolites such as amino acids, antibiotics, anticancer drugs, tissue cells etc. [1]–[3]. This technology is favoured by recent trends towards environmentally-friendly technologies, particularly because MBRs do not require additives, function at moderate operating conditions, and reduce by-product formation [1]. The efficiency of MBRs is dependent mainly on the transport of solutes through the bioreactor, and this is influenced by biochemical, geometric, and hydrodynamic parameters [2], [4]. This paper considers the numerical solution of the convection-diffusion equation, for solute transport through a fixed-film MBR. This analysis is important for simulation of the performance (i.e. efficiency and effectiveness) of the bioreactor. The governing equation for mass transport of solutes through the bioreactor is the convection-diffusion equation, with Monod kinetics [5]:

$$u\frac{\partial c}{\partial z} + v\frac{\partial c}{\partial r} = D_{AB}\left[\frac{1}{r}\frac{\partial}{\partial r}\left(r\frac{\partial c}{\partial r}\right) + \frac{\partial^2 c}{\partial z^2}\right] - \frac{V_M c}{K_m + c} \tag{4.1}$$

where c is the local substrate concentration, u and v are the axial and radial velocity components respectively, D_{AB} is the substrate diffusion coefficient, V_M is the maximum rate of reaction, and K_m is the saturation (or Michaelis) constant. Eq. (4.1) is made dimensionless by introducing the following variables:

$$\begin{gathered} U = \frac{u}{u_0};\quad V = \frac{v}{v_0};\quad C = \frac{c}{c_0};\quad \phi = \sqrt{\frac{V_M R_1^2}{c_0 D_{AB}}} \\ K_m^* = \frac{K_m}{c_0};\quad Z = \frac{z}{L};\quad R = \frac{r}{R_1};\quad \varphi = \frac{R_1}{L} \end{gathered} \tag{4.2}$$

Eq. (4.1) then becomes:

$$\varphi Pe_u U\frac{\partial C}{\partial Z} + Pe_v V\frac{\partial C}{\partial R} = \left[\frac{1}{R}\frac{\partial}{\partial R}\left(R\frac{\partial C}{\partial R}\right) + \varphi^2\frac{\partial^2 C}{\partial Z^2}\right] - \frac{\phi^2 C}{K_m^* + C} \tag{4.3}$$

Where the axial and radial Peclet numbers $\left(Pe_{u,v}\right)$ are respectively defined as:

$$Pe_u = \frac{u_0 R_1}{D_{AB}};\quad Pe_v = \frac{v_0 R_1}{D_{AB}} \tag{4.4}$$

The velocity profiles, *U* and *V,* in Eq. (4.3) are solutions of the *z* and *r*-components of the Navier-Stokes equations, respectively [6]:

$$U = -\frac{1}{4}(1 - R^2)\frac{dP}{dZ} \tag{4.5}$$

and

$$V = \varphi\left(\frac{u_0}{v_0}\right)\left[\frac{R}{8}\left(1 - \frac{R^2}{2}\right)\right]\frac{d^2P}{dZ^2} \tag{4.6}$$

Where *P* is the dimensionless fluid pressure, which is a function of the membrane hydraulic permeability κ. When the membrane hydraulic permeability κ is much smaller than unity, Eq (4.3) reduces to:

$$U^*\frac{\partial C}{\partial Z} + Pe_u\kappa\beta(2R - R^3)\frac{\partial C}{\partial R} = \left[\frac{1}{R}\frac{\partial}{\partial R}\left(R\frac{\partial C}{\partial R}\right) + \varphi^2\frac{\partial^2 C}{\partial Z^2}\right] - \frac{\phi^2 C}{K_m^* + C} \tag{4.7}$$

Where

$$U^* = -4Pe_u\kappa\beta\left[\frac{1}{(f-1)} + Z\right](1 - R^2)\ , \qquad f \neq 1 \tag{4.8}$$

The fraction retentate, *f*, is defined as the ratio of the outlet to the inlet axial velocity (*f* = 0 for the dead-end mode and *f* ~ 1 for the closed-shell mode), β is the dimensionless transmembrane pressure. The corresponding boundary conditions are:

$$\begin{aligned} B.C.1 \quad at\ Z = 0 \quad \forall R \quad C = 1 \\ B.C.2 \quad at\ R = 0 \quad \forall Z \quad \frac{\partial C}{\partial R} = 0 \\ B.C.3 \quad at\ R = 1 \quad \forall Z \quad \frac{\partial C}{\partial Z} = \frac{2}{\varphi Pe_u}\frac{\partial C}{\partial R} \end{aligned} \tag{4.9}$$

Boundary condition 1 (B.C.1) corresponds to a uniform inlet substrate concentration; B.C.2 corresponds to cylindrical symmetry at the center of the membrane lumen; B.C. 3 corresponds to continuity of the substrate flux at the lumen-matrix interface [7]. The solution of Eq. (4.7) is based on the following general assumptions: (i) the system is isothermal; (ii) the flow regime is laminar and fully developed; (iii) the fluid is Newtonian, homogenous, and has constant physical and transport properties (iv) the membrane hydraulic permeability is constant.

4.2 Analytical Models

The Graetz Problem [8] is one of the oldest forced-convection problems, describing the steady-temperature distribution and rate of heat transfer in tube flow. The evaluation of Eq. (4.7) for concentration profiles in a tubular reactor is mathematical analogous to the Graetz problem [5], [9]. In the original Graetz problem however there is no reaction (or source) term, axial diffusion and radial convection is ignored. The assumption of negligible axial diffusion and radial convection is common in the majority of analytical models currently in use [7], [10]–[12]. Radial convective flows have been shown to significantly improve MBR efficiency [4], [13]–[15]. In the dead-end ultrafiltration mode, particularly, the assumption of negligible radial convective flow is not justifiable. Nagy [15] investigated the effect of radial convective flows (Pe_v) on the mass transfer rates of solutes through a biocatalytic membrane layer. Analytical solutions of Eq. (4.7) for the zero-order and first-order limits of the Monod equation were provided. This analysis, however, was restricted to the matrix/fiber region of the membrane and hence the radial velocity was assumed constant, and axial convective and diffusive flows were ignored. At axial Peclet numbers (Pe_u) smaller than unity large concentration gradients exist in the membrane lumen, and ignoring axial diffusion is also not justified [6], [7].

The model proposed by Godongwana *et al.*[6] follows the approach suggested by Davis [9], *i.e*. writing the solution of Eq. (4.7) in terms of known functions. The model accounts for radial convective flow and axial diffusion, for the limiting case of first-order kinetics. In that model, Eq. (4.7) was solved by separation of variables and regular perturbation, resulting in the asymptotic expansion:

$$C(\theta, x) = \sum_{m=1}^{\infty} \sum_{n=0}^{N} B_m F_m(\theta) T_n(x) \kappa^n \tag{4.10}$$

Making use of the following change of variables:

$$\xi = -\frac{2Pe_u \kappa \beta}{\varphi^2}\left[\frac{1}{(f-1)} + Z\right] \tag{4.11}$$

$$\theta = -\left(\frac{\varphi^2}{4Pe_u \kappa \beta}\right)\xi^2 \tag{4.12}$$

$$x = \lambda_m R \tag{4.13}$$

Where $F(\theta)$ in Eq. (4.10) is represented by the Kummer function [16]:

$$F_m(\theta) = M\left[\frac{-(\lambda_m^2 + \phi^2/K_m^*)}{4Pe_u\kappa\beta}, \frac{1}{2}, \theta\right] \tag{4.14}$$

The zero-order and first-order approximations of *T(x)* in Eq. (4.10) are, respectively:

$$T_0(x) = J_0(x) \tag{4.15}$$

and

$$T_1(x) = \sigma_1\left[\frac{(x)^2 J_2(x)}{3!!} + \sigma_2\frac{(x)^3 J_3(x)}{5!!} + \sigma_3\frac{(x)^4 J_4(x)}{7!!}\right] \tag{4.16}$$

where λ_m are the eigenvalues, J_n is the Bessel function of the first kind of order *n* [16].

$$\sigma_1 = -\frac{3Pe_u\beta}{2\lambda_m^2}, \quad \sigma_2 = -\frac{20}{3\lambda_m^2}, \quad and \quad \sigma_3 = \frac{35}{4\lambda_m^2} \tag{4.17}$$

The eigenvalues are obtained from B.C.3 of Eq. (4.9), and are roots of the equation:

$$\begin{aligned}\frac{\varphi\xi}{2\kappa\beta}(\lambda_m^2 + \phi^2/K_m^*)M\left[\frac{-(\lambda_m^2 + \phi^2/K_m^*)}{4Pe_u\kappa\beta} + 1, \frac{3}{2}, \theta\right] \\ = 2\lambda_m\frac{J_1(\lambda)}{J_0(\lambda)}M\left[\frac{-(\lambda_m^2 + \phi^2/K_m^*)}{4Pe_u\kappa\beta}, \frac{1}{2}, \theta\right]\end{aligned} \tag{4.18}$$

Table 4.1: Positive roots of Eq.(4.18), *f* = 0.

	Z = 0	*Z = 0.2*	*Z = 0.4*	*Z = 0.6*	*Z = 0.8*	*Z = 1.0*
λ_1	2.142	2.191	2.242	2.294	2.349	3.832
λ_2	4.968	5.060	5.162	5.273	5.394	7.016
λ_3	7.891	8.000	8.131	8.285	8.462	10.173
λ_4	10.885	10.997	11.140	11.320	11.541	13.324
λ_5	13.929	14.037	14.181	14.376	14.630	16.471
λ_6	17.004	17.107	17.249	17.450	17.728	19.616
λ_7	20.101	20.198	20.337	20.541	20.835	22.760
λ_8	23.211	23.305	23.440	23.644	23.949	25.904
λ_9	26.331	26.422	26.554	26.757	27.070	29.047
λ_{10}	29.458	29.547	29.677	29.88	30.197	32.190

Table 4.2: Positive roots of Eq.(4.18), *f* = 0.8.

	Z = 0	*Z = 0.2*	*Z = 0.4*	*Z = 0.6*	*Z = 0.8*	*Z = 1.0*
λ_1	1.518	1.538	1.559	1.581	1.604	1.628
λ_2	4.234	4.248	4.264	4.280	4.298	4.318
λ_3	7.256	7.265	7.275	7.286	7.299	7.312
λ_4	10.347	10.354	10.362	10.370	10.379	10.389
λ_5	13.463	13.468	13.475	13.481	13.489	13.497
λ_6	16.589	16.594	16.599	16.605	16.611	16.618
λ_7	19.721	19.726	19.730	19.736	19.741	19.748
λ_8	22.857	22.861	22.865	22.870	22.875	22.881
λ_9	25.995	25.999	26.003	26.007	26.012	26.017
λ_{10}	29.134	29.138	29.142	29.146	29.151	29.156

The first ten eigenvalues at different axial positions are listed in Table 4.1 and Table 4.2 for *f* = 0 and *f* = 0.8, respectively. The coefficient B_m is obtained by imposing the inlet condition B.C.1 of Eq. (4.9) and employing Lommel integrals to give [6]:

$$B_m = \frac{2}{\lambda_m M\left[\frac{-(\lambda_m^2 + \phi^2/K_m^*)}{4Pe_u\kappa\beta}, \frac{1}{2}, \theta_0\right]}\left[\frac{J_1(\lambda_m)}{J_0^2(\lambda_m) + J_1^2(\lambda_m)}\right] \tag{4.19}$$

The assumption of first order-kinetics ($K_m^* \gg C$), used in the above analysis allows for analytical evaluation of Eq. (4.7); however it limits the range of inlet substrate concentrations. The complete non-linear form of Eq. (4.7) is not amenable to analytical evaluation, and hence was solved using a finite-difference scheme described in Section 4.3.

4.3 Finite-Difference Scheme

A finite-difference representation of Eq. (4.7) is obtained by employing first-order upwind difference quotients for the derivatives on the LHS:

$$\left(\frac{\partial C}{\partial R}\right)_{i,j} = \frac{C_{i,j} - C_{i-1,j}}{h} + O(h) \tag{4.20}$$

$$\left(\frac{\partial C}{\partial Z}\right)_{i,j} = \frac{C_{i,j} - C_{i,j-1}}{k} + O(k) \tag{4.21}$$

And second-order central-differences for the derivatives on the RHS of Eq.(4.7):

$$\left(\frac{\partial^2 C}{\partial R^2}\right)_{i,j} = \frac{C_{i+1,j} - 2C_{i,j} + C_{i-1,j}}{h^2} + O(h)^2 \tag{4.22}$$

$$\left(\frac{\partial^2 C}{\partial Z^2}\right)_{i,j} = \frac{C_{i,j+1} - 2C_{i,j} + C_{i,j-1}}{k^2} + O(k)^2 \tag{4.23}$$

Resulting in the general difference equation:

$$\alpha_1 C_{i-1,j} + \left(\alpha_2 + \frac{\alpha_3}{K_m^* + C_{i.j}}\right) C_{i,j} + \alpha_4 C_{i+1,j} + \alpha_5 C_{i,j-1} + \alpha_6 C_{i,j+1} = 0 \tag{4.24}$$

Where

$$\alpha_1 = -\left[hPe_u \kappa\beta(2R - R^3) + 1 - \frac{h}{R}\right] \tag{4.25}$$

$$\alpha_2 = \left(\frac{h^2}{k}\right) U^* + hPe_u \kappa\beta(2R - R^3) + 2\varphi^2 \left(\frac{h^2}{k^2}\right) + 2 - \frac{h}{R} \tag{4.26}$$

$$\alpha_3 = h^2 \phi^2 \tag{4.27}$$

$$\alpha_4 = -1 \tag{4.28}$$

$$\alpha_5 = -h^2 \left(\frac{U^*}{k} + \frac{\varphi^2}{k^2}\right) \tag{4.29}$$

$$\alpha_6 = -\varphi^2 \left(\frac{h^2}{k^2}\right) \tag{4.30}$$

The corresponding difference quotients of the boundary conditions in Eq. (4.9) are:

$$\begin{aligned}
&B.C.1 \quad at\ j = 1 \quad \forall i \quad C_{i,j} = e^{-Pe_v VR} \\
&B.C.2 \quad at\ i = 1 \quad \forall j \quad \frac{C_{i,j} - C_{i-1,j}}{h} = 0 \\
&B.C.3 \quad at\ i = m \quad \forall j \quad \frac{C_{i+1,j} - C_{i,j}}{h} = \frac{\varphi Pe_u}{2} \frac{C_{i,j} - C_{i,j-1}}{k} \\
&B.C.4 \quad at\ j = n \quad \forall i \quad \frac{C_{i,j} - C_{i,j-1}}{k} = 0
\end{aligned} \tag{4.31}$$

Boundary condition 1 is an approximation of the inlet condition in Eq (4.9), and is obtained by assuming the net diffusive and convective flux in the radial direction is negligible at the membrane entrance. Boundary condition 4 implies there is no diffusive transport at the membrane exit. The solution domain is a regular 2-dimensional grid, and is sub-divided into *m*-intervals (of size *h*) in the *r*-dimension and *n*-intervals (of size *k*) in the *z*-dimension. The

difference equation (4.24), including the boundary conditions of Eq. (4.31), is solved by making use of the multivariate Newton-Rapshon iteration scheme:

$$\boldsymbol{C}_{(n+1)} = \boldsymbol{C}_n - \frac{\boldsymbol{F}(\boldsymbol{C_n})}{\boldsymbol{J}_n} \tag{4.32}$$

Where ***F(C***) is the residual Eq. (4.24), and ***J*** is the tridiagonal Jacobian matrix:

$$\boldsymbol{J} = \begin{bmatrix} D & B & 0 & & 0 & 0 & 0 \\ E & D & B & \cdots & 0 & 0 & 0 \\ 0 & E & D & & 0 & 0 & 0 \\ & \vdots & & \ddots & & \vdots & \\ 0 & 0 & 0 & & D & B & 0 \\ 0 & 0 & 0 & \cdots & E & D & B \\ 0 & 0 & 0 & & 0 & E & D \end{bmatrix} \tag{4.33}$$

The matrix elements *B*, *D*, and *E* are, respectively:

$$B = \alpha_4 + \alpha_5 \tag{4.34}$$

$$D = \alpha_2 + \alpha_3 \left[\frac{1}{K_m^* + C_{i.j}} + \frac{C_{i.j}}{\left(K_m^* + C_{i.j}\right)^2} \right] \tag{4.35}$$

$$E = \alpha_1 + \alpha_6 \tag{4.36}$$

The Newton-Raphson iteration scheme was implemented on MATLAB R2014a and the procedure is shown in Figure 4.1. The algorithm begins with an initial guess of the solute concentration at each grid point; an initial guess of zero was used. Based on this guess, the residual column vector and the Jacobian matrix can be evaluated. The magnitude (Euclidean norm) of the quotient of the residual vector and Jacobian matrix, *d**C***, is evaluated. The iteration is repeated with new solute concentration guess values until the Euclidean norm is less than the prescribed tolerance.

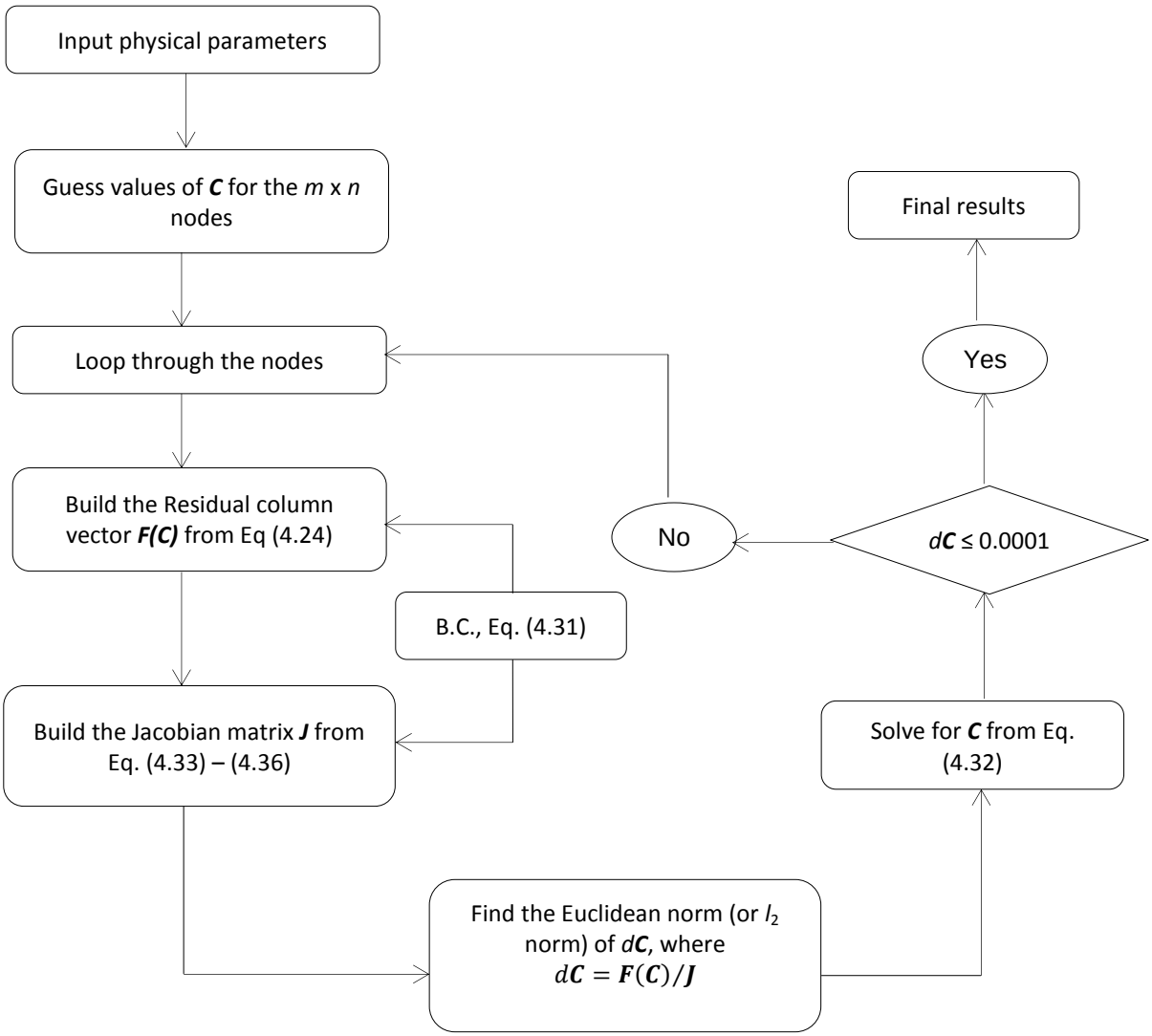

Figure 4.1: The Newton-Raphson Algorithm for solving Eq. (4.24).

4.4 Results

4.4.1 Numerical solution

The implicit finite-difference scheme was shown to be unconditionally stable for the different values of *h* and *k* listed in Table 4.3. The results are shown in Figure 4.2 and Figure 4.3 for the parameter values listed in Table 4.4. The computing times listed in Table 4.3 were obtained on a Lenovo M93P (3.2 GHz) 8GB Ram computer. Figures 4.2 and 4.3 illustrate the effect of the fraction retentate *f* on the solute concentration profiles. In the dead-end mode (*f* = 0) there is increased radial convective flow as shown by the streamlines in Figure 4.2. This increased radial flow allows for more solute contact with the biofilm, and hence improved conversion, resulting in higher MBR efficiency. In this mode however the solute is limited to only the entrance-half of the

MBR as shown in Figure 4.2. Increasing the fraction retentate to f = 0.8 allows for a uniform distribution of the solute (Figure 4.3), however radial convective flow is significantly reduced. This result implies that an optimum f value should be sought for enhanced MBR efficiency. The concentration profiles are consistent with the numerical results of Ye *et al*. [17], with the solute concentration decreasing linearly in the axial direction while exhibiting a flat profile in the radial direction, as indicated by the colour coded concentrations in Figure 4.2 and Figure 4.3.

The developed finite-difference scheme also allows for the evaluation of the effect on the concentration profiles of the radial and axial convective velocity, the convective mass transfer rates, the reaction rates, and the aspect ratio. The sensitivity analysis of these parameters however has been omitted in the current paper.

Table 4.3: **Computation times for different sizes of *h* and *k*.**

Simulation	Number of radial nodes (*m*)	Number of axial nodes (*n*)	Total number of solution nodes	Total iteration time (s)
1.	32	32	1,024	13.302
2.	64	64	4,096	55.130
3.	128	128	16,384	505.108

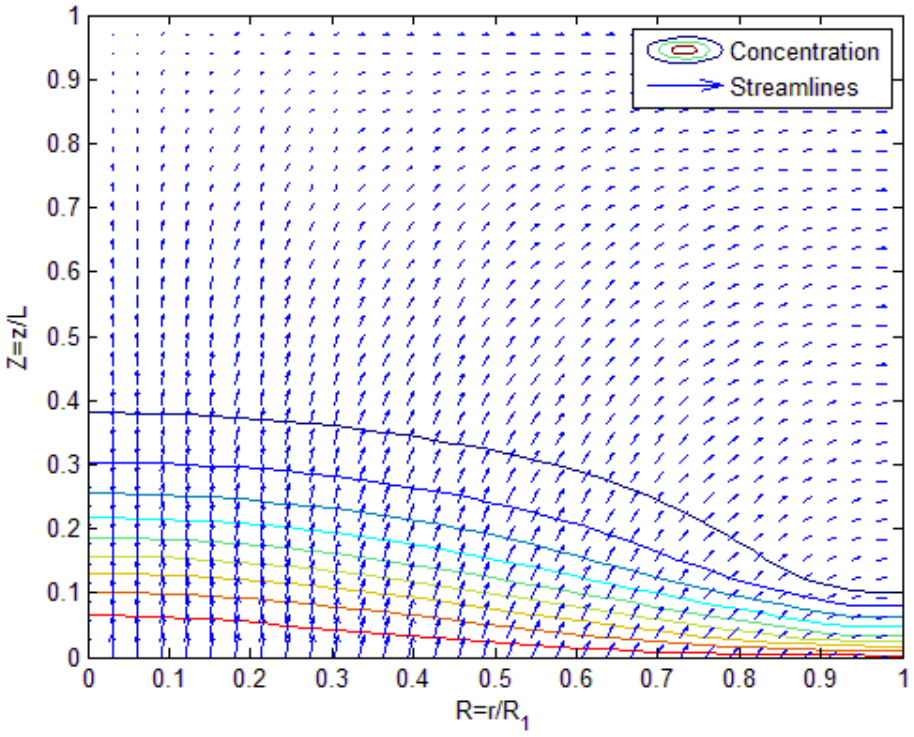

Figure 4.2: Solute concentration profiles for *m* = *n* = 64 when *f* = 0.

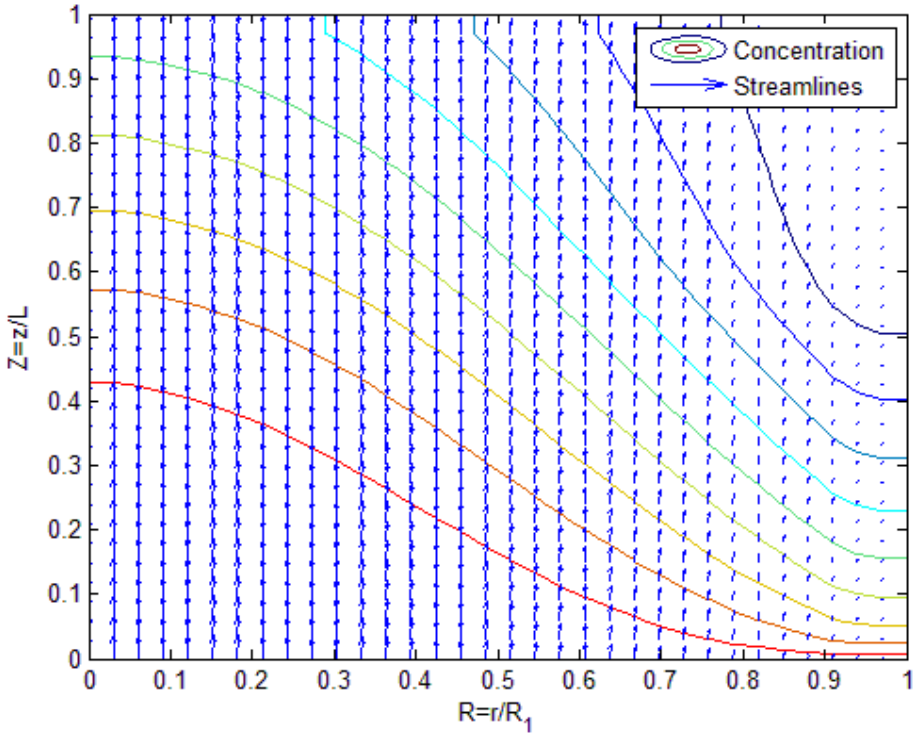

Figure 4.3: Solute concentration profiles for *m* = *n* = 64 when *f* = 0.8.

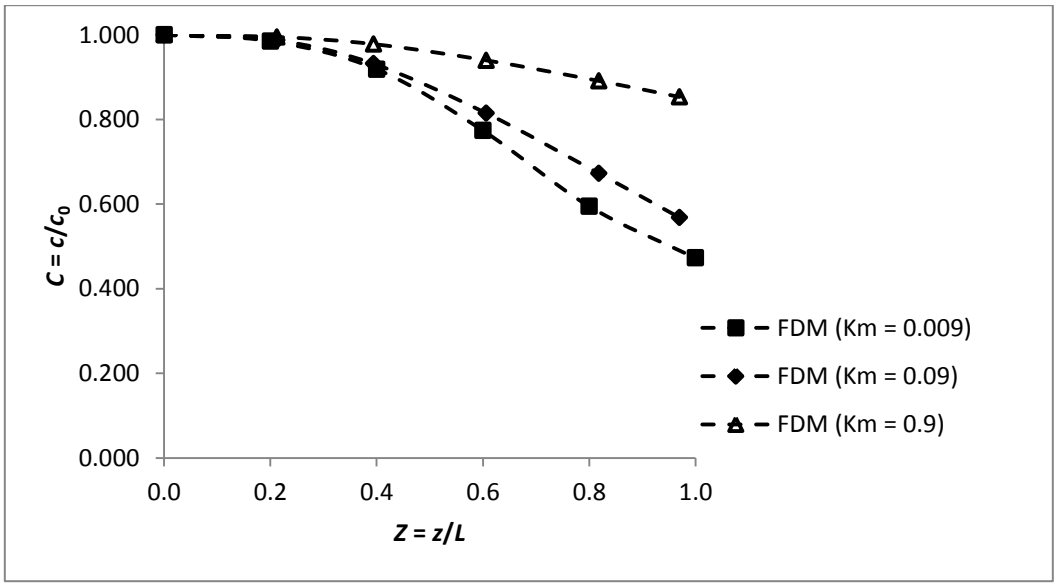

Figure 4.4: Solute concentration profiles from the Finite Difference Method (FDM) for different saturation constants K_m, when *f* = 0.8.

Figure 4.4 is a plot of the solute concentration profile, from the FDM scheme, for different dimensionless saturation constants when *f* = 0.8. At a low K_m^* value of 0.009 the dimensionless outlet solute concentration is 0.472, whereas increasing K_m^* to 0.9 reduces the outlet concentration to only 0.853. This result is expected since a lower K_m^* value is consistent with a

higher biofilm/enzyme affinity for the substrate [18]. This result also illustrates the significance of the appropriate choice of substrate on bioreactor design.

4.4.2 Comparison with analytical solution

In Figure 4.5 the FDM scheme is compared with the analytical model presented in Section 4.2 for the open-shell mode (f = 0.8). The analytical model predicts a linear decrease in the solute concentration inside the membrane lumen to 47% of the original concentration. This result is consistent, qualitatively, with the result of Heath and Belfort [7,17] for the parameter values listed in Table 4.4. The FDM scheme predicts the same outlet concentration; however the decrease is gradual close to the entrance and rises with increasing length. The discrepancies between the two profiles arise from the assumption of first-order kinetics, assumed in developing the analytical solution. These two profiles suggest the open-mode is suitable for microbial growth since the substrate is not depleted inside the lumen.

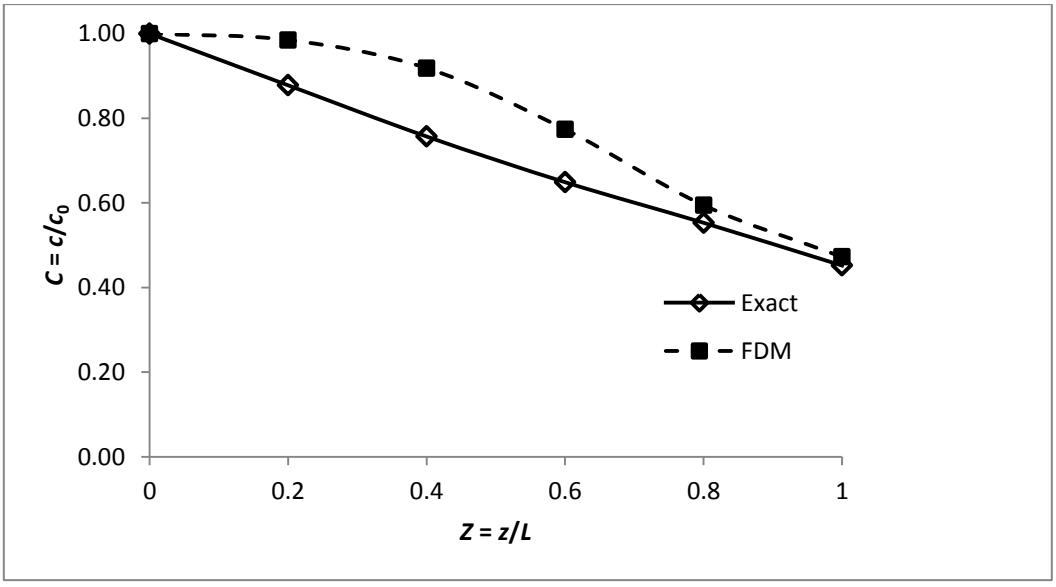

Figure 4.5: A comparison of the analytical versus the FDM solution for solute concentration profiles when f = 0.8.

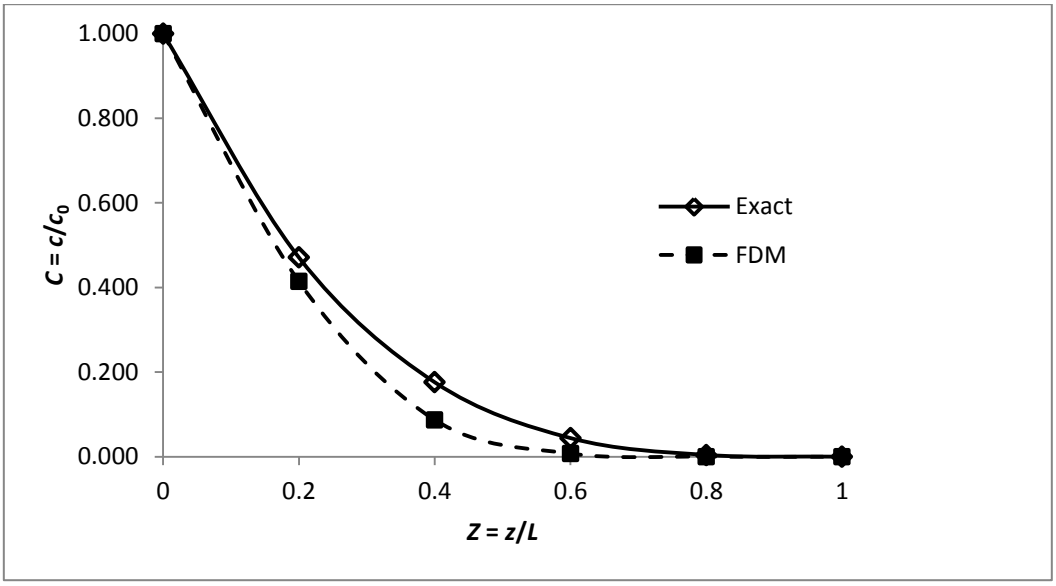

Figure 4.6: A comparison of the analytical versus the FDM solution for solute concentration profiles when $f = 0$.

Table 4.4: Parameter values used to determine the concentration profile [6]**.**

Model parameter	Symbol	Unit	Basic measured value
Membrane hydraulic permeability	k_m	m/Pas	3.82×10^{-11}
Membrane inner radius	R_1	m	1.30×10^{-4}
Effective membrane length	L	m	5.7×10^{-2}
Lumen-side entrance axial velocity	u_0	m s^{-1}	1.67×10^{-3}
Permeation velocity	v_0	m s^{-1}	1.91×10^{-7}
Lumen-side inlet fluid pressure	p_0	Pa	106 325
Shell-side fluid pressure	p_S	Pa	101 325
Glucose diffusivity	D_{AB}	m^2 s	1.0×10^{-10}
solution density	ρ	kg m^{-3}	998.0
solution viscosity	μ	Pas	9.7×10^{-4}
Glucose inlet concentration	c_0	g dm^{-3}	2.00
Kinetic constants	V_M/K_m	s^{-1}	1.00

The rapid decline in the solute concentration in Figure 4.6 is due to increased radial convective flow in the dead-end mode. This results in non-uniform microbial growth/tapering as observed by Godongwana *et al.* [19] for the bacterium *Streptomyces coelicolor* on a ceramic membrane. This

phenomenon can be reduced either by increasing the solute flowrate or increasing the fraction retentate *f*. The numerical scheme matches the analytical model approximately on a small interval close to the origin. The divergence again is attributed to the assumption of first-order kinetics.

4.5 Conclusion

A numerical solution of the dimensionless convection-diffusion equation, with non-linear kinetics, was developed. The numerical scheme was performed using the Newton-Raphson method, and was shown to be unconditionally stable for different step-sizes (*h* and *k*). The analysis provides for evaluation of concentration profiles of solutes through a membrane bioreactor. The numerical solution was compared to a regular perturbation solution for two modes of operation, *i.e.* the dead-end mode and open-shell mode. In the dead-end mode the numerical results closely matched the perturbation solution. The assumption of linear kinetics, commonly used in literature models, was shown to result in inaccuracies in the open-shell mode. The numerical solution allows for the evaluation of the influence of the general operating parameters of a MBR on the concentration profiles. The fraction retentate (*f*) was shown to be an important optimisation parameter for improved MBR efficiency.

4.6 Summary

This chapter of the thesis served to validate the analytic solutions developed in Chapter 3, particularly the first-order limit of the Monod equation. An analytical solution of the differential mass balance equation was only plausible when zero-order or first-order kinetics was assumed. The use of these assumptions in developing the model limited the range of concentrations in the MBR. The significance of the numerical analysis, therefore, was in the identification of the range of applicability of the analytical model developed in Chapter 3.

Nomenclature

c	substrate concentration (g dm^{-3})
c_0	substrate feed concentration (g dm^{-3})
$C = c/c_0$	dimensionless substrate concentration
D_{AB}	substrate diffusivity (m^2 s^{-1})
$f = u_1/u_0$	fraction retentate
h	step-size in the r-dimension (m)
i	grid point index in the r-dimension
j	grid point index in the z-dimension
$J_n(\lambda)$	Bessel function of order n of the first kind
k	step-size in the z-dimension (m)
K_m	saturation (or Michaelis) constant (g dm^{-3})
K_m^*	dimensionless Michaelis constant
L	membrane effective length (m)
$M(a,b,\theta)$	Kummer function of the first kind
$Pe_u = u_0R_1/D_{AB}$	axial Peclet number
$Pe_v = v_0R_1/D_{AB}$	radial Peclet number
r	radial spatial coordinate (m)
$R = r/R_1$	dimensionless radial spatial coordinate
R_1	membrane lumen radius (m)
u	axial velocity (m s^{-1})
u_0	feed axial velocity (m s^{-1})
$U = u/u_0$	dimensionless axial velocity
v	radial velocity (m s^{-1})
$V = v/v_0$	dimensionless radial velocity
V_M	maximum rate of reaction (g dm^{-3} s^{-1})
z	axial spatial coordinate (m)
$Z = z/L$	dimensionless axial spatial coordinate

Greek letters

α	coefficients of finite difference scheme, defined in text
$\beta = P_0 - P_2$	dimensionless transmembrane pressure
κ	dimensinless membrane hydraulic permeability

ϕ	Thiele modulus
$\varphi = R_1/L$	aspect ratio
λ_m	eigen values, m = 1, 2, …

Acknowledgements

The authors would like to thank the National Research Foundation (RSA) and the Fulbright Program (U.S. Department of State) for supporting this work. The *MATLAB* code for the Newton-Raphson algorithm was developed with the assistance of Professor Jeff Heys of Montana State University.

References

[1] L. Giorno and E. Drioli, “Biocatalytic membrane reactors : applications and perspectives,” *Tibtech*, vol. 18, no. August, pp. 339–349, 2000.

[2] C. Charcosset, “Membrane processes in biotechnology: an overview.,” *Biotechnol. Adv.*, vol. 24, no. 5, pp. 482–492, 2006.

[3] D. F. Stamatialis, B. J. Papenburg, M. Giron, S. N. M. Bettahalli, S. Schmitmeier, and M. Wessling, “Medical applications of membranes : drug delivery , artificial organs and tissue engineering,” *J. Memb. Sci.*, vol. 308, pp. 1–34, 2008.

[4] S. Curcio, V. Calabro, and G. Iorio, “A theoretical and experimental analysis of a membrane bioreactor performance in recycle configuration,” *J. Memb. Sci.*, vol. 273, no. 1–2, pp. 129–142, Mar. 2006.

[5] B. R. Bird, W. E. Stewart, and E. N. Lightfoot, *Transport Phenomena*, 2nd ed. New York: John Wiley & Sons, 2002.

[6] B. Godongwana, D. Solomons, and M. S. Sheldon, “A solution of the convective-diffusion equation for solute mass transfer inside a capillary membrane bioreactor,” *Int. J. Chem. Eng.*, 2010.

[7] C. Heath and G. Belfort, “Immobilization of suspended mammalian cells: analysis of hollow fiber and microcapsule bioreactors.,” *Adv. Biochem. Eng. Biotechnol.*, vol. 34, pp. 1–31, Jan. 1987.

[8] L. Graetz, “Über die wärmeleitungsfähigkeit von flüssigkeiten,” *Ann. der Phys. und Chemie*, vol. 18, pp. 79–94, 1883.

[9] E. J. Davis, “Exact solutions for a class of heat and mass transfer problems,” *Can. J. Chem. Eng.*, vol. 51, pp. 562–572, 1973.

[10] L. R. Waterland, A. S. Michaelis, and C. R. Robertson, “A theoretical model for enzymatic catalysis using asymmetric hollow fiber membranes,” *Am. Inst. Chem. Eng. J.*, vol. 20, no. 1, pp. 50–59, 1974.

[11] V. K. Jayaraman, “The solution of hollow fiber bioreactor design equations.,” *Biotechnol. Prog.*, vol. 8, no. 5, pp. 462–464, 1992.

[12] E. Nagy, *Basic Equations of the Mass Transport Through a Membrane Layer*. Boston: Elsevier, 2012.

[13] L. J. Kelsey, M. R. Pillarella, and A. L. Zydney, “Theoretical analysis of convective flow profiles in a hollow-fiber membrane bioreactor,” *Chem. Eng. Sci.*, vol. 45, no. 11, pp. 3211–3220, 1990.

[14] V. Calabrò, S. Curcio, and G. Iorio, “A theoretical analysis of transport phenomena in a hollow fiber membrane bioreactor with immobilized biocatalyst,” *J. Memb. Sci.*, vol. 206, no. 1–2, pp. 217–241, Aug. 2002.

[15] E. Nagy, “Basic equations of mass transfer through biocatalytic membrane layer,” *Asia-Pacific J. Chem. Eng.*, vol. 4, pp. 270–278, 2009.

[16] M. Abramowitz and I. A. Stegun, *Handbook of Mathematical Functions*. New York, 1965.

[17] H. Ye, D. B. Das, J. T. Triffitt, and Z. Cui, “Modelling nutrient transport in hollow fibre membrane bioreactors for growing three-dimensional bone tissue,” *J. Memb. Sci.*, vol. 272, pp. 169–178, 2006.

[18] M. L. Shuler and F. K. Kargi, *Bioprocess Engineering: basic concepts*, 2nd ed. New Jersey: Pearson, 2014.

[19] B. Godongwana, D. De Jager, M. S. Sheldon, and W. Edwards, “The effect of Streptomyces coelicolor development on the hydrodynamics of a vertically orientated capillary membrane gradostat reactor,” *J. Memb. Sci.*, vol. 333, no. 1–2, pp. 79–87, 2009.

CHAPTER 5: RESULTS

Analysis of Bioreactor Performance

Godongwana, B. 2015. Effectiveness factors and conversion in a biocatalytic membrane reactor. *PLoSONE,* **minor revisions required.**

(Accepted: 01 February 2016; Manuscript ID: Bunta_PONE-D-16-00394)

5. ANALYSIS OF BIOREACTOR PERFORMANCE

Abstract

Analytical expressions of the effectiveness factor of a biocatalytic membrane reactor, and its asymptote as the Thiele modulus becomes large, are presented. The evaluation of the effectiveness factor is based on the solution of the governing equations for solute transport in the two regions of the reactor, i.e. the lumen and the matrix (immobilised with biofilm). The lumen solution accounts for both axial diffusion and radial convective flow, while the matrix solution is based on Robin-type boundary conditions. The effectiveness factor is shown to be a function of the Thiele modulus, the partition coefficient, the Sherwood number, the Peclet number, and membrane thickness. Three regions of Thiele moduli are defined in the effectiveness factor graphs. These correspond with reaction rate limited, internal-diffusion limited, and external mass transfer limited solute transport. Radial convective flows were shown to only improve the effectiveness factor in the region of internal diffusion limitation. The assumption of first order kinetics is shown to be applicable only in the Thiele modulus regions of internal and external mass transfer limitation. An iteration scheme is also presented for estimating the effectiveness factor when the solute fractional conversion is known. The model is validated with experimental data from a membrane gradostat reactor immobilised with *Phanerochaete chrysosporium* for the production of lignin and manganese peroxidases. The developed model and experimental data allow for the determination of the Thiele modulus at which the effectiveness factor and fractional conversion are optimal.

Keywords: Biocatalysis; Effectiveness factor; Mass transfer; Substrate transport; Regular perturbation; Thiele modulus.

5.1 Introduction

Membrane bioreactors (MBR's) offer a number of advantages over traditional bioreactors and their use for various bioconversions have been extensively reported [1-3]. The main challenge in the use of MBR's remains the diffusional resistance of the membrane which adversely affects their performance [4,5]. The effectiveness factor (η), defined as the ratio of the observed rate of reaction to the hypothetical rate in the absence of mass transfer limitations [6], is generally used to evaluate the performance of a catalytic reactor. A thorough review of mathematical methods employed in evaluating exact solutions of this parameter was given by Aris [6]. This study presented effectiveness factors for single and multiple reactions taking place in various shapes of porous catalysts. Webster and co-workers [7,8] presented analytical models for a membrane bioreactor immobilized with whole cells, based on both Robin-type and Dirichlet-type boundary conditions. The former boundary type accounts for external mass transfer limitations, while the latter assumes the concentration at the membrane wall is known. Willaert *et al*. [9] obtained identical effectiveness factor expressions to Webster and Shuler [7] based on Dirichlet boundary conditions. In these studies, as well as in the majority of available exact solutions [10-12], axial diffusion and radial convective flows are neglected and the kinetics are generally considered linear. These assumptions are not always justified [13] and are imposed with the intention of attaining closed-form expression of the transport equation. The analytical solution of the mass balance equation is not always feasible, and a number of numerical schemes have been developed for this purpose [14-20]. Analytical models however are preferred for their simplicity.

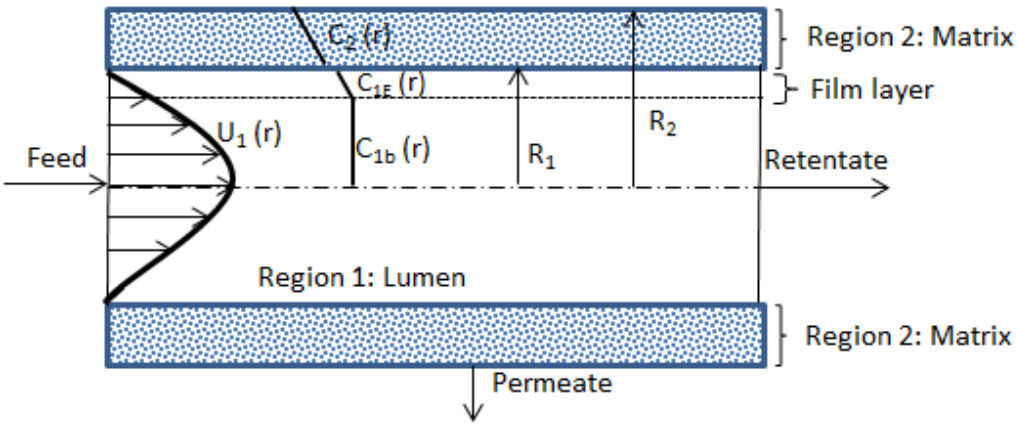

Figure 5.1: A cross-section of the membrane bioreactor.

The current analysis is aimed at developing expressions of the effectiveness factor for an MBR immobilized with biofilm, based on the model developed by Godongwana *et al*. [13].

The asymptotic behaviour as the Thiele-modulus becomes large will be considered. The models are based on the MBR system shown in Figure 5.1, and the following conditions of operation are assumed: (1) the system is isothermal; (2) the flow regime within the membrane lumen is fully developed, laminar, and homogeneous; (3) the physical and transport parameters are constant; (4) in the membrane matrix the flow is only one dimensional (i.e. there are no axial components of the velocity in the membrane matrix due to the morphology of the membrane wall).

5.2 Mathematical formulation

5.2.1 Governing equations

The governing equations for solute transport in the lumen and matrix of the MBR are respectively:

$$u_1 \frac{\partial c_1}{\partial z} + v_1 \frac{\partial c_1}{\partial r} = D_1 \left[\frac{1}{r} \frac{\partial}{\partial r} \left(r \frac{\partial c_1}{\partial r} \right) + \frac{\partial^2 c_1}{\partial z^2} \right] \tag{5.1}$$

$$v_2 \frac{\partial c_2}{\partial r} + \frac{D_2}{r} \frac{\partial}{\partial r} \left(r \frac{\partial c_2}{\partial r} \right) = \frac{V_M c_2}{K_m + c_2} \tag{5.2}$$

The associated boundary conditions are:

$$B.C.1 \quad at \ z = 0 \quad \forall r \quad c_1 = c_0 \tag{5.3a}$$

$$B.C.2 \quad at \ r = 0 \quad \forall z \quad \frac{\partial c_1}{\partial r} = 0 \tag{5.3b}$$

$$B.C.3 \quad at \ r = R_1 \quad \forall z \quad \frac{\partial c_1}{\partial z} = \frac{2D_1}{u_1 R_1} \frac{\partial c_1}{\partial r} \tag{5.3c}$$

$$B.C.4 \quad at \ r = R_1 \quad \forall z \quad k_a (c_{1b} - c_{1E}) = -D_2 \frac{\partial c_2}{\partial r} \tag{5.3d}$$

$$B.C.5 \quad at \ r = R_2 \quad \forall z \quad \frac{\partial c_2}{\partial r} = 0 \tag{5.3e}$$

where u and v are the axial and radial velocity components, respectively; c_1 and c_2 are the local substrate concentrations in the lumen and fiber matrix, respectively; c_{1b} is the bulk lumen concentration; c_{1E} is the concentration on the internal surface of the membrane; D_1 and D_2 are the substrate diffusion coefficients in the lumen and matrix, respectively; k_a is the mass transfer coefficient; K_m is the saturation constant; and V_M is the maximum rate of reaction.

Boundary condition 1 (B.C.1) corresponds to a uniform inlet substrate concentration; B.C.2 corresponds to cylindrical symmetry at the centre of the membrane lumen; B.C.3 and B.C.4

corresponds to continuity of the substrate flux at the lumen-matrix interface; and B.C.5 implies there is no diffusion across the matrix-shell interface. In single-substrate limited biofilms, V_M in Eq. (5.2) is given by [21]:

$$V_M = \frac{\mu_{max} X}{Y_{X/S}} \tag{5.4}$$

where X is the average biofilm density, μ_{max} is the maximum specific growth rate, and $Y_{x/s}$ is the yield of biofilm per unit substrate.

5.2.2 MBR lumen (Region 1)

In the lumen-side of the MBR, Eq. (5.1) in dimensionless form becomes:

$$\varphi Pe_u U_1 \frac{\partial C_1}{\partial Z} - \varphi^2 \frac{\partial^2 C_1}{\partial Z^2} = \frac{1}{R}\left(\frac{\partial C_1}{\partial R} + R\frac{\partial^2 C_1}{\partial R^2}\right) - Pe_v V_1 \frac{\partial C_1}{\partial R} \tag{5.5}$$

where:

$$U = \frac{u}{u_0};\ V = \frac{v}{v_0};\ C = \frac{c}{c_0};\ Z = \frac{z}{L};\ R = \frac{r}{R_1};\ \varphi = \frac{R_1}{L}$$
$$Pe_u = \frac{u_0 R_1}{D_1};\ Pe_v = \frac{v_0 R_1}{D_1} \tag{5.6}$$

The solution of Eq. (5.5) was given by Godongwana *et al.* [13] as an asymptotic expansion in terms of the membrane hydraulic permeability κ:

$$C_1(\theta, x) = \sum_{m=1}^{\infty}\sum_{n=0}^{N} B_m F_m(\theta) T_n(x) \kappa^n \tag{5.7}$$

Where

$$\theta = -\left(\frac{\varphi^2}{4Pe_u \kappa\beta}\right)\xi^2;\quad \xi = -\frac{2Pe_u\kappa\beta}{\varphi^2}\left[\frac{1}{(f-1)} + Z\right];\quad \text{and}\quad x = \lambda_m R \tag{5.8}$$

and $F_m(\theta)$ in Eq. (5.7) is the Kummer function:

$$F_m(\theta) = M\left(-\frac{\lambda_m^2}{4Pe_u\kappa\beta}, \frac{1}{2}, \theta\right) \tag{5.9}$$

The zero-order and first-order approximations of $T_n(x)$ in Eq. (5.7) are, respectively:

$$T_0(x) = J_0(x) \tag{5.10}$$

and

$$T_1(x) = \sigma_1 \left[\frac{(x)^2 J_2(x)}{3!!} + \sigma_2 \frac{(x)^3 J_3(x)}{5!!} + \sigma_3 \frac{(x)^4 J_4(x)}{7!!} \right] \tag{5.11}$$

where λ_m are the eigenvalues, J_n is the Bessel function of the first kind of order n.

$$\sigma_1 = -\frac{3Pe_u\beta}{2\lambda_m^2}, \quad \sigma_2 = -\frac{20}{3\lambda_m^2}, \quad and \quad \sigma_3 = \frac{35}{4\lambda_m^2} \tag{5.12}$$

The eigenvalues are obtained from B.C.3 in Eq. (5.3c), and are roots of the equation [20]:

$$\frac{\lambda_m \varphi \xi}{\kappa\beta} M\left(-\frac{\lambda_m^2}{4Pe_u\kappa\beta} + 1, \frac{3}{2}, \theta\right) = 4\frac{J_1(\lambda_m)}{J_0(\lambda_m)} M\left(\frac{-\lambda_m^2}{4Pe_u\kappa\beta}, \frac{1}{2}, \theta\right) \tag{5.13}$$

The coefficient B_m is obtained by imposing the inlet condition B.C.1 of Eq.(5.3a):

$$B_m = \frac{2}{\lambda_m M\left(-\frac{\lambda_m^2}{4Pe_u\kappa\beta}, \frac{1}{2}, \theta_0\right)} \left[\frac{J_1(\lambda_m)}{J_0^2(\lambda_m) + J_1^2(\lambda_m)} \right] \tag{5.14}$$

5.2.3 MBR Matrix (Region 2)

5.2.3.1 First-order Kinetics

The rate of solute consumption inside the membrane matrix is governed by Monod kinetics. Assuming the first-order limit, i.e. $K_m >> c$, Eq. (5.2) for the matrix in dimensionless form becomes:

$$\frac{d^2C_2}{dR^2} + \left(\frac{1}{R} - Pe_v V_2\right)\frac{dC_2}{dR} - \phi^2 C_2 = 0 \tag{5.15}$$

where the first-order Thiele modulus ϕ is defined as:

$$\phi = \sqrt{\frac{V_M R_1^2}{K_m D_2}} \tag{5.16}$$

Eq. (5.15) is amenable to an analytical solution by regular perturbation only when the hydraulic permeability is much smaller than unity $\kappa << 1$. For brevity only the zero-order approximation will be considered here, the first order perturbation approximation is given in Appendix B (B.1 – B.2) following the procedure of Godongwana *et al* [13]. Equation (5.15) then reduces to:

$$\frac{d^2C_2}{dR^2} + \frac{1}{R}\frac{dC_2}{dR} - \phi^2 C_2 = 0 \tag{5.17}$$

Equation (5.17) is evaluated subject to B.C.4, which in dimensionless form becomes:

$$Sh\left(C_b - {}^{C_2}/_{\gamma}\right) = -\frac{dC_2}{dR}\bigg|_{R=1} \tag{5.18}$$

Where γ is the partition coefficient and *Sh* is the Sherwood number. A good estimate of *Sh* for hollow fiber membranes is given by Wickramasinghe *et al*. [22]:

$$Sh = 1.11 Re^{0.47} Sc^{0.33} \tag{5.19}$$

where $Sc = \mu/\rho D_{AB}$ is the Schmidt number and $Re = \rho v R_1/\mu$ is the Reynolds number. The dimensionless bulk lumen concentration is defined as:

$$C_b = 2\int_0^1 C_1(\theta, x) R dR = 2\sum_{m=1}^{\infty} \frac{B_m}{\lambda_m} \cdot M\left(-\frac{\lambda_m^2}{4Pe_u \kappa\beta}, \frac{1}{2}, \theta_1\right) \cdot J_1(\lambda_m) \tag{5.20}$$

Equation (5.17) is the modified Bessel equation and has a solution of the form [23]:

$$C_2 = B_1 I_0(\phi R) + B_2 K_0(\phi R) \tag{5.21}$$

where I_0 and K_0 are the modified Bessel functions of the first kind and second kind, respectively. The constants B_1 and B_2 are obtained with the use of B.C.4 and B.C.5 as:

$$B_1 = \frac{K_1(\phi R_2) \cdot \gamma C_b}{[K_0(\phi) \cdot I_1(\phi R_2) + I_0(\phi) \cdot K_1(\phi R_2)] + \psi} \tag{5.22}$$

and

$$B_2 = \frac{I_1(\phi R_2) \cdot \gamma C_b}{[K_0(\phi) \cdot I_1(\phi R_2) + I_0(\phi) \cdot K_1(\phi R_2)] + \psi} \tag{5.23}$$

where

$$\psi = \frac{\gamma\phi}{Sh}[K_1(\phi)\cdot I_1(\phi R_2) + I_1(\phi)\cdot K_1(\phi R_2)] \tag{5.24}$$

The effectiveness, η, factor is defined as:

$$\eta = \frac{-2\pi r_1 L D_2 \left.\frac{\partial c_2}{\partial r}\right|_{r=r_1}}{\pi L(r_2^2 - r_1^2)\frac{V_M c_b}{K_m + c_b}} \tag{5.25}$$

In dimensionless form:

$$\eta = \frac{-2(\delta+1)}{\phi_0^2(R_2^2-1)}\left.\frac{\partial C_2}{\partial R}\right|_{R=1} \tag{5.26}$$

where $\delta = \frac{K_m^*}{C_b}$ and ϕ_0 is the zero-order Thiele modulus defined as:

$$\phi_0 = \sqrt{\frac{V_M R_1^2}{c_0 D_2}} \tag{5.27}$$

Assuming first-order kinetics ($\delta >> 1$) Eq. (5.26) reduces to:

$$\eta_1 = \frac{-2}{\phi^2(R_2^2-1)C_b}\left.\frac{\partial C_2}{\partial R}\right|_{R=1} \tag{5.28}$$

Substituting Eqs. (5.20)- (5.24) into Eq (5.28) gives:

$$\eta_1 = \frac{2\gamma[K_1(\phi)\cdot I_1(\phi R_2) - I_1(\phi)\cdot K_1(\phi R_2)]}{\phi(R_2^2-1)\{[K_0(\phi)\cdot I_1(\phi R_2) + I_0(\phi)\cdot K_1(\phi R_2)] + \psi\}} \tag{5.29}$$

The reciprocal of the effectiveness factor is generally considered a mass transfer resistance [6,8,24]. Thus, the reciprocal of Eq. (5.29) is the sum of the internal resistance and the external resistance (ψ) to mass transfer. This is explicit in the asymptotic form of Eq. (5.29) given in Appendix B:

$$\frac{1}{\eta_1} \sim \frac{\phi(R_2^2-1)}{2}\left\{\frac{\phi}{Sh} + \frac{1}{\gamma}coth[\phi(R_2-1)]\right\} \quad , as\ \phi \to \infty \tag{5.30}$$

The first and second terms inside the curly brackets in Eq. (5.30) represent the external resistance and internal resistance to mass transfer, respectively. The series-of-resistances

nature of Eqs. (5.29) and (5.30) is a result of using the Robin-type boundary condition, B.C.4, in the evaluation of Eq. (5.17). In both equations the parameters with the greatest influence on the effectiveness factor are: the Thiele modulus, partition coefficient, Sherwood number, and membrane thickness. The influence of the Peclet (Pe_u) number on the effectiveness factor is presented in Appendix B (B.2). By definition η = 1 when the Thiele modulus, ϕ, becomes zero since this value of the Thiele modulus corresponds with a reaction rate-controlled transfer with no mass transfer limitations.

5.2.3.2 Zero-order Kinetics

Assuming the zero-order limit, i.e. $K_m << c$, the dimensionless form of Eq. (5.2) becomes:

$$\frac{d^2C_2}{dR^2} + \frac{1}{R}\frac{dC_2}{dR} - \phi_0^2 = 0 \tag{5.31}$$

Equation (5.31), subject to B.C. 4 and B.C.5, has a solution of the form:

$$C_2 = \frac{\phi_0^2}{4}\left\{(R^2-1) - 2\left[R_2^2 lnR + \frac{\gamma}{Sh}(R_2^2-1)\right]\right\} + \gamma C_b \tag{5.32}$$

The dimensionless zero-order effectiveness factor from Eq. (5.26) is:

$$\eta_0 = -\frac{2}{\phi_0^2(R_2^2-1)}\frac{\partial C_2}{\partial R}\Big|_{R=1} = 1 \tag{5.33}$$

5.2.3.3 Non-linear Kinetics

The effectiveness factor allows for the determination of the overall reaction rate in terms of the Thiele modulus. However, when the reaction kinetics are non-linear as was assumed in the previous sections Eq. (5.26) is not amenable to an analytical solution. A practical measure of evaluating the effectiveness factor is attained by making the following approximation:

$$\frac{dC_2}{dR}\Big|_{R=1} = \frac{C_2|_{R=R_2} - C_2|_{R=1}}{(R_2-1)}, \quad (R_2-1) \ll 1 \tag{5.34}$$

Substituting Eq. (5.34) into Eq. (5.26) gives:

$$\Upsilon = 1 - \left[C_2|_{R=1} - \frac{\eta \phi_0^2 (R_2^2 - 1)(R_2 - 1)}{2(\delta + 1)} \right], \quad (R_2 - 1) \ll 1 \tag{5.35}$$

where Υ is the fractional conversion. Equation (5.35) allows for empirical determination of the effectiveness factor when the fractional conversion is known, from the following procedure: (i) guess the wall concentration ($C_2|_{R=R_1}$) and obtain the concentration gradient from Eq. (5.34), (ii) substitute the concentration gradient $\left.\frac{dC_2}{dR}\right|_{R=1}$ into Eq. (5.26) to obtain the effectiveness factor, (iii) substitute the effectiveness factor η into Eq. (5.35) and compare the experimental conversion to the attained value, and (iv) repeat the procedure until the experimental conversion is equal to the value obtained from the iteration.

5.3 Results

Figure 5.2 is a plot of effectiveness factors and corresponding asymptotes, from Eq. (5.29) and (5.30) respectively, as functions of the normalized Thiele modulus Φ for different values of the Sherwood number. The normalized modulus is defined as:

$$\Phi = \frac{\phi}{2}(R_2^2 - 1) \tag{5.36}$$

Equation (5.30) provides a simple mathematical approximation to Eq. (5.29) and for $\Phi > 1$ gives exact values for the effectiveness factor, as shown in Figure 5.2. Three regions of Thiele moduli may be defined from Figure 5.2, as characterised by the effectiveness factor. In the first region ($\Phi < 0.01$) the effectiveness factor is unity, and the rate of solute transport in the MBR is controlled by the rate of reaction. When the MBR is operated in this region the diffusional resistance offered by the membrane is negligible. In the second region ($0.01 < \Phi < 0.1$) the rate of solute transport is limited only by internal diffusion through the membrane, and hence the effectiveness factor is not a function of the Sherwood number. In the third region ($\Phi > 0.1$) external mass transfer limitations control the rate of solute transport through the MBR, and the effectiveness factor is greatly influenced by the Sherwood number. This result is consistent with the Robin-type boundary condition.

Table 5.1: Parameter values used to determine the effectiveness factor in Figure 5.3 [25]

Model parameter	Symbol	Unit	Basic measured value
Membrane inner radius	R_1	m	6.98×10^{-4}
Membrane outer radius	R_2	m	9.63×10^{-4}
Effective membrane length	L	m	0.230
Lumen-side entrance velocity	u_0	ms^{-1}	3.04×10^{-4}
Permeation velocity	v_0	$m\ s^{-1}$	8.82×10^{-6}
Glucose diffusivity	D_{AB}	$m^2\ s$	1.59×10^{-9}
Glucose inlet concentration	c_0	$g\ dm^{-3}$	10.00
Maximum specific growth rate	μ_{max}	h^{-1}	0.035
Saturation constant	K_m	$g\ dm^{-3}$	9.350
Yield of biofilm per substrate	$Y_{x/s}$	g/g	0.202

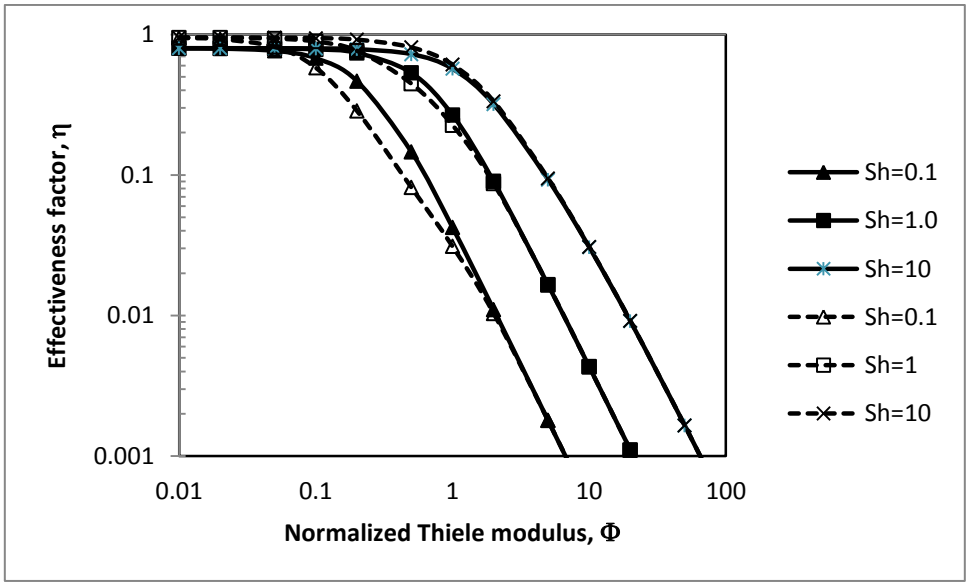

Figure 5.2: Effectiveness factors (–) and asymptotes (---) vs Thiele modulus at different Sherwood numbers.

Figure 5.2 may suggest operating the MBR at low values of the Thiele modulus for high effectiveness factors, however substrate conversion at these low values is minimal as can be seen in Figure 5.3. This figure presents experimental values of conversion and the effectiveness factor for an MBR used for the production of Lignin and Manganese Peroxidases from *Phanerochaete chrysosporium*. The operating parameters of the MBR and kinetic constants of

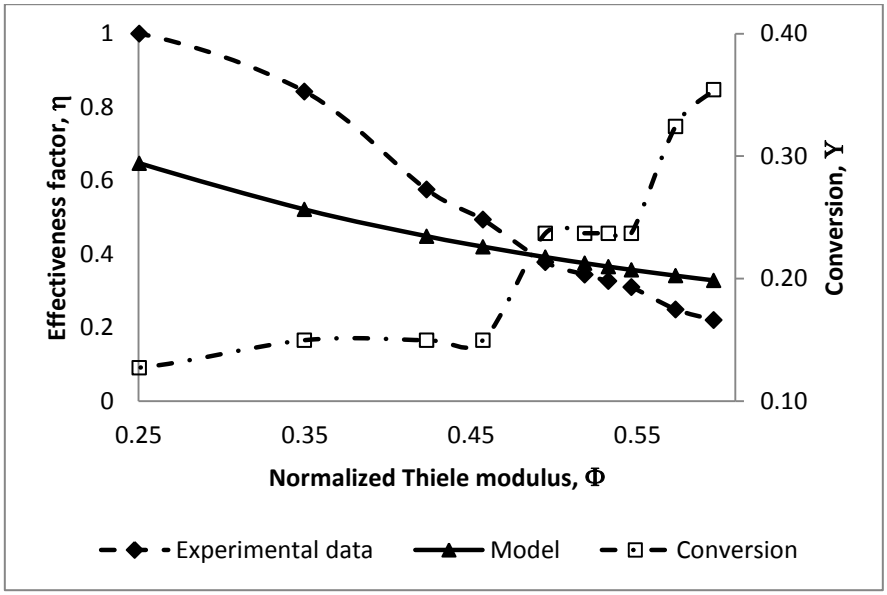

Figure 5.3: Effectiveness factor and glucose conversion vs normalized Thiele modulus.

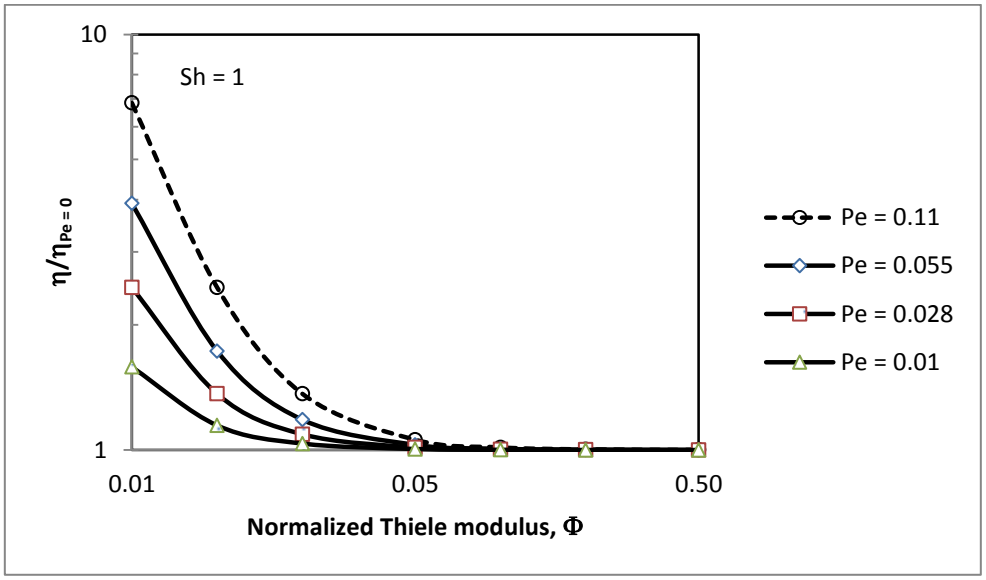

Figure 5.4: Relative increase in effectiveness factor vs normalized Thiele modulus at different Peclet numbers.

the biofilm are listed in Table 5.1. The operation of the MBR is detailed in Appendix C. Figure 5.3 provides a basis for performing rigour optimisation studies of an operating Thiele modulus at which both substrate conversion and the effectiveness factor are optimal. This point corresponds with low effectiveness factors when the objective is to maximise solute conversion [19]. However, parametric optimisation was not part of the current study, and therefore the optimal Thiele modulus was not defined for the current MBR.

The experimental effectiveness factor in Figure 5.3 is obtained from Eq. (5.35) and is plotted against the first-order model of Eq. (5.29). The two plots exhibit the same trend, with the model underestimating the effectiveness factor at values of $\Phi < 0.5$. This is because at low values of the Thiele modulus solute transport is reaction rate controlled and the first-order kinetics premise assumes a lower rate of reaction than the maximum. At higher values of the Thiele modulus solute transport is limited by internal and external diffusion, and the first-order model approximately matches the experimental effectiveness factor.

In the region of internal diffusional limitation ($0.01 < \Phi < 0.1$) radial convective flows can significantly improve the effectiveness factor, as illustrated in Figure 5.4. In this figure the relative increases in the effectiveness factor ($\eta/\eta_{Pe=0}$) are plotted against normalised Thiele moduli for different values of the radial Peclet number. The effectiveness factors in Figure 5.4 are obtained from Eq. (B.10) in Appendix B. The increase in η with Pe_v is only restricted to the region of internal diffusional limitation. The maximum relative increase in the effectiveness factor is obtained in the transitional region from kinetic to internal-diffusional control ($\Phi \approx 0.01$), and minimal in the boundary region between internal-diffusional control and external mass transfer limitation. Increasing Pe_v outside this region may drastically reduce the contact time between the substrate and the biocatalyst, and hence lead to reduced substrate conversions as was shown by Calabro *et al.* [17]. In this region ($\Phi > 0.1$), as previously discussed the effectiveness factor can be improved by increased Sherwood numbers.

5.4 Conclusion

Mathematical models have been developed for solute concentration profiles and effectiveness factors in an MBR, assuming the zero-order and first-order limits of the Michaelis-Menten (or Monod) equation. The first-order kinetic model was shown to be applicable only when the MBR is operated at high Thiele moduli. Experimental results show that the effectiveness factor decreases with increasing Thiele modulus, while the fractional conversion increases with an increase in this parameter. The developed model allows for the determination of the operating point at which both the conversion and effectiveness factor are optimal. It was also shown that the radial Peclet number can significantly improve the performance of an MBR operating under internal diffusional limitations.

5.5 Summary

This chapter addressed the main objective of the thesis, i.e. to evaluate the nature of the dependence of the MBR effectiveness on convective mass and momentum transfer. A novel mathematical solution of the effectiveness factor as a function of the Thiele modulus, the partition coefficient, the Sherwood number, and the Peclet number was presented. Prior to this study, there were no analytical (or closed-form) solutions of the effectiveness factor which accounted for both diffusive and convective mass transfer in a biocatalytic MBR. The most significant finding from the application of the developed model was that radial convective flows only improved bioreactor performance under internal-diffusional limitations. This result has significant implications in the future design and operation of MBRs. Prospective studies emanating from the current work are summarised in Chapter 6.

Nomenclature

B_m	constants of integration of Bessel's equation, m = 1, 2
c	substrate concentration (g dm^{-3})
c_b	bulk lumen concentration (g dm^{-3})
c_0	substrate feed concentration (g dm^{-3})
$C = c/c_0$	dimensionless substrate concentration
D_{AB}	substrate diffusivity (m^2 s^{-1})
$f = u_1/u_0$	fraction retentate
$J_n(\lambda)$	Bessel function of order n of the first kind
k_a	mass transfer coefficient (m s^{-1})
k_m	membrane hydraulic permeability (m Pa^{-1}s^{-1})
K_m	saturation (or Monod constant) (g dm^{-3})
$K_m^* = K_m/c_0$	dimensionless Monod constant
L	membrane effective length (m)
$M(a,b,\theta)$	Kummer function of the first kind
$Pe_u = u_0R_1/D_{AB}$	axial Peclet number
$Pe_v = v_0R_1/D_{AB}$	radial Peclet number
r	radial spatial coordinate (m)
$R = r/R_1$	dimensionless radial spatial coordinate
R_1	membrane lumen radius (m)
$Re = \rho u_0R_1/\mu$	Reynolds number
$Sc = \mu/\rho D_{AB}$	Schmidt number
$Sh = k_aR_1/D_{AB}$	Sherwood number
u	axial velocity (m s^{-1})
u_0	feed axial velocity (m s^{-1})
$U = u/u_0$	dimensionless axial velocity
v	radial velocity (m s^{-1})
$v_0 = k_m(p_0 - p_S)$	permeation velocity (m s^{-1})
$V = v/v_0$	dimensionless radial velocity
V_M	maximum rate of reaction (g dm^{-3} s^{-1})
X	average biofilm density (g dm^{-3})
$Y_{x/s}$	yield of biofim per unit substrate
z	axial spatial coordinate (m)
$Z = z/L$	dimensionless axial spatial coordinate

Greek letters

β	dimensionless transmembrane pressure
γ	membrane partition coefficient
$\delta = K_m/c_0C_b$	modified dimensionless Monod constant
$\epsilon = \frac{1}{\phi}$	substitution variable
η	effectiveness factor for general kinetics
η_0	effectiveness factor for zero-order kinetics
η_1	effectiveness factor for first-order kinetics
θ	substitution variable
$\kappa = \mu k_m L/R_1^2$	dimensionless membrane hydraulic permeability
λ_m	eigen values, m = 1, 2, …
μ	solution dynamic viscosity (Pa s)
μ_{max}	maximum specific growth rate (s^{-1})
ρ	solution density (kg m^{-3})
$\varphi = R_1/L$	aspect ratio
ϕ	Thiele modulus
Φ	normalized Thiele modulus
ψ	external resistance to mass transfer
Υ	fractional conversion

Acknowledgements

This work was funded by the National Research Foundation (NRF) of South Africa. Special thanks to Prof S.K. Ntwampe and Prof M.S. Sheldon for making available the data used in Figure **5.3**.

References

[1] Chang, H.N. & Furusaki, S. 1991. Membrane bioreactors: present and prospects. *Advances in Biochemical Engineering Biotechnology*, 44: 27-64.

[2] Giorno, L. & Drioli, E. 2000. Biocatalytic membrane reactors: applications and perspectives. *Trends in Biotechnology*, 18: 339-349.

[3] Charcosset, C. 2006. Membrane processes in biotechnology: an overview. *Biotechnology Advances*, 24: 482-492.

[4] Curcio, S., Calabro, V. & Iorio, G. 2006. A theoretical and experimental analysis of a membrane bioreactor performance in recycle configuration. *Journal of Membrane Science* 273, 129-142.

[5] Nagy, E. 2012. *Basic Equations of the Mass Transport Through a Membrane Layer*. Boston: Elsevier.

[6] Aris, R. 1975. *The mathematical theory of diffusion and reaction in permeable catalysts. vol. 1, The theory of the steady state*. Oxford: Clarendon.

[7] Webster, I.A. & Shuler, M.L. 1978. Mathematical models for hollow-fiber enzyme reactors. *Biotechnology and Bioengineering*, 20: 1541-1556.

[8] Webster, I.A., Shuler, M.L. & Rony, P.R. 1979. Whole-cell hollow fiber reactor: effectiveness factors. *Biotechnology and Bioengineering*, 21: 1725-1748.

[9] Willaert, R., Smets, A. & De Vuyst, L. 1999. Mass transfer limitations in diffusion-limited isotropic hollow fiber bioreactors. *Biotechnology Techniques*, 13: 317-323.

[10] Waterland, L.R., Michaelis, A.S. & Robertson, C.R. 1974. A theoretical model for enzymatic catalysis using asymmetric hollow fiber membranes. *American Institute of Chemical Engineers Journal*, 20: 50-59.

[11] Ye, H., Das, D.B., Triffitt, J.T. & Cui, Z. 2006. Modelling nutrient transport in hollow fiber membrane bioreactors for growing three-dimensional bone tissue. *Journal of Membrane Science,* 272: 169 – 178.

[12] Jayaraman, V.K. 1992. The solution of hollow fiber bioreactor design equations. *Biotechnology Progress*, 8: 462-464.

[13] Godongwana, B., Solomons, D. & Sheldon, M.S. 2010. A solution of the convective-diffusion equation for solute mass transfer inside a capillary membrane bioreactor. *International Journal of Chemical Engineering*, 2010: 1-12.

[14] Dall-Bauman, L., Ilias, S. & Govind, R. 1990. Analysis of hollow fiber bioreactor wastewater treatment. *Biotechnology and Bioengineering*, 35: 837-842.

[15] Tanyolac, A. & Beyenal, H. 1996. Effectiveness factor for a hollow-fiber biofilm reactor at maximum substrate consumption. *The Chemical Engineering Journal*, 62: 149-154.

[16] Jayaraman, V.K. & Kulkarni, B.D. 1997. An efficient algorithm for solving hollow-fiber bioreactor design equations. *The Chemical Engineering Journal*, 65:77-80.

[17] Calabro, V., Curcio, S. & Iorio, G. 2002. A theoretical analysis of transport phenomena in a hollow fiber membrane bioreactor with immobilized biocatalyst. *Journal of Membrane Science,* 206: 217-241.

[18] Gonzo, E.E. & Gottifredi, J.C. 2007. A simple and accurate method for simulation of hollow fiber biocatalyst membrane reactors. *Biochemical Engineering Journal*, 37: 80-85.

[19] Nagy, E., Dudás, J., Mazzei, R., Drioli, E. & Giorno, L. 2015. Description of the diffusive – convective mass transport in a hollow-fiber biphasic biocatalytic membrane reactor. *Journal of Membrane Science*, 482: 144-157.

[20] Godongwana, B., Solomons, D. & Sheldon, M.S. 2015. A finite difference solution of solute transport through a membrane bioreactor. *Mathematical Problems in Engineering*, 2015: 1-8.

[21] Lewandowski, Z. & Beyenal, H. 2007. *Fundamentals of Biofilm Research*. Boca Raton: CRC.

[22] Wickramasinghe, S.R., Garcia, J.D. & Han, B. 2002. Mass and momentum transfer in hollow fibre blood oxygenators. *Journal of Membrane Science*, 208: 247-256.

[23] Olver, F.W.J., Lozier, D.W., Boisvert, R.F. & Clark, C.W. (eds). 2010. *NIST handbook of mathematical functions.* New York: Cambridge University Press.

[24] Lieb, T.M. & Pereira, C.J. 2007. Reaction kinetics. In Green, D.W. & Perry, R.H. (eds). 2007. *Perry's chemical engineer's handbook*. 8th ed. New York: McGraw Hill.

[25] Ntwampe, S.K.O. & Sheldon, M.S. 2006. Quantifying growth kinetics of Phanerochaete chrysosporium immobilised on a vertically orientated polysulphone capillary membrane: biofilm development and substrate consumption. *Biochemical Engineering Journal*, 30: 147-151.

CHAPTER 6: GENERAL CONCLUSIONS AND PROSPECTS

6. GENERAL CONCLUSIONS AND PROSPECTS

6.1 Summary

The purpose of this study was to quantify the efficiency of a biocatalytic membrane reactor used for the production of enzymes. This was done by developing exact solutions of the concentration and velocity profiles in the different regions of the membrane bioreactor (MBR). The emphasis of this study was on the influence of radial convective flows, which have generally been neglected in previous analytical studies (Jayaraman, 1992; Willaert *et al*., 1999; Cabrera *et al*., 2001; Ye *et al*, 2006). The efficiency of the MBR was measured by means of the effectiveness factor.

In the first section of results, Chapter 3, an analytical model for substrate concentration profiles in the lumen of the MBR was developed. The model was based on the solution of the Navier-Stokes equations and Darcy's law for velocity profiles, and the convective-diffusion equation for the solute concentration profiles. The model allowed for the evaluation of the influence of both hydrodynamic and mass transfer operating parameters on the performance of the MBR. These parameters include the fraction retentate (f), the transmembrane pressure (β), the membrane hydraulic permeability (κ), the Reynolds number, the axial and radial Peclet numbers, and the dimensions of the MBR. The significant findings on the hydrodynamic studies were on the influence of the fraction retentate, defined as the ratio of the retentate (exit) and feed flowrates. This parameter defines the mode of operation of the MBR (f = 0 for the dead end mode, and f = 1 for the closed shell). In the dead-end mode it was found that there was increased radial convective flow, and hence more solute contact with the enzymes/biofilm immobilised on the surface of the membrane. The improved solute-biofilm contact however was only limited to the entrance half of the MBR. In the closed shell mode there was uniform distribution of solute, however, radial convective flows were significantly reduced. The developed model therefore allowed for the evaluation of an optimum f value, where both the distribution of solutes and radial convective flows could be maximised.

The concentration profiles developed from the analytical model were compared to the results of Heath and Belfort (Ye *et al.*, 2006). The model of Heath and Belfort was representative of the common assumptions made in developing concentration profiles in hollow fiber MBRs; and these include: (i) negligible axial diffusion, (ii) negligible membrane resistance to mass transfer, and (iii) negligible radial convective flows in the MBR. While there was good agreement between the two models, the abovementioned assumptions were shown to severely limit the applicability

of the latter model. As previously discussed, recent designs of MBRs seek to overcome diffusional limitations inherent in these devices by exploiting radial convective flows. The developed model from the current study allowed for the evaluation of the influence of axial diffusion, membrane resistance and radial convective flows on the solute concentration profiles in the MBR.

In Chapter 4 the second-order elliptic differential balance equation, with non-linear kinetics, was solved for concentration profiles in the MBR. The numerical scheme was executed using the Newton-Raphson algorithm, and was shown to be unconditionally stable for different step sizes. The significant findings from the FDM scheme was that the uniform solute distribution, in the open-shell mode, was more favourable for microbial growth than the dead-end mode. This result was consistent with the findings from the analytical solution (developed in Chapter 3), and also confirmed the tapering biofilm phenomenon observed by Godongwana *et al*. (2009). The numerical scheme of Chapter 4 served to validate the perturbation technique employed in Chapter 3, which was also the basis for the analysis in Chapter 5.

In Chapter 5 an exact solution of the effectiveness factor (η) for the MBR was presented as a function of the Thiele modulus (Φ), the Sherwood number (*Sh*), the Peclet number (*Pe*) and dimensions of the MBR. Effectiveness factor plots and their asymptotes were developed and compared to experimental data. Three regions of Thiele moduli were defined from the plots, corresponding with: kinetic control (Φ < 0.01), internal-diffusion control (0.01 < Φ < 0.1), and external mass transfer limitation (Φ > 0.1). It was shown that operation of the MBR at low Thiele moduli was not optimal since substrate conversion at these values was minimal. Conversely, at high Thiele moduli solute transport was limited by diffusion through the membrane. The developed model therefore allowed for the determination of the optimal Thiele modulus, at which both substrate conversion and the effectiveness factor were optimal.

The theoretical model developed for the effectiveness factor confirmed previous experimental studies, and a recent numerical analysis (Nagy *et al*, 2015), on the importance of radial convective flows on the performance of the MBR. The more significant finding from the current study was that radial convective flows improve bioreactor performance in a limited range of Thiele moduli, and this range was found to coincide with the region of internal diffusion limitation (0.01 < Φ < 0.1). Outside this range, the effectiveness factor was shown to be improved only by increased Sherwood numbers (or reduced “boundary layer” thickness). The maximum relative increase in the effectiveness factor ($\eta/\eta_{Pe=0}$) was observed to be in the transitional region from

kinetic to internal-diffusional control ($\Phi \approx 0.01$), and minimal in the boundary region between internal-diffusional control and external mass transfer limitation.

6.2 Prospects

- Mass transfer in MBRs is governed by the flow behavior (or fluid dynamics) of the nutrient feed, and this is greatly dependent on the mode of operation. In the dead-end mode it was shown that radial convective flows are improved, while non-uniform (or channeling) flows were also observed. The closed shell mode on the other hand was shown to produce more distributed flows, however radial convection was reduced in this mode. This result necessitates an optimisation study on the best mode of operation for improved distribution of solutes and radial convective flows.

- As previously discussed, an MBR should ideally operate in a reaction-limited regime rather than a diffusion-limited regime. However, it was shown in the current study that the reaction-limited regime is characterised by low substrate conversions. This result highlights the existence of an optimal Thiele modulus at which both substrate conversion and effectiveness factors are improved. Currently such optimisation studies are not available.

- The current study presented a novel mathematical analysis of the influence of convective flows on the performance of a catalytic membrane reactor, measured by the effectiveness factor. The differential balance (convective-diffusion) equations were solved analytically for the zero-order and first-order limiting forms of the Michaelis-Menten (or Monod) equation. The resulting concentration profiles were compared to results from an FDM numerical scheme based on non-linear kinetics. These results showed that at low Thiele moduli ($\Phi < 0.5$), the first-order kinetics assumption underestimates the effectiveness factor. Currently there are no analytical expressions of the effectiveness factor, when non-linear kinetics are assumed in the rate of consumption of solutes. Such solutions will provide for more efficient designs of MBRs, and form the basis for rigor optimization studies.

- Finally, in the solutions of both momentum and mass transfer differential balance equations transient states and angular variations were ignored. Extending the current

analysis to include both these effects may be important in designing process control mechanism during start-up, and for studying systems of non-cylindrical symmetry.

BIBILIOGRAPHY

BIBLIOGRAPHY

Abdullah, N.S., Jones, D.R. & Das, D.B. 2009. Nutrient transport in bioreactors for bone tissue growth: why do hollow fiber membrane bioreactors work? *Chemical Engineering Science,* 64: 109 – 125.

Aris, R. 1975. *The mathematical theory of diffusion and reaction in permeable catalysts. vol. 1, The theory of the steady state*. Oxford: Clarendon.

Bird, R.B., Stewart, W.E. & Lightfoot, E.N. 2002. *Transport phenomena.* 2nd ed. New York: John Wiley.

Biazar, J., Tango, M., Babolian, E. & Islam, R. 2003. Solution of the kinetic modelling of lactic acid fermentation using Adomian decomposition method. *Applied Mathematics and Computation,* 144: 433-439.

Bizukojc, M. & Ledakowicz, S. 2003. Morphological structured model for growth and citric acid accumulation by *aspergillus niger*. *Enzyme and Microbial Technology,* 32: 268-281.

Blanch, H.W. 1981. Microbial growth kinetics. *Chemical Engineering Communications,* 8: 181-211.

Brotherton, J.D. & Chau, P.C. 1995. Analysis of convective flow effects on the performance of an intercalated-spiral alternate-dead-ended hollow fiber bioreactor. *Chemical Engineering Science,* 50: 3813 – 3828.

Bungay, H.R., Humphrey, A.E. & Tsao, G.T. 1998. Biochemical engineering. In **Perry, R.H., Green, D.W. & Maloney, J.O.** (eds). 1998. *Perry's chemical engineer's handbook*. 7th ed. New York: McGraw Hill.

Calabro, V., Curcio, S. & Iorio, G. 2002. A theoretical analysis of transport phenomena in a hollow fiber membrane bioreactor with immobilized biocatalyst. *Journal of Membrane Science* 206, 217-241.

Cabrera, M.I., Luna, J.A. & Grau, R.J. 2001. Solving design equations for a hollow fiber bioreactor with arbitrary kinetics. *Chemical Engineering Journal*, 84: 445 – 461.

Catapano, G., Iorio, G., Drioli, E., Lombardi, C.P., Crucitti, F., Doglietto, G.B. & Bellantone, M. 1990. Theoretical and experimental analysis of a hybrid bioartificial membrane pancreas: a distributed parameter model taking into account Starling fluxes. *Journal of Membrane Science,* 52: 351 – 378.

Chang, H.N. & Furusaki, S. 1991. Membrane bioreactors: present and prospects. *Advances in Biochemical Engineering Biotechnology*, 44: 27-64.

Cicek, N. 2003. A review of membrane bioreactors and their potential application in the treatment of agricultural wastewater. *Canadian Biosystems Engineering*, 45: 6.37 - 6.49.

Contois, D.E. 1959. Kinetics of bacterial growth: relationship between population density and specific growth rate of continuous culture. *Journal of General Microbiology,* 21: 40.

Curcio, S., Calabro, V. & Iorio, G. 2006. A theoretical and experimental analysis of a membrane bioreactor performance in recycle configuration. *Journal of Membrane Science,* 273: 129 – 142.

Dall-Bauman, L., Ilias, S. & Govind, R. 1990. Analysis of hollow fiber bioreactor wastewater treatment. *Biotechnology and Bioengineering*, 35: 837-842.

De Jager, D. 2013. Membrane bioreactor application within the South African textile industry: pilot to full scale. Unpublished DTech thesis, Cape Peninsula University of Technology, Cape Town.

De Napoli, I.E., Zanetti, E.M., Fragomeni, G., Guizio, E., Audenino, A.L. & Catapano, G. 2014. Transport modelling of convection-enhanced hollow fiber membrane bioreactors for therapeutic applications. *Journal of Membrane Science,* 471: 347 – 361.

Doran, P.M. 2013. *Bioprocess engineering principles*. 2nd ed. London: Academic Press.

Eakman, J.M., Fredrickson, A.G. & Tsuchiya, H.M. 1966. Statistics and dynamics of microbial cell populations. *Chemical Engineering Progress Symposium Series,* 62: 37-49.

Giorno, L. & Drioli, E. 2000. Biocatalytic membrane reactors: applications and perspectives. *Trends in Biotechnology*, 18: 339 – 349.

Godin, F.B., Cooper, D.G. & Rey, A.D. 1999. Development and solution of a cell mass population balance model applied to the SCF process. *Chemical Engineering Science,* 54: 565-578.

Godongwana, B., Sheldon, M.S. & Solomons, D.M. 2007. Momentum transfer inside a vertically orientated capillary membrane bioreactor. *Journal of Membrane Science,* 303: 86 –99.

Godongwana, B., De Jager, D., Sheldon, M.S. & Edwards, W. 2009. The effect of Streptomyces coelicolor on the hydrodynamics of a vertically orientated capillary membrane bioreactor. *Journal of Membrane Science,* 303: 86 – 99.

Godongwana, B., Solomons, D. & Sheldon, M.S. 2010. A solution of the convective-diffusion equation for solute mass transfer inside a capillary membrane bioreactor. *International Journal of Chemical Engineering*, 2010: 1 – 12.

Heath, C. & Belfort, G. 1987. Immobilization of suspended mammalian cells: analysis of hollow fiber and microcapsule bioreactors. *Advances in Biochemical Engineering,* 34: 1-31.

Jayaraman, V.K. 1992. The solution of hollow fiber bioreactor design equations. *Biotechnology Progress*, 8: 462-464.

Kelsey, L.J., Pillarella, M.R. & Zydney, A.L. 1990. Theoretical analysis of convective flow profiles in a hollow fiber membrane bioreactor. *Chemical Engineering Science,* 45: 3211 – 3220.

Knazek R.A., Gullino, P.M., Kohler, P.O. & Dedrick, R.L. 1972. Cell culture on artificial capillaries: an approach to tissue growth in vitro. *Science,* 178: 65 – 67.

Koska, J., Bowen, B.D. & Piret, J.M. 1997. Protein transport in packed bed ultrafiltration hollow-fiber bioreactors. *Chemical Engineering Science,* 52: 2251 – 2263.

Labecki, M., Bowen, B.D. & Piret, J. M. 2001. Protein transport in ultrafiltration hollow-fiber bioreactors for mammalian cell culture. In Wang, W.K. (ed). 2001. *Membrane separations in biotechnology*. New York: Marcel Dekker.

Lee, J. & Kim, D.H. 2006. An approximation method for the effectiveness factor in porous catalysts. *Chemical Engineering Science,* 61: 5127 – 5136.

Leukes, W.D. 1999. Development and characterisation of a membrane gradostat bioreactor for the bioremediation of aromatic pollutants using white rot fungi. Unpublished PhD thesis, Rhodes University, Grahamstown.

Lewandowski, Z. & Beyenal, H. 2007. *Fundamentals of biofilm research*. Boca Raton: CRC.

Li, K. & Tan, X. 2001. Mass transfer and chemical reaction in hollow-fiber membrane reactors. *American Institute of Chemical Engineers Journal,* 47: 427-435.

Liou, J.-J., Srienc, F. & Friedrickson, A.G. 1997. Solutions of population balance models based on a successive generations approach. *Chemical Engineering Science,* 52: 1529-1540.

Mantzaris, N.V., Liou, J-J., Daoutidis, P. & Srienc, F. 1999. Numerical solution of a mass structured cell population balance model in an environment of changing stubstrate concentration. *Journal of Biotechnology,* 71: 157-174.

Merchuk, J.C. & Asenjo, J.A. 1994. Fundamentals of bioreactor design. In **Asenjo, J.A. & Merchuk, J.C.** (eds). 1994. *Bioreactor system design*. Boca Raton: CRC Press.

Mitchell, D.A., Von Meien, O.F., Krieger, N. & Dalsenter, F.D.H. 2004. A review of recent developments in modelling of microbial growth kinetics and intraparticle phenomena in solid-state fermentation. *Biochemical Engineering Journal,* 17: 15-26.

Monod, J. 1949. The growth of bacterial cultures. *Annual Review of Microbiology,* 3: 371–394.

Montgomery, R. 2004. Development of biobased products. *Bioresource Technology,* 91: 1 –21.

Moser, H. 1958. The dynamics of bacterial populations maintained in the chemostat. *Carnegie Institution of Washington Publication* 614. Washington D.C.

Moussy, Y. 2003. Convective flow through a hollow fiber bioartificial liver. *Artificial Organs,* 27: 1041 – 1049.

Nagy, E. 2009. Basic equations of mass transfer through biocatalytic membrane layer. *Asia-Pacific Journal of Chemical Engineering,* 4: 270 – 278.

Nagy, E. & Kulcsar, E. 2009. Mass transport through biocatalytic membrane reactor. *Desalination,* 245: 422 – 436.

Nagy, E. 2012. *Basic Equations of the Mass Transport Through a Membrane Layer*. Boston: Elsevier.

Nagy, E., Lepossa, A. & Prettl, Z. 2012. Mass transfer through a biocatalytic membrane reactor. *Industrial and Engineering Chemistry Research,* 51:1636 – 1646.

Nagy, E., Dudás, J., Mazzei, R., Drioli, E. & Giorno, L. 2015. Description of the diffusive – convective mass transport in a hollow-fiber biphasic biocatalytic membrane reactor. *Journal of Membrane Science*, 482: 144 – 157.

Narang, A. & Pilyugin, S.S. 2007. Bacterial gene regulation in diauxic and non-diauxic growth. *Journal of Theoretical Biology,* 244: 326-348.

Nielsen, J., Nikolajsen, K. & Villadsen, J. 1991. Structured modeling of a microbial system: 1. a theoretical study of lactic acid fermentation. *Biotechnology and Bioengineering,* 38: 1-10.

Nielsen, J. 1992. Modelling the growth of filamentous fungi. *Advances in Biochemical Engineering/Biotechnology,* 46: 187-223.

Nielsen, J. & Villadsen, J. 1992. Modelling of microbial kinetics. *Chemical Engineering Science,* 47: 4225-4270.

Nielsen, J. 2006. Microbial process kinetics. In **Ratledge, C. & Kristiansen, B.** (eds). 2006. *Basic biotechnology*. 3rd ed. Cambridge: Cambridge University Press.

Ntwampe, S.K.O. & Sheldon, M.S. 2006. Quantifying growth kinetics of Phanerochaete chrysosporium immobilised on a vertically orientated polysulphone capillary membrane: biofilm development and substrate consumption. *Biochemical Engineering Journal*, 30: 147-151.

Okpokwasili, G.C. & Nweke, C.O. 2005. Microbial growth and substrate utilization kinetics. *African Journal of Biotechnology,* 5: 305-317.

Olver, F.W.J., Lozier, D.W., Boisvert, R.F. & Clark, C.W. (eds). 2010. *NIST handbook of mathematical functions.* New York: Cambridge University Press.

Ramkrishna, D. 1979. Statistical models of cell populations. *Advances in Biochemical Engineering,* 11: 1-48.

Rony, P.R. 1971. Multiphase catalysis. II. Hollow-fiber catalysis. *Biotechnology and Bioengineering,* 13: 431 – 447.

Salmon, P.M. & Robertson, C.R. 1994. In **Asenjo, J.A. & Merchuk, J.C.** (eds). 1994. *Bioreactor system design*. Boca Raton: CRC Press.

Sartor, M., Kaschek, M. & Mavrov, V. 2008. Feasibility study for evaluating the client application of membrane bioreactor (MBR) technology for decentralised municipal waste water treatment in Vietnam. *Desalination,* 224: 172 – 177.

Sheldon, M.S. & Small, H.J. 2005. Immobilisation and biofilm development of *Phanerochaete chrysosporium* on polysulphone and ceramic membranes. *Journal of Membrane Science,* 263: 30-37.

Sheldon, M.S. 2008. Modelling and scale-up of a membrane gradostat bioreactor. Unpublished DTech thesis, Cape Peninsula University of Technology, Cape Town.

Sheldon, M.S., Mohammed, K. & Ntwampe, S.K.O. 2008. An investigation of biphasic growth kinetics for Phanerochaete chrysosporium (BKMF-1767) immobilised in a membrane gradostat reactor using flow-cells. *Enzyme and Microbial Technology,* 42: 353 – 361.

Shuler, M.L. & Kargi, F. 2014. *Bioprocess engineering*. 2nd ed. New Jersey: Pearson.

Sonmezisik, M., Tanyolac, D., Seker, S. & Tanyolac, A. 1998. The double-substrate growth kinetics of *sulfolobus solfataricus*, a thermophilic sulphur-removing archeabacterum. *Biochemical Engineering Journal,* 1: 243-248.

Taylor, D.G., Piret, J.M. & Bowen, B.D. 1994. Protein polarization in isotropic membrane hollow-fiber bioreactors. *American Institute of Chemical Engineers Journal,* 40: 321 – 333.

Tien, M. & Kirk, T.K. 1988. Lignin peroxidase of *Phanerochaete chrysosporium*. *Methods in Enzymology*, 16: 238-249.

Truskey, G.A., Yuan, F. & Katz, D.F. 2009. *Transport phenomena in biological systems*. New Jersey: Prentice Hall.

Tsuchiya, H.M., Fredrickson, A.G. & Aris, R. 1966. Dynamics of microbial cell populations. *Advances in Chemical Engineering,* 6: 125-206

Van Reis, R. & Zydney, A. 2007. Bioprocess membrane technology. *Journal of Membrane Science,* 297: 16 – 50.

Webster, I.A., Shuler, M.L. & Rony, P.R. 1979. Whole-cell hollow fiber reactor: effectiveness factors. *Biotechnology and Bioengineering*, 21: 1725-1748.

Willaert, R. Smets, A. & De Vuyst, L. 1999. Mass transfer limitations in diffusion-limited isotropic hollow fiber bioreactors. *Biotechnology Techniques,* 13: 317-323.

Ye, H., Das, D.B., Triffitt, J.T. & Cui, Z. 2006. Modelling nutrient transport in hollow fiber membrane bioreactors for growing three-dimensional bone tissue. *Journal of Membrane Science,* 272: 169 – 178.

APPENDIX A: The Lumen Region

APPENDIX A

A.1 Momentum transfer analysis

The *z*-component of the non-conservative form of the Navier-Stokes equation in cylindrical coordinates is made dimensionless by introducing the variables in Eq. (3.3) and the following additional variables:

$$P = \frac{pR_1^2}{\mu u_0 L}; \quad \tau = \frac{\mu t}{\rho R_1^2}; \quad Fr = \frac{u_0^2}{gR_1} \tag{A.1}$$

where *p* and *P* are the fluid pressure and dimensionless fluid pressure, respectively; *t* and τ are the time and dimensionless time, respectively; μ is the solution dynamic viscosity; and *Fr* is the Froude number. The dimensionless form of the Navier-Stokes thus becomes:

$$\frac{\partial U}{\partial \tau} = \left[\frac{1}{R}\frac{\partial}{\partial R}\left(R\frac{\partial U}{\partial R}\right) + \varphi^2\frac{\partial^2 U}{\partial Z^2}\right] - \frac{dP}{dZ} + \frac{Re}{Fr} \tag{A.2}$$

and the continuity equation:

$$\frac{1}{R}\frac{\partial (RV)}{\partial R} = -\varphi\left(\frac{u_0}{v_0}\right)\frac{\partial U}{\partial Z} \tag{A.3}$$

Ignoring normal stresses $\frac{\partial^2 U}{\partial Z^2}$ and considering steady-state conditions, the solution of Eq. (A.2) is obtained by integrating twice and making use of the boundary conditions listed in Table 3.1 (B.C.4 and B.C.5) to obtain:

$$U = -\frac{1}{4}(1 - R^2)\left(\frac{dP}{dZ} - \frac{Re}{Fr}\right) \tag{A.4}$$

The dimensionless radial velocity profile *V* is obtained by substituting Eq. (A.4) into Eq. (A.3) and imposing B.C. 6 (Table 3.1):

$$V = \varphi\left(\frac{u_0}{v_0}\right)\left[\frac{R}{8}\left(1 - \frac{R^2}{2}\right)\right]\frac{d^2 P}{dZ^2} \tag{A.5}$$

The dimensionless pressure profile *P* is obtained by imposing B.C.7, where the matrix velocity V_M is governed by Darcy's law:

$$V_M = -\left(\frac{u_0}{v_0}\right)\kappa(P_S - P_0) \tag{A.6}$$

where the dimensionless membrane hydraulic permeability κ is given by:

$$\kappa = \frac{\mu k_m L}{R_1^2} \tag{A.7}$$

Substituting Eq. (A.5) and (A.6) into Eq. (3.7g) results in:

$$\frac{\varphi}{16}\frac{d^2P}{dZ^2} = -\kappa(P_S - P_0) \tag{A.8}$$

Eq. (A.8) is solved by applying B.C.8 to give:

$$P = \beta cosh\left(4\sqrt{\varphi^{-1}\kappa}\right)Z + \frac{\varphi a}{4\sqrt{\varphi^{-1}\kappa}} sinh\left(4\sqrt{\varphi^{-1}\kappa}\right)Z + P_S \tag{A.9}$$

where the dimensionless entrance pressure drop *a* in Eq. (A.9) is obtained by defining a fraction retentate, *f*, as the ratio of the exit to the inlet velocity, i.e. $f = U_1/U_0$:

$$a = \frac{4\sqrt{\varphi^{-1}\kappa}\beta sinh\left(4\sqrt{\varphi^{-1}\kappa}\right) - ReFr^{-1}(1-f)}{\varphi\left[f - cosh\left(4\sqrt{\varphi^{-1}\kappa}\right)\right]} \tag{A.10}$$

A.2 Solution of the coefficient B_{1m}

Imposing the inlet condition Eq. (3.7a) into Eq. (3.46) gives:

$$C(\theta_0, x) = \sum_{m=1}^{\infty}\sum_{n=0}^{N} F_m(\theta_0)T_n(x)\kappa^n = 1, \quad at\ Z = 0 \tag{A.11}$$

For the zero-order approximation of the radial function *T(R)*, Eq. (A.11) becomes:

$$\sum_{m=1}^{\infty} M\left(\frac{A\lambda_m^2}{2\varphi^2}, \frac{1}{2}, \theta_0\right) B_{1m} J_0(\lambda_m R) = 1, \quad at\ Z = 0 \tag{A.12}$$

Equation (3.29) is a Sturm-Liouville type differential equation, thus the eigenfuctions of Eq. (3.29) are orthogonal. This property allows for the solution of B_{1n} in Eq. (A.12) by multiplying both the L.H.S. and the R.H.S. by $J_0(\lambda_{mx}R)R$ and integrating with respect to R over the interval 0 – 1.

$$\int_0^1 J_0(\lambda_{mx}R)R\left\{\sum_{m=1}^{\infty} M\left(\frac{A\lambda_m^2}{2\varphi^2},\frac{1}{2},\theta_0\right)B_{1m}J_0(\lambda_m R)\right\}dR = \int_0^1 J_0(\lambda_{mx}R)RdR \tag{A.13}$$

The R.H.S. of Eq. (A.13) is evaluated by making use of the following property of Bessel functions:

$$\int_0^z r^v J_{v-1}(r)dr = z^v J_v(z) \tag{A.14}$$

The R.H.S of Eq. (A.13) then becomes:

$$R.H.S. = \frac{J_1(\lambda_{mx})}{\lambda_{mx}} \tag{A.15}$$

The L.H.S of Eq. (A.13) may be evaluated by making use of Lommel integrals:

$$\int_0^x J_n(\alpha_k r)J_n(\alpha_m r)rdr = 0 \quad (k \neq m) \tag{A.16}$$

$$\int_0^x rJ_n^2(\alpha_m r)dr = \frac{x^2}{2}\left[J_n'(\alpha_m x)^2 + \left(1 - \frac{n^2}{\alpha_m^2 x^2}\right)J_n^2(\alpha_m x)\right] \tag{A.17}$$

To give the following equation:

$$L.H.S. = \frac{B_{1m}}{2}M\left(\frac{A\lambda_m^2}{2\varphi^2},\frac{1}{2},\theta_0\right)[J_0^2(\lambda_m) + J_1^2(\lambda_m)] \tag{A.18}$$

Substituting Eqs. (A.15) and (A.18) back into the R.H.S. and L.H.S. of Eq. (A.13), respectively:

$$B_{1m} = \frac{2}{\lambda_m M\left(\frac{A\lambda_m^2}{2\varphi^2},\frac{1}{2},\theta_0\right)}\left[\frac{J_1(\lambda_m)}{J_0^2(\lambda_m) + J_1^2(\lambda_m)}\right] \tag{A.19}$$

A.3 Mathematical architecture for the solution of *T*(*x*)

We define a parameter *p* in Laplace space as:

$$p = \frac{1}{\sqrt{1+s^2}} \tag{A.20}$$

Such that the Laplace transform of the function we are evaluating, e.g. $J_n(x)$, can be expressed in terms of this parameter. The properties of the parameter *p* can easily be extrapolated. The following properties of *p* are all noteworthy, differentiation:

$$p' = -sp^3 \tag{A.21}$$

Integration:

$$\int p^n s ds = \frac{p^{n-2}}{2-n}, \quad n \neq 2 \tag{A.22}$$

Inverse Laplace Transform:

$$\begin{gathered} \mathcal{L}^{-1}\{p\} = J_0(x) \\ \mathcal{L}^{-1}\{p^{2n+1}\} = \frac{x^n J_n(x)}{(2n-1)!!} \end{gathered} \tag{A.23}$$

Laplace Transforms involving the first-order Bessel function:

$$\mathcal{L}^{-1}\{J_1(x)\} = 1 - sp \tag{A.24}$$

More relations involving *p*:

$$s^2 = p^{-2} - 1 \tag{A.25}$$

$$\begin{gathered} \frac{d}{ds}[1-sp] = -p^3, \quad and \ \frac{d^2}{ds^2}[1-sp] = 3sp^5 \\ \frac{d^3}{ds^3}[1-sp] = 15p^7 - 12p^5, \quad and \ \frac{d^4}{ds^4}[1-sp] = 60sp^7 - 105sp^9 \end{gathered} \tag{A.26}$$

We also define the following polynomial in *p*, which is significant for the first and second-order approximations of *T*(*x*) in Sections A.4 and A.5, respectively:

$$u(p) = p^5 + i_1 p^7 + i_2 p^9 \tag{A.27}$$

Then it is easy to show that the second derivative of the product *su*(*p*) with respect to the Laplace variable *s* is:

$$\frac{d^2}{ds^2}[su(p)] = s[20p^7 + 7(6i_1 - 5)p^9 + 9(8i_2 - 7i_1)p^{11} + 99i_2p^{13}] \tag{A.28}$$

The fourth derivative of the product *su*(*p*) with respect to the Laplace variable *s* is:

$$\begin{aligned}\frac{d^4}{ds^4}[su(p)] = s[&840p^9 - 63(60 - 48i_1)p^{11} + 9 \cdot 11(35 - 112i_1 + 80i_2)p^{13} - \quad 9 \cdot 11 \\ &\cdot 13(20i_2 - 7i_1)p^{15} + 9 \cdot 11 \cdot 13 \cdot 15i_2p^{17}]\end{aligned} \tag{A.29}$$

Both Eqs. (A.28) and (A.29) will become important in Section A.5.

A.4 Solution of the first-order approximation function, $T_1(x)$, in Eq. (3.40)

If the function *g*(*s*) is taken as the Laplace transform of the function $T_1(x)$, i.e. $\mathcal{L}\{T_1(x)\} = g(s)$, then the Laplace transform of Eq. (3.40) yields:

$$-s^2\frac{d}{ds}g(s) - sg(s) - \frac{d}{ds}g(s) = \frac{\delta}{2\lambda_m^4}\{\mathcal{L}[x^4J_1(x)] - 2\lambda_m^2\mathcal{L}[x^2J_1(x)]\} \tag{A.30}$$

In terms of the parameter *p*, defined in Section A.3, this equation may be written as:

$$p^{-2}\frac{d}{ds}g(s) + sg(s) = -\frac{\delta}{2\lambda_m^4}\left\{\frac{d^4}{ds^4}(1 - sp) - 2\lambda_m^2\frac{d^2}{ds^2}(1 - sp)\right\} \tag{A.31}$$

The right-hand side of Eq. (A.31) is evaluated from the relations involving *p* in Section A.3 (A.26). Multiplying through by *p* Eq. (A.31) becomes:

$$\frac{d}{ds}[p^{-1}g(s)] = -\frac{\delta}{2\lambda_m^4}\{-60sp^8 + 105sp^{10} + 6\lambda_m^2sp^6\} \tag{A.32}$$

Integrating Eq. (A.32) with respect to *s*, to find the Laplace space solution:

$$g(s) = -\frac{3\delta}{4\lambda_m^2}\left(p^5 - \frac{20}{3\lambda_m^2}p^7 + \frac{35}{4\lambda_m^2}p^9\right) \tag{A.33}$$

For convenience of expressing the solutions of the first and second-order approximations, $T_1(x)$ and $T_2(x)$ respectively, the following constants and function are defined:

$$g(s) = i_3 u(p) \tag{A.34}$$

$$i_1 = -\frac{20}{3\lambda_m^2}, \quad i_2 = \frac{35}{4\lambda_m^2}, \quad i_3 = -\frac{3\delta}{4\lambda_m^2} \tag{A.35}$$

The polynomial $u(p)$ in Eq. (A.34) was defined in Eq. (A.27). The inverse Laplace transform of the function $g(s)$ in Eq. (A.33) is the solution of $T_1(x)$:

$$T_1(x) = \mathcal{L}^{-1}\{g(s)\} = i_3\mathcal{L}^{-1}\{p^5 - i_1 p^7 + i_2 p^9\} = i_3\left[\frac{x^2 J_2(x)}{3!!} + i_1\frac{x^3 J_3(x)}{5!!} + i_2\frac{x^4 J_4(x)}{7!!}\right] \tag{A.36}$$

A.5 Solution of the second-order approximation function, $T_2(x)$, in Eq. (3.43)

Similar to the first-order approximation, the Laplace transform of the second-order approximation, for $\mathcal{L}\{T_2(x)\} = h(s)$, yields:

$$-s^2\frac{d}{ds}h(s) - sh(s) - \frac{d}{ds}h(s) = \frac{\delta}{2\lambda_m^4}\{\mathcal{L}[x^4 T_1'(x)] - 2\lambda_m^2\mathcal{L}[x^2 T_1'(x)]\} \tag{A.37}$$

In terms of the parameter p, defined in Section A.3, this equation may be written as:

$$p^{-2}\frac{d}{ds}h(s) + sh(s) = -\frac{2i_3^2}{3\lambda_m^2}\left\{\frac{d^4}{ds^4}su - 2\lambda_m^2\frac{d^2}{ds^2}su\right\} \tag{A.38}$$

The expressions for the second and fourth derivatives of $su(p)$ are given in Section A.3 (A.28-A.29). The first order differential equation in $h(s)$ has an integrating factor p^{-1}, so again Eq. (A.38) is multiplied by p to obtain:

$$\begin{aligned}\frac{d}{ds}[p^{-1}h(s)] = \frac{2i_3^2 s}{3\lambda_m^4}\{&[840p^{10} - 63(60 - 48i_1)p^{12} + 99(35 - 112i_1 + 80i_2)p^{14} + 9\cdot 11\\ &\cdot 13(7i_1 - 20i_2)p^{16} + 9\cdot 11\cdot 13\cdot 15 i_2 p^{18}]\\ &- 2\lambda_m^2[20p^8 + 7(6i_1 - 5)p^{10} + 9(8i_2 - 7i_1)p^{12} - 99 i_2 p^{14}]\}\end{aligned} \tag{A.39}$$

The integral of Eq. (A.39), after simplifying by grouping terms with like powers of *p*, is:

$$
\begin{aligned}
p^{-1}h(s) = \frac{2i_3^2}{3\lambda_m^2}\Bigg\{ & \frac{20}{3}\lambda_m^2 p^6 - \left[105 - \frac{7}{3}\lambda_m^2(6i_1 - 5)\right]p^8 \\
& + \frac{9}{10}[7(60 - 48i_1) + 2\lambda_m^2(8i_2 - 7i_1)]p^{10} \\
& - \frac{9\cdot 11}{12}[(35 - 112i_1 + 80i_2) + 2\lambda_m^2 i_2]p^{12} - \frac{9\cdot 11\cdot 13}{14}(7i_1 - 20i_2)p^{14} \\
& - \frac{9\cdot 11\cdot 13\cdot 15}{16} i_2 p^{16}\Bigg\}
\end{aligned}
\tag{A.40}
$$

Recalling that $\mathcal{L}\{T_2(x)\} = h(s)$, the second order approximation of Eq. (3.25) is simply the inverse Laplace transform of Eq. (A.40):

$$
\begin{aligned}
T_2(x) = \frac{3\delta^2}{2\lambda_m^6}\Bigg\{ & \frac{20}{3}\lambda_m^2 \frac{x^3 J_3(x)}{5!!} - \left[105 - \frac{7}{3}\lambda_m^2(6i_1 - 5)\right]\frac{x^4 J_4(x)}{7!!} \\
& + \frac{9}{10}[7(60 - 48i_1) + 2\lambda_m^2(8i_2 - 7i_1)]\frac{x^5 J_5(x)}{9!!} \\
& - \frac{9\cdot 11}{12}[(35 - 112i_1 + 80i_2) + 2\lambda_m^2 i_2]\frac{x^6 J_6(x)}{11!!} \\
& - \frac{9\cdot 11\cdot 13}{14}(7i_1 - 20i_2)\frac{x^7 J_7(x)}{13!!} - \frac{9\cdot 11\cdot 13\cdot 15}{16} i_2 \frac{x^8 J_8(x)}{15!!}\Bigg\}
\end{aligned}
\tag{A.41}
$$

APPENDIX B: Biocatalytic Matrix

APPENDIX B

B.1 Architecture for the solution

The solution of the solute concentration profile through the membrane matrix follows the same procedure given in Appendix A (A.3 – A.5) for the lumen. However, Eq. (5.17) is the modified Bessel equation instead of the Bessel equation described in Appendix A. We now define the parameter *p* as:

$$p = \frac{1}{\sqrt{s^2 - 1}} \tag{B.1}$$

With the following inverse Laplace transform properties:

$$\mathcal{L}^{-1}\{p\} = I_0(x)$$
$$\mathcal{L}^{-1}\{p^{2n+1}\} = \frac{\sqrt{\pi}}{\Gamma(n + 1/2)}\left(\frac{x}{2}\right)^n I_n(x) \tag{B.2}$$

B.2 Biocatalytic membrane concentration profile

The solution of Eq. (5.15) may be approximated by an asymptotic expansion:

$$C_2 = C_2^{(0)} + \kappa C_2^{(1)} + \kappa^2 C_2^{(2)} + \cdots \kappa^n C_n^{(n)} \tag{B.3}$$

The zero-order approximation $C_2^{(0)}$ was given in Section 5.2.3 as:

$$C_2^{(0)} = B_1 I_0(\phi R) + B_2 K_0(\phi R) \tag{B.4}$$

The first-order approximation $C_2^{(1)}$ is a solution of the equation:

$$\frac{d^2 C_2^{(1)}}{dR^2} + \frac{1}{R}\frac{dC_2^{(1)}}{dR} + \phi^2 C_2^{(1)} = 2Pe_u\beta\left[R\left(1 - \frac{R^2}{2}\right)\right]\frac{dC_2^{(0)}}{dR} \tag{B.5}$$

The modified Bessel function $K_v(x)$ tends to zero as $|x| \to \infty$ for all values of *v*. The contribution of this function in Eq. (B.5) is therefore only significant as $x \to 0$. In this region the limiting form of $K_v(x)$ is (Olver *et al.*, 2010):

$$K_v(x) \sim \frac{1}{2}\Gamma(v)\left(\frac{1}{2}x\right)^{-v} \quad (v > 0) \tag{B.6}$$

where $\Gamma(n)$ is the Gamma function. Making use of the architecture in Section B.1 and following the procedure in Appendix A, the first-order approximation is given by:

$$C_2^{(1)} = \frac{Pe_u \beta \kappa}{\phi^2}\left\{\frac{3\sqrt{\pi}B_1}{2}\left[\frac{(\phi R)^2 I_2(\phi R)}{2^2\Gamma\left(2\frac{1}{2}\right)} + \alpha_1 \frac{(\phi R)^3 I_3(\phi R)}{2^3\Gamma\left(3\frac{1}{2}\right)} + \alpha_2 \frac{(\phi R)^4 I_4(\phi R)}{2^4\Gamma\left(4\frac{1}{2}\right)}\right] - \frac{B_2}{\phi^2}[(\phi R)^2 - 2\phi^2 + 4]\right\} \tag{B.7}$$

where

$$\alpha_1 = -\frac{20}{3\phi^2}, \quad \text{and} \quad \alpha_2 = -\frac{35}{4\phi^2} \tag{B.8}$$

The effectiveness factor is obtained by substituting the derivatives of Eqs. (B.4) and (B.7) into Eq. (5.28), making use of the following property of Bessel functions (Olver *et al.*, 2010):

$$\left(\frac{1}{z}\frac{d}{dz}\right)^k \{z^v I_v(z)\} = z^{v-k} I_{v-k}(z) \tag{B.9}$$

This gives:

$$\eta = \frac{2\gamma[K_1(\phi)\cdot I_1(\phi R_2) - I_1(\phi)\cdot K_1(\phi R_2) - \xi]}{\phi(R_2^2 - 1)\{[K_0(\phi)\cdot I_1(\phi R_2) + I_0(\phi)\cdot K_1(\phi R_2)] + \psi\}} \tag{B.10}$$

where

$$\xi = Pe_u \beta \kappa \left\{\frac{3\sqrt{\pi}\cdot K_1(\phi R_2)}{8}\left[\frac{I_1(\phi)}{\Gamma\left(2\frac{1}{2}\right)} + \alpha_1 \frac{\phi I_2(\phi)}{2\Gamma\left(3\frac{1}{2}\right)} + \alpha_2 \frac{\phi^2 I_3(\phi)}{4\Gamma\left(4\frac{1}{2}\right)}\right] - \frac{2I_1(\phi R_2)}{\phi^3}\right\} \tag{B.11}$$

B.3 Asymptotic solution of the Effectiveness factor ($\phi \to \infty$)

Eq. (5.17) may be written as:

$$\frac{\epsilon^2}{R}\frac{d}{dR}\left(R\frac{dC_2}{dR}\right) - C_2 = 0 \tag{B.12}$$

where:

$$\epsilon = \frac{1}{\phi} \tag{B.13}$$

The solution of Eq. (5.17) may be approximated by an asymptotic expansion when $\epsilon \ll 1$ as:

$$C_2 = \sum_{n=0}^{N} \epsilon^n b_n \tag{B.14}$$

In order to keep the second-order derivative in the solution of the coefficient b_0 in Eq. (B.14), the following variable is defined:

$$\omega = \frac{1-R}{\epsilon} \tag{B.15}$$

Eq. (B.12) then becomes:

$$\frac{d^2C_2}{d\omega^2} - \frac{\epsilon}{(1-\epsilon\omega)}\frac{dC_2}{d\omega} - C_2 = 0 \tag{B.16}$$

The leading order term sub-problem is:

$$\frac{d^2b_0}{d\omega^2} - b_0 = 0 \tag{B.17}$$

The corresponding boundary conditions are B.C.4 and B.C.5 of Eq. (5.3):

$$\left.\frac{db_0}{d\omega}\right|_{\omega=0} = \epsilon Sh\left[C_b - \frac{b_0(0)}{\gamma}\right] \tag{B.18a}$$

and

$$\left.\frac{db_0}{d\omega}\right|_{\omega=(1-R_2)/\epsilon} = 0 \tag{B.18b}$$

The solution of Eq. (B.17), subject to the boundary conditions of Eq. (B.18) is:

$$b_0 = \Lambda_1 e^{\omega} + \Lambda_2 e^{-\omega} \tag{B.19}$$

where

$$\Lambda_1 = \frac{1}{\phi\left(1+\frac{Sh}{\phi\gamma}\right)}\left\{\frac{\left(1-\frac{Sh}{\phi\gamma}\right)ShC_b e^{-[\phi(R_2-1)]}}{sinh[\phi(R_2-1)] + \frac{Sh}{\phi\gamma}cosh[\phi(R_2-1)]} + ShC_b\right\} \tag{B.20}$$

and

$$\Lambda_2 = \frac{1}{\phi}\left\{\frac{ShC_b e^{-[\phi(R_2-1)]}}{sinh[\phi(R_2-1)] + \frac{Sh}{\phi\gamma}cosh[\phi(R_2-1)]}\right\} \tag{B.21}$$

The effectiveness factor is obtained by taking the derivative of Eq. (B.19) and substituting into Eq. (5.28) to obtain:

$$\frac{1}{\eta_1} \sim \frac{\phi(R_2^2-1)}{2}\left\{\frac{\phi}{Sh} + \frac{1}{\gamma}coth[\phi(R_2-1)]\right\} \tag{B.22}$$

APPENDIX C: Materials and Methods

APPENDIX C

C.1 Introduction

This section provides a description of the materials and methods that were used to validate the theoretical models developed in Chapters 3 - 5. A summary of the procedures that were used to prepare the reagents and the fungus will be given. The experimental procedure that were followed to cultivate *P. chrysosporium* for continuous enzyme production, in a single fibre capillary membrane bioreactor (MBR), was previously explained by Leukes (1999); Sheldon and Small (2005); Ntwampe and Sheldon (2006); Godongwana *et al.* (2007).

C.2 Description of materials

C.2.1 Microorganism

The WRF, *P. chrysosporium* strain BKM-F-1767 (ATCC 24725), was used in all the experiments. Cultures of the fungus were maintained on supplemented malt agar slants, and were grown on petri plates containing growth medium at 37ºC, according to Tien and Kirk (1988). The resulting mycelia was homogenised with sterile distilled water, to form a spore-mycelia mixture, which was then filtered to obtain a pure spore solution. The pure spore solution was freeze-dried to a temperature of -70ºC and stored at 4ºC. For an experimental run the freeze-dried spores were homogenised, with sterile distilled water, to make up the required spore solution concentration. For each biofilm growth experimental run 3×10^6 spores were prepared and inoculated onto the external skin of the capillary polysulphone membrane using reverse filtration.

C.2.2 Nutrient medium

A nutrient medium was used to provide the fungus with low-molecular mass nutrient sources, such as carbon and nitrogen, and was also the standard medium as described by Tien and Kirk (1988). The nutrient medium contained (in 1 liter): 100ml Basal medium, 100ml of 10% glucose stock solution, 100ml of 0.1M 2,2-dimethylsuccinate, 10ml thiamin, 25ml ammonium tartrate, 100ml of 0.02M veratryl alcohol, 60ml trace elements, and 505ml of sterile distilled water. The nutrient medium was supplied through the membrane lumen to the fungus, immobilized on the external skin of the capillary membrane, at a flow rate of 6.20 ml/hr using a Watson Marlow 505S perilstatic pump (Dune Engineering, RSA).

C.2.3 Polysulphone capillary membrane

The MBR used in this study consisted of a single capillary, made of surface modified polysulphone, encased in a glass bioreactor. The capillary membranes were produced and supplied by the Institute of Polymer Science at the University of Stellenbosch (RSA). The membranes are characterized by an internally skinned and externally un-skinned region of microvoids, approximately 0.15mm long and 0.015mm thick, as shown by the scanning electron microscope (SEM) image in Figure C.1. These membranes have inner diameters of approximately 1.395mm and outer diameters of 1.925mm.

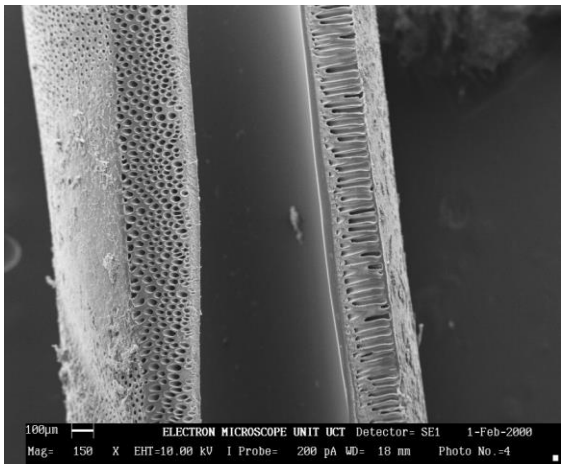

Figure C.1: An SEM image of the capillary membrane (Godongwana *et al.* 2007).

C.2.4 Air pump

A Hailea ACO 9220 diaphragm air pump was used to supply humidified air to the shell of the MBR at a throughput 240 L/hr. The air supplied by the pump was filter-sterilised, using a 0.22µm Cameo filter, before being fed to the humidifier.

C.2.5 Humidifier

A 500ml Schott bottle, half-filled with sterile distilled water, was used as a humidifier. The humidifier was connected to the MBR and the diaphragm air pump by silicone tubing (ID = 3cm; OD = 5cm). The air from the diaphragm pump was first filter-sterilised and humidified before being fed to the shell side of the MBR.

C.2.6 Pressure transducers

The MBR was fitted with two Vega (United Kingdom) pressure transducers (model: BAR14.X1CA1GV1), which were connected to a computer for online pressure readings. The two pressure transducers were connected at the inlet and outlet of the MBR, as previously shown in Figure 3.1. LabView® was utilised for acquiring, transforming and displaying the data from the pressure transducers. The shell side pressure of the MBR, p_S, was at atmospheric pressure (101.325 kPa) for both the control and biofilm growth experiments.

C.3 Description of experiments

C.3.1 Control experiments

Before performing the biofilm growth experimental runs, experiments with no biofilm growth were undertaken to serve as a control. The control experiments also involved validation of the properties of both the nutrient solution and polysulphone capillary membrane.

Table C.1: The dimensions of the single fibre capillary membrane bioreactor.

Membrane inner radius	R_1	m	6.98×10^{-04}
Membrane outer radius	R_2	m	9.10×10^{-04}
Extra capillary space radius	R_3	m	5.91×10^{-03}
Glass manifold inner radius	R_4	m	10.91×10^{-03}
Effective membrane length	L	m	0.230

The dimensions of the MBR are indicated in Table C.1. The capillary membrane, described in Section C.2.3, was fixed to the centre of the glass reactor using epoxy glue, one side at a time, and left over night to dry. Silicone tubing (ID = 3cm; OD = 5cm) was connected and used to feed the bioreactor with distilled water. The one end of the bioreactor was clamped, to force the distilled water through the membrane (i.e. dead-end filtration). The tubing to and from the bioreactor was fitted with a splitter to allow pressure transducers to be connected. Distilled water was pumped at varying flowrates from a 500ml bottle to the bioreactor using a Watson Marlow 505S peristaltic pump. The system was allowed to run for about an hour for all the tubing to be filled with water, before the inlet and outlet pressure readings were taken. Pressure readings were taken until the system reached steady-state.

The inlet and outlet pressure readings were used in the developed hydrodynamic models (Chapter 3) to firstly validate the accuracy of the developed model, and secondly, to predict various model parameters such as membrane hydraulic permeability; the pressure and velocity profiles along the length of the membrane.

C.3.2 Biofilm growth experiments

When carrying out the biofilm growth experiments precautionary sterilisation measures had to be taken in all the preparation steps, to prevent contamination. It was important that the membranes were handled gently and with the minimum amount of distortion. All the tubing, glassware and bioreactors that were used were autoclaved for 20min at 120 ºC. A 4% formaldehyde solution was used to chemically sterilize the lumen side of the capillary membranes. The formaldehyde solution was run for 6 hours through the system, and thereafter the bioreactor was rinsed with autoclaved distilled water for 12hr to remove all the traces of formaldehyde.

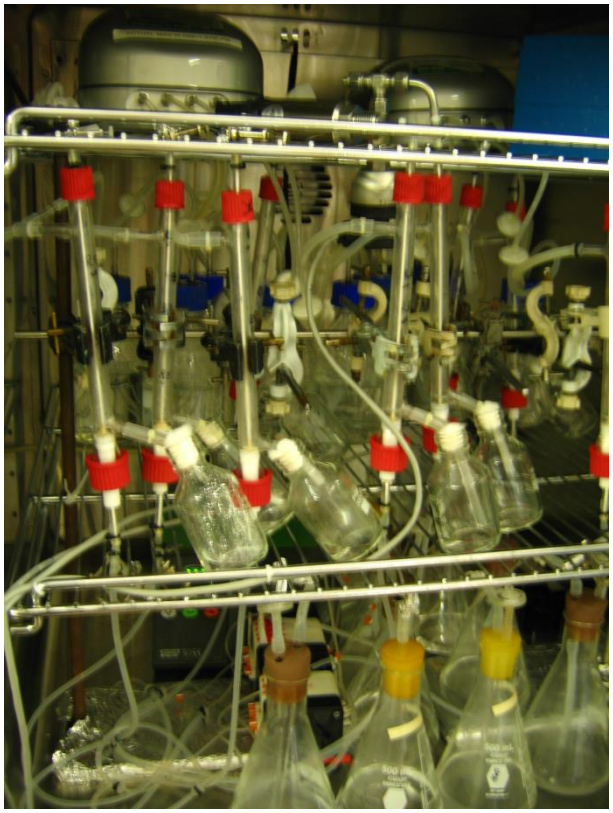

Figure C.2: A pictorial view of the single-fibre capillary membrane bioreactor

After the sterilization and rinsing process, the membrane was inoculated with 3.0×10^{6} *P. chrysosporium* spores. Inoculation was achieved by forcing the spore solution from the shell

side of the membrane, through the membrane, to the lumen side (reverse filtration). Immediately after the inoculation process, the system was fed with nutrients, supplied at a flow rate of 6.20 ml/hr on the lumen side of the membrane. When more than one MBR system was running, as shown in Figure C.2, individual nutrient feeds were used so as to minimise the risk of contamination. The nutrient solution was allowed to fill-up the membrane lumen, before the pump was stopped and the system was left for 24hr for the spores to germinate and acclimatise to their new environment (referred to as the lag phase).

Following the 24hr lag-period, the nutrient supply was continued, and the system was allowed to run with as little disturbance as possible. The mode of operation was dead-end; the nutrient was forced to permeate through the walls of the membrane, to the fungus immobilized on the external skin of the membrane. Permeate was collected daily using 50ml bottles. The pH and redox potential of the permeate solution was monitored daily, using a Hanna HI 8314 pH meter in order to check whether the reactors were biochemically similar. A redox potential of above 200mV was used as an indicator of LiP and MnP activity (Leukes, 1999). An experimental run consisted of 10 reactors connected to individual nutrient feeds as shown in Figure C.2.

C.3.3 Scanning electron microscope preparation

After biofilm growth was visible in all the bioreactors, one bioreactor was stopped every 24hr and prepared for SEM imaging. Samples of the membrane, with biofilm growth, were cut with a sterile blade and placed into a 10% gluteraldehyde solution to preserve the biofilm. The samples were then taken through an alcohol dehydration series. This involved placing the samples in different concentrations of alcohol for at least 10 minutes each. Once the samples were in 100% alcohol they were taken to the Electron Microscopic Unit (EMU) at the University of Cape Town, where they were critical point dried and sputter coated with gold/palladium for examination with the SEM. The SEM that was used was a fully analytical Leo S440 SEM. The SEM images were used to determine the biofilm thicknesses over time.

C.3.4 Hydraulic permeability

Two batches of membranes were used for all the experiments covered in this thesis, and the hydraulic permeability of each batch was determined experimentally. The hydraulic permeabilities were obtained by running distilled water through the lumen side of the MBR at five different flowrates of 1.72, 3.19, 4.86, 6.18 and 13.56 ml/hr; and measuring the pressures at the

inlet and outlet of the MBR operated in the dead-end mode at 20°C, as explained in Section C.2.6.

An investigation of the effect of temperature on the hydraulic permeability of the membranes was also performed. The hydraulic permeability of membranes at two differing temperatures of 20°C and 37°C was compared. For the bioreactor operated at 37°C the flowrates used were: 6.90, 13.56, 20.28, 26.94 and 33.66 ml/hr.

C.4 Results

The dry biofilm density from the MBR was determined using a helium pycnometer (Accupyc, 1330). The calibration of the pycnometer was done by using a steel sphere with a known volume before taking measurements on a series of biofilm samples. The results listed in Table C.2 were obtained for the average biofilm density and substrate conversion, for an inlet glucose concentration of 10 g/dm^3 (Ntwampe and Sheldon, 2006). These results were used in validating the developed theoretical models presented in Chapter 3 – 5.

Table C.2: Experimental results used to validate the effectiveness factor correlations.

Time (hr)	*Biofilm density* (g/dm^3)	*Substrate conversion*
72	410	0.149
120	700	0.149
168	900	0.237
216	1000	0.237
264	1190	0.354

The kinetic constants were listed in Table 5.1 and will not be repeated here.

INDEX

T

V

W

MISCELLANEOUS NOTATION

$\frac{D}{Dt}$	substantial or total derivative
$\frac{\partial}{\partial x}$	partial derivative
$\int$	integral
n!	factorial
n!!	double factorial (e.g. 6!! = 6·4·2)
Σ	overall summation
Π	overall product
∇^n	Laplacian operator, where *n* = 0, 1, 2, 3…
$\approx$	approximately equal
$\sim$	asymptotically equal
<, >, $\leq$ $\geq$	inequality, inclusion
$\neq$	unequal
>>, <<	much larger than, much smaller than